Muon Ionization Cooling Experiment

Coupling Solenoid Magnet Engineering Design Report

2008-12-03

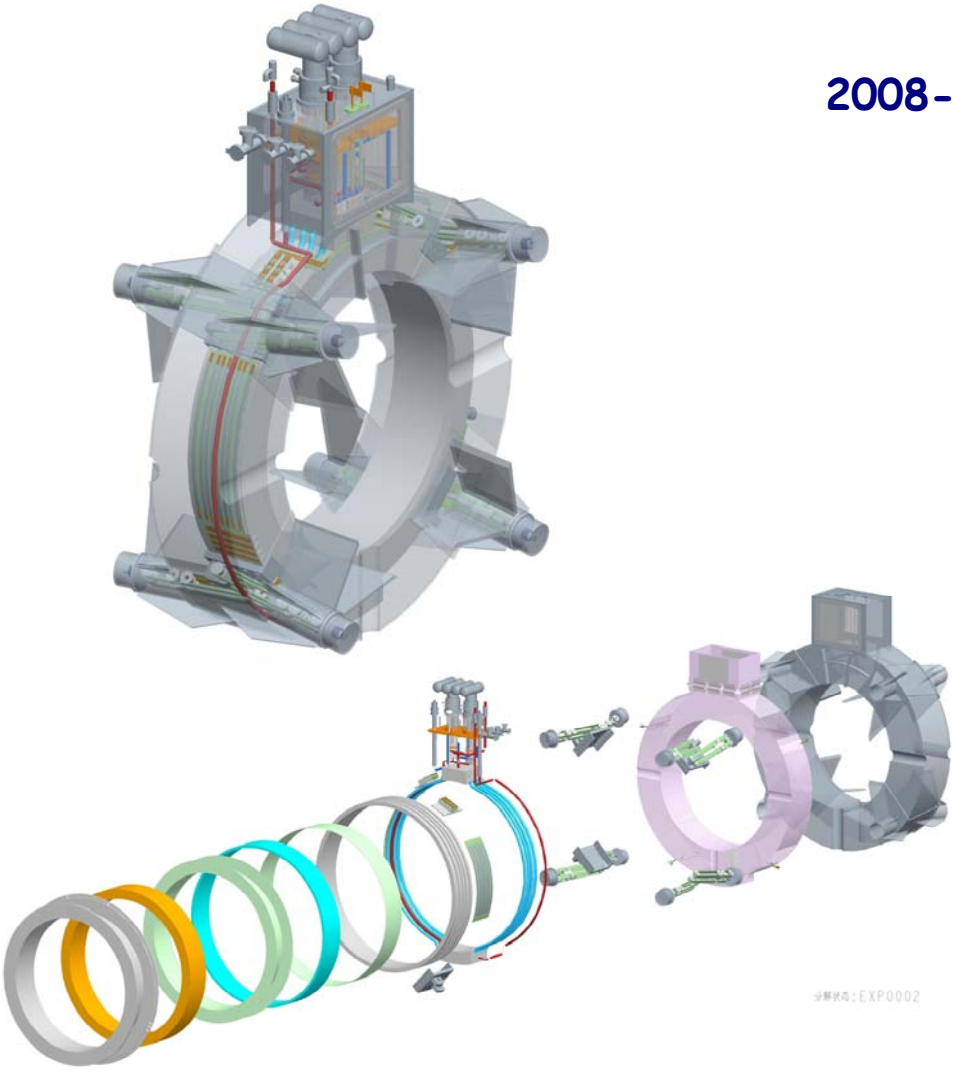

Institute of Cryogenics and Superconductivity Technology

Harbin Institute of Technology

Harbin, China

TABLE OF CONTENTS

1 Introduction

The development of a muon collider or a neutrino factory requires that beams of low emittance muons are to be produced. A key to producing low emittance muons is muon ionization cooling. The international Muon Ionization Cooling Experiment (MICE) will be a demonstration of muon cooling in a configuration of superconducting magnets and absorbers that may be useful for a neutrino factory. The proposed MICE experiment will test cooling on a low intensity muon beam generated by a plunging target in the proton beam of the ISIS ring at the Rutherford Appleton Laboratory in the United Kingdom. Ionization cooling occurs when there is a net loss of transverse muon momentum when the muons pass through the absorber material and are reaccelerated by adjacent RF cavities.

The MICE magnetic channel consists of seven magnet assemblies composed of eighteen superconducting solenoid coils spread over a length of over 12 meters [1]. The solenoid channel is physically symmetric about its centre, which is defined locally as z = 0. There are three types of magnets: 1) the focusing magnets that produce the magnetic field in the absorbers within the absorber focus coil module (AFC module), 2) the coupling magnets that generate the magnetic field for the RF coupling coil module (RFCC module), and 3) the tracker solenoids that generate the uniform and matching fields within the tracker module. The MICE channel consists of three AFC modules, two RFCC modules and two tracker modules.

As shown in Fig.1-1, the muon beam enters from the lower left and is measured by time-of-flight (TOF) and Cherenkov detectors and a first solenoidal tracking spectrometer. It then enters the cooling section, where it is alternately slowed down in absorbers and reaccelerated by RF cavities, while being focused by a lattice of superconducting solenoids. Finally it is re-measured by a second solenoidal tracking spectrometer and its muon identity confirmed by Cherenkov and TOF detectors and a calorimeter.

The muon beam longitudinal momentum is recovered to its original by accelerating the beam with four normal conducting 201.25-MHz closed RF cavities that are in an around 2.5T magnetic field produced by a coupling magnet after cooled by passing through the AFC module. Each cavity has a pair of thin curved beryllium windows to close the conventional open beam irises, which allows for independent control of the phase in each cavity and for the RF power to be fed separately. The single superconducting coil package that surrounds the RF cavities is mounted on a vacuum vessel. The coupling coil confines the beam in the cavity module and, in particular, within the radius of the cavity beam windows.

The RF vacuum is shared between the cavities and the vacuum vessel around the cavities such that there is no differential pressure on the thin beryllium windows. The RFCC vacuum vessel is also designed to withstand the longitudinal magnetic forces generated by the coupling magnet at its various operating modes. The magnetic forces are then carried to the base plate of the experiment through the RFCC module stand. The vacuum within the RFCC vessel is totally isolated from the insulating vacuum within the coupling magnet vessel. A cross-section of the RFCC module is

shown in Fig.1-2.

A coupling magnet assembly consists of a single coil that fits into a cryostat vacuum vessel. The coupling magnet is designed to operate in a channel where the fields from other magnets can interact with the magnet. As shown in Fig.1-2, the size and shape of the coupling magnet is determined by the RF cavities. The inner diameter of the coupling magnet is determined by the diameter of the 201.25 MHz RF cavities and the vacuum vessel that must go around the cavities. The length of the coupling magnet is determined by the space needed for the cavity RF couplers and the cavity tuners.

The updated engineering design were carried out by the ICST/HIT according to the "A Technical Agreement on the MICE and MuCool Coupling Solenoid Magnet Fabrication, Assembly, Test and Shipping" issued in September, 2007 and experience learnt form test coils' winding in collaboration with Lawrence Berkeley National Laboratory.

In this engineering design report, the updated coupling magnet design is presented in detail. The coupling magnet mainly consists of the coil assembly and the cryostat assembly. The coil assembly is composed of the coil winding pack and its case. The cryostat comprises the cooling circuit system, cold mass support system, heat shields and thermal intercepts, magnet leads, cryocoolers and helium re-condenser, vacuum chamber, and instrumentation as shown in Fig.1-3.

The main differences between the previous design reviewed in May, 2007 and the updated design include:

1. The inner radius of the coupling coil is changed from 744mm to 750mm considering very tight space on the inner side of the magnet.
2. The coil cold mass assembly is designed different from the previous one in terms of winding, mandrel fabrication, cooling and quench protection assembly (see details in the report).
3. A double-band cold mass support system is presented instead of a single-band system considering the shipping load during long-term transportation.
4. Two drop-in PTR coolers are to be used for cooling the coupling magnet for the sake of easy removal from the cryostat during transportation.
5. Thermal shields are designed to be supported from the vacuum vessel by four pairs of G-10 rods instead of being supported onto the cold mass support assembly as previous design.
6. The cooling configuration for the warm end of the HTS leads is designed different from the previous one (see details in the report).

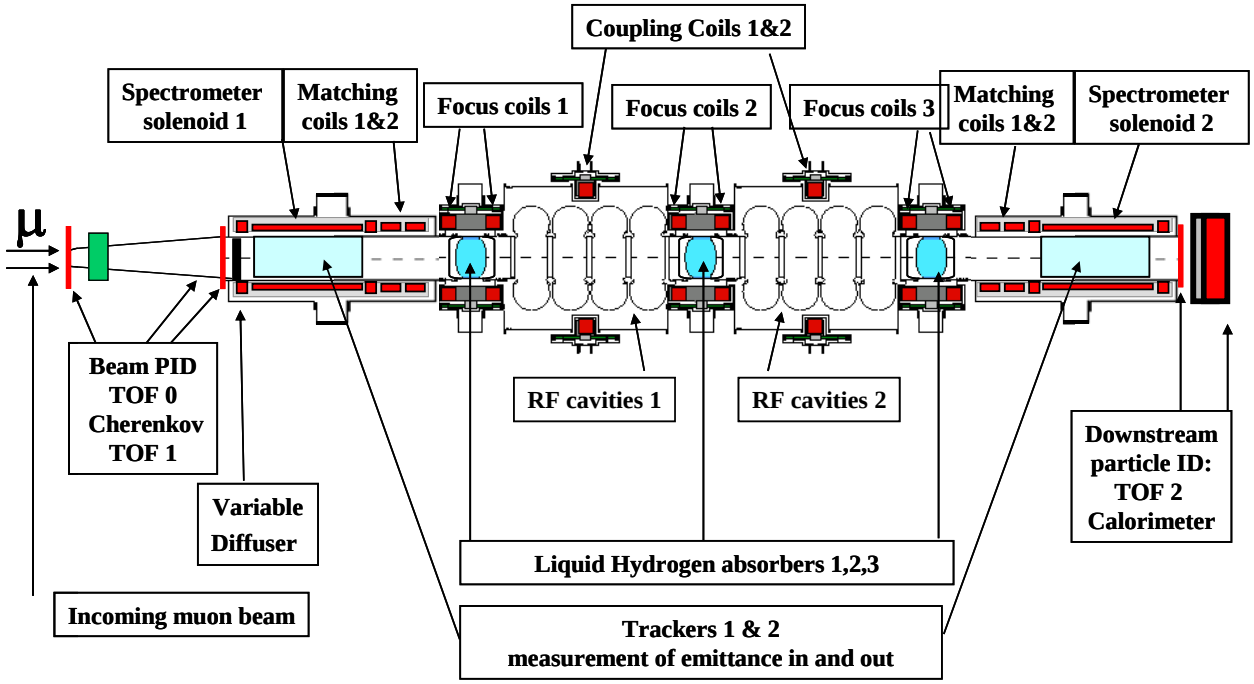

Fig.1-1 MICE Layout

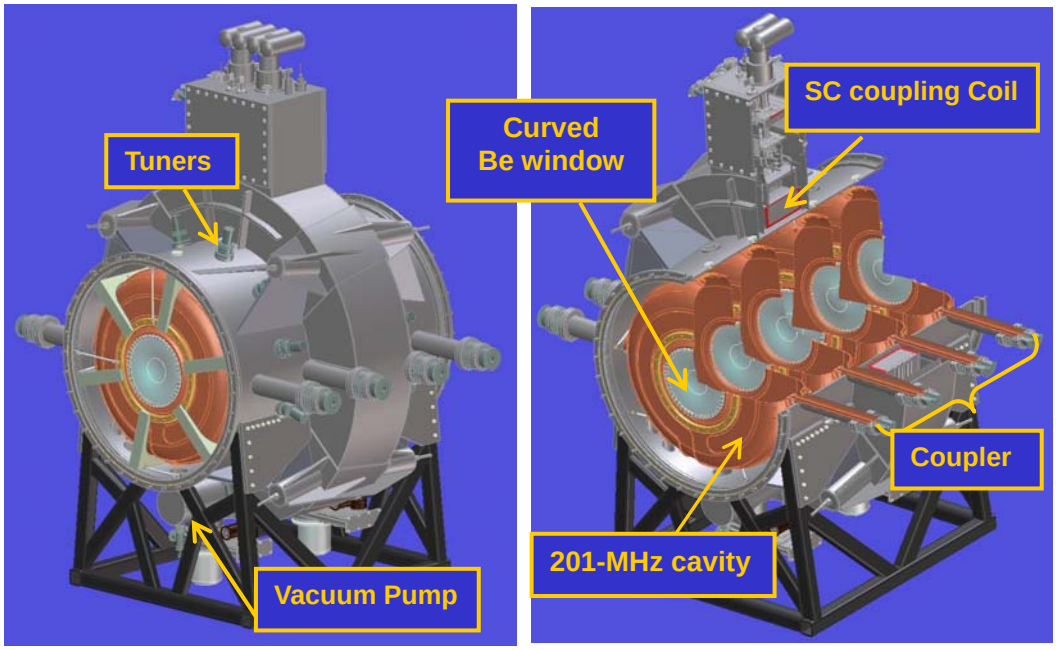

Fig.1-2 RFCC module

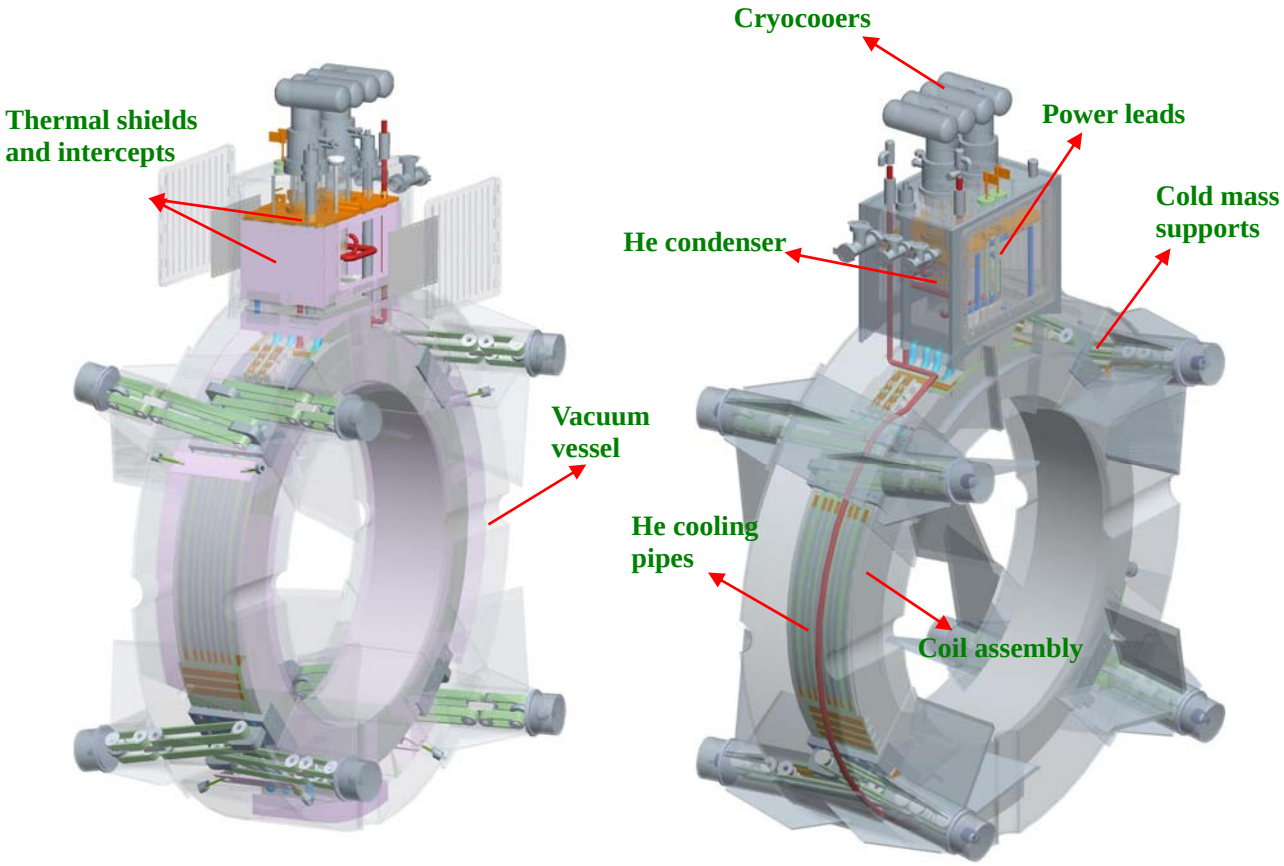

Fig.1-3 Overall 3D view of coupling magnet

2 Basic Design Parameters

2.1 Technical requirement for coupling magnet design

According to "A Technical Agreement between the LBNL and the HIT on the MICE and MuCool Coupling Solenoid Magnet Fabrication, Assembly, Test and Shipping" in September, 2007:

- The coupling magnet assembly consists of a single coil that fits into a cryostat vacuum vessel.
- The coupling magnet is designed to operate in a channel where the fields from other magnets can interact with the magnet.
- The size and shape of the coupling magnet is determined by the RF cavities. The inner diameter of the coupling magnet is determined by the diameter of the 201.25 MHz RF cavities and the vacuum vessel that must go around the cavities. The length of the coupling magnet is determined by the space needed for the cavity RF couplers and the cavity tuners.
- The coupling magnet is to be cooled by using two cryocoolers that produce up to 1.5 W at 4.2 K each. The connection of the cooler to the magnet is designed to maximize the coupling magnet operating temperature margin.
- The coupling solenoid will be powered by using a single 300 A, 0-20V unipolar power supply that is connected to the magnet through a single pair of binary leads that are designed to carry a maximum current of 250 A. The high temperature superconducting (HTS) leads are to be applied between the first stage of the cooler and the magnet in order to reduce the heat leak, which operates at around 4.2 K.
- The coupling magnet is to be passively protected by cold diodes and resistors across sections of coil and by quench back from the 6061 aluminum mandrel. Sub–division of the coupling magnet using cold diodes and resistors will result in lower quench voltages and a lower hot spot temperature.
- The coupling magnet cold mass support is to be a self-centering support system consisting of eight tension bands so that the magnet center does not change as the magnet is cooled down. The support system is designed to carry a sustained longitudinal force up to 500 kN (50 tons) in either direction during the anticipated operating and failure modes of the experiment and to withstand a 2.5g shipping load at any direction during warm transportation.

Table 2-1 shows some of detailed requirement for the coupling magnet design

Table 2-1 Requirements for engineering design of coupling magnet*

Inner diameter of inner vacuum vessel (mm)	1389±3
Length of vacuum vessel (mm)	489±2
Inner radius of coil (mm)	750
Coil to ground insulation (mm)	≥1
Thickness of coil (mm)	102.5
Length of coil (mm)	285

Layers of coil	96
Turns per layer	166±3
Space between 4.2K cold mass and heat shields (mm)	>5
Space between vacuum vessel and heat shields (mm)	>20
ΔT between the cold mass and second-stage cold head	<0.2 K
Intercept temperature for the cold mass support	<70K
Temperature on the heat shield	<80K
Cooling capacity at the first-stage cold head	55W/60K，45W/50K
Cooling capacity at the second-stage cold head	1.5 W/4.2K
4.2Kheat load along the cold mass support	<0.25W
Spring constant for the cold mass support	$>2x10^{8}N\text{-}m^{-1}$
Radial force on the cold mass	<50kN
Longitudinal force on the cold mass	500kN
Design pressure for cooling tubing	20bar (290psig)
Design pressure for helium vessels	4bara (44psig)
Relief pressure for relief valves of cooling tubing	≤3bar (29psig)
Relief pressure for burst disc of cooling tubing	3.3bar (32psig)- 4bar (44psig)
Design outer pressure for vacuum chamber	1bar (15psig)
Design inner pressure for vacuum chamber	0.3bar (4.4psig)
Relief pressure for vacuum chamber	0.14bar (2psig)
Relief pressure for burst disc of vacuum chamber	0.3bar (4.4psig)
Copper leads (A)	optimized design current 220A, maximum operating current 250A
HTS leads	nominal 220A, 500A at 64K, 0.5T
Magnetic field around the warm end of HTS leads	≤0.5T, otherwise, shielding needed
Magnetic field around the cooler drive motor	<0.05T, otherwise, shielding needed

*A Technical Agreement on MICE Coupling Solenoid Magnet Fabrication, Assembly, Test and Shipping, issued on 09/27/2007.

2.2 Basic parameters of coupling coils

The MICE coupling coil is a single 285 mm long solenoid wound on a 6061-T6-Al mandrel. The inner radius of the coil is 750 mm and its thickness is 110.4 mm at room temperature. Table 2-3 shows the basic parameters of the coil.

Table 2-3 Basic parameters for the coupling magnet

	p = 240 MeV/c and β= 420 mm		p = 200 MeV/c and β= 400 mm	
Parameter	**Flip**	**Non-flip**	**Flip**	**Non-flip**
Coil Length (mm)	285		285	
Coil Inner Radius (mm)	750		750	

Coil Thickness (mm)	110.4		110.4	
Number of Layers	96		96	
No. Turns per Layer	166±3		166±3	
Magnet Self Inductance (H)	591.8		591.8	
Magnet J (A mm^{-2})*	106.85	100.76	89.02	83.97
Magnet Current (A)*	210.1	198.2	175.1	165.2
Magnet Stored Energy (MJ)**	13.1	11.6	9.07	8.08
Peak Induction in Coil (T)*	7.3	7.0	6.1	5.9
Coil Temperature Margin (K)	~0.8	~1.1	~1.4	~1.7

*For the standard case with p = 200 MeV/c and beta = 420 mm based on the 300K dimensions of coil. For the worse case with p = 240 MeV/c and beta = 420 mm, to multiply value by 1.2.

** For the standard case with p = 200 MeV/c and beta = 420 mm based on the 300K dimensions of coil. For the worse case with p = 240 MeV/c and beta = 420 mm, to multiply value by 1.44.

2.3 Superconductor

The superconductor to be used for the coupling solenoid is a commercial copper matrix NbTi conductor originally used for MRI magnets with a copper to superconductor ratio of four. The copper in the conductor has a minimum residual resistance ratio RRR of 70. The conductor consists of 222 filaments that are nominally 41μm in diameter, and the conductor nominal twist pitch is 13 mm. The conductor has insulated dimensions of 1.65 mm by 1.00 mm, (The bare dimension are 1.60 mm by 0.95 mm).The dimensions of the insulated conductor are 1.0 by 1.65 mm, and the conductor is rounded to prevent insulation cracking. The design critical current for the conductor is 760 A at 4.2 K and 5.0 T. The conductor n value is greater than 35 at 5T.

Fig. 2-1 shows the cross section of the conductor. A typical short sample test is shown in Fig. 2-2. The critical current versus the magnetic induction is shown in Fig. 2-3. From the test result, the conductor smallest critical current at 5T and 4.2K is 793A and greater than the critical current parameters specification (>760 A).

The load line shown in Fig. 2-4 is plotted based on the typical short sample test curve. The coupling magnet is to operate in the MICE channel where the fields from other magnets can interact with it. It will work in two modes due to the polarity change of two focusing coils in the AFC module. One is gradient mode (flip mode), and the other is solenoid mode (non-flip mode). For each mode, the coupling magnet will work at the standard case with p = 200 MeV/c (average momentum of the muons traveling along the channel) and beta = 420 mm (beam beta at the center of the absorbers) or at the worse case with p = 240 MeV/c and beta = 420 mm. The worst case is to operate the MICE in the flip mode with p =240MeV/c and beta = 420 mm. Using this conductor at the worst case, the magnet temperature margin is expected to be about 0.8 K when the induction at high field point is 7.4 T under the full current of 210 A and the cold mass temperature at 4.2 K.

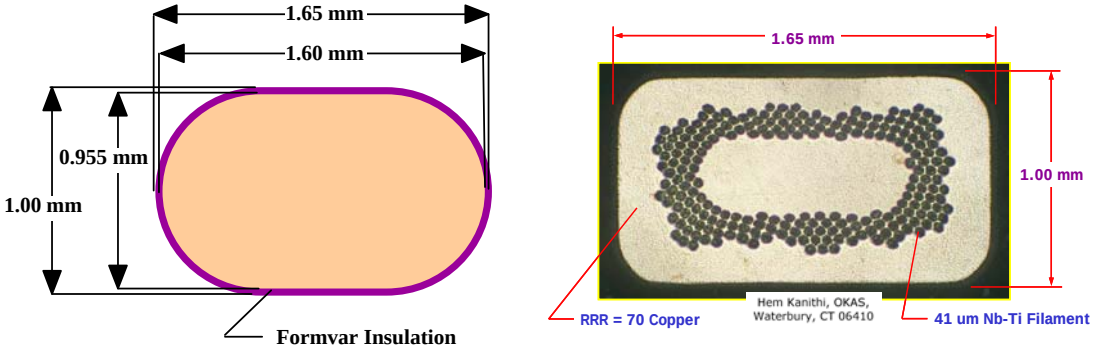

Fig. 2-1 Cross section of conductor

Table 2-2 Parameters for superconductors

Parameter	**Value**
Insulated dimension	1.00mm x 1.65mm
Cu to S/C Ratio	4.0 ± 0.5
Cu RRR	>70
No. Filaments	222
Filament Diameter	~41 μm
Filament twist Pitch	19 mm ± 6
Ic(4.2K, 5T)	> 760 A
n	> 35 @ 5T

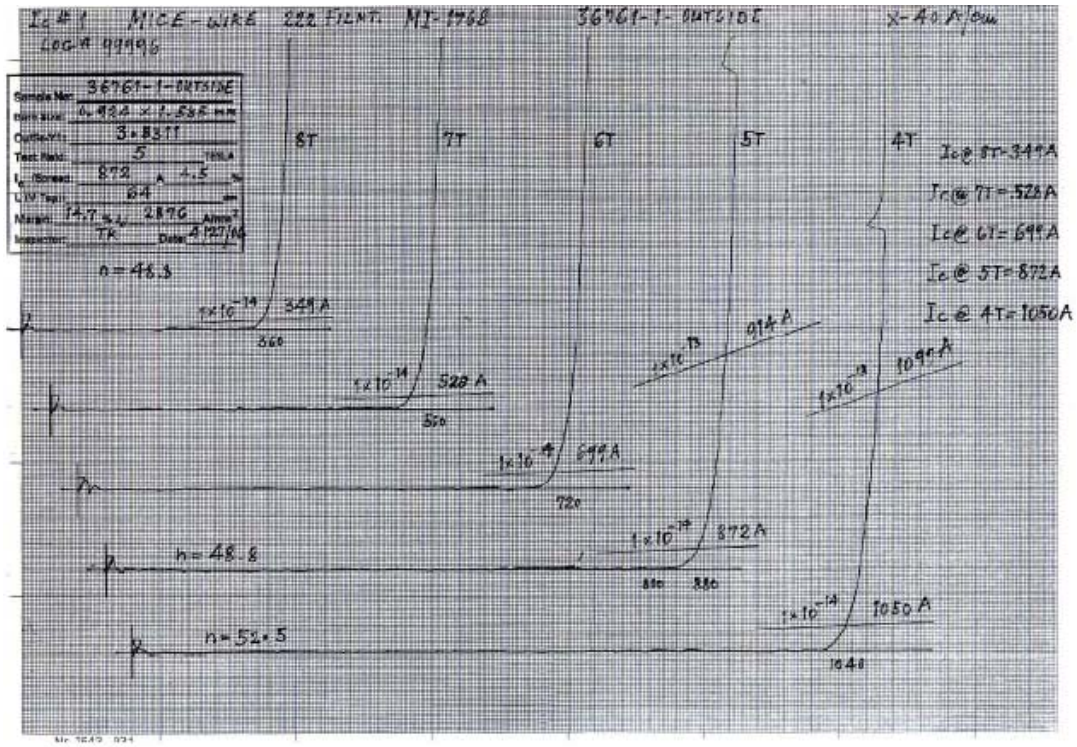

Fig.2-2 Typical short sample test plot

B Tesla)	Ic(36760-1A)	Ic(36761-1A)	Ic(36679-B)
4	957	1042	998
5	793	867	826
6	634	697	662
7	476	526	498
8	314	351	330

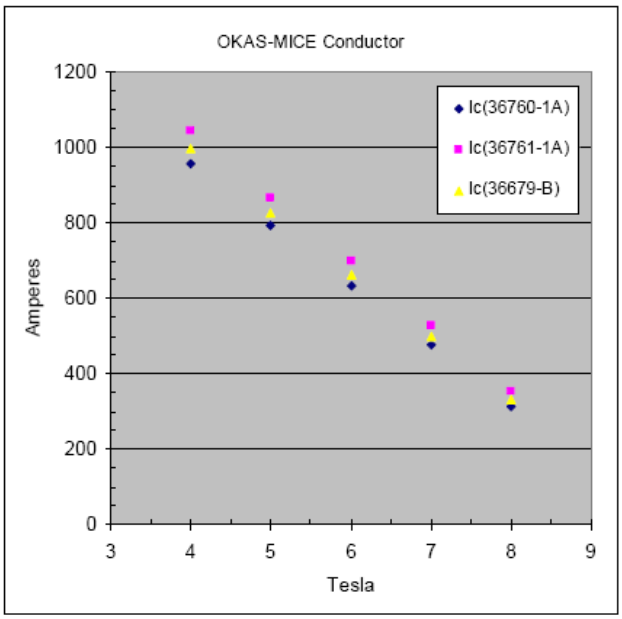

Fig. 2-3 Critical current vs. Magnetic field at 4.2K

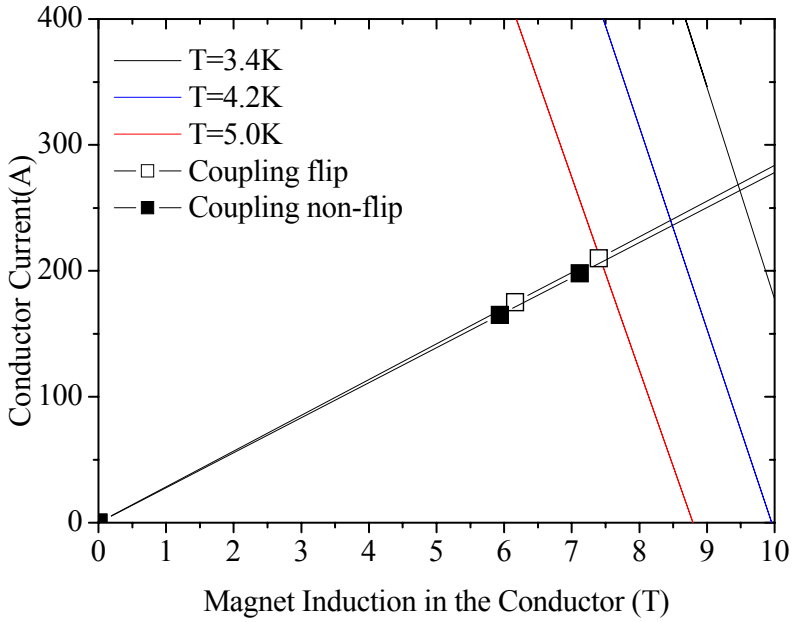

Fig. 2-4 Load line for coupling magnet at different modes

2.4 Main structure parameters for coupling magnet

Table 2-4 presents the main structure parameters for the coupling magnet design. Fig. 2-5 shows the cross-section of the coil assembly.

Table 2-4 Main structure parameters for the coupling magnet

	Updated design	Previous design
Inner diameter of inner vacuum shell (mm)	**1387** (1389±3)	1389
Thickness of inner vacuum shell (mm)	4.0	4.0

Outer diameter of outer vacuum shell (mm)	**2278±6**	**2160**
Thickness of outer vacuum shell (mm)	10.0	10.0
Length of vacuum chamber (mm)	489	489
Inner diameter of inner shield (mm)	1431	---
Outer diameter of outer shield (mm)	2056	---
Thickness of heat shield (mm)	4.0 (Al)	2.0 (Cu)
Inner radius of coil (mm)	**750**	**744**
G-10 insulations for coil-to-ground (mm)	1.0 (0.5x2)	1.0 (0.5x2)
Insulations between coil and end plates (mm)	3.5	3.0
Thickness of coil (mm)*	**110.4**	102.5
Length of coil (mm)	285	285
Layers of coil	96	96
Turns per layer	166±3	166±3
Thickness of coil bobbin (mm)	19 (without considering pre-tension and slip-plane)	13 (w/o considering pre-tension and slip-plane)
Thickness of coil end plates (mm)	18.5	19
Thickness of cover plate (mm)	45	15
Thickness of banding (mm)**	10~27	13~25
Space between 4.2K surface and heat shield (mm)	10	9.7
Space between heat shield and 300K (mm)	18	18

Note: *Due to the thickness of the fiber glass cloth used for layer-to-layer insulation is 0.1mm, plus the thickness of the epoxy, the total thickness for each layer of coil is about 1.15mm, so the thickness of the coil is 110.4 instead of 102.5. **The thickness of the banding is also up to the fabrication process for the coil case.

For the interface design between the RF cavities and coupling magnet, as shown in Fig. 1-2, the magnet cryostat is bounded by the center two cavity couplers and vacuum ports. In order to maximize the coil length, the magnet vacuum vessel has to be designed to fit around the RF cavity couplers, tuners and vacuum pump out ports. There are indentations at different locations on the vacuum vessel to fit in the 130 mm OD coupler tubes and the cavity vacuum pumping ports. There is a 3 mm clearance space between the RFCC vacuum vessel and the coupling coil vacuum vessel. The clearance between the cryostat vacuum vessel and the coupler tube is 3 mm as well. The spacing between the center coupler tubes is 517 mm. The RFCC vacuum vessel is 6.4 mm thick under the coupling coil. The coupling coil inner vacuum vessel is 4 mm thick. At other locations, the RFCC vacuum vessel is 19.1 mm thick. The indented section of the coupling coil cryostat vessel is about 4 mm thick with a radius of 68 mm. The tube indent is a problem here. Of the total space between the inside of the indent tube and the end wall of the cold mass (at 300 K) is of 29 mm, about 8 mm is taken up with the vacuum vessel wall and the radiation shield. The local radiation heat will be large.

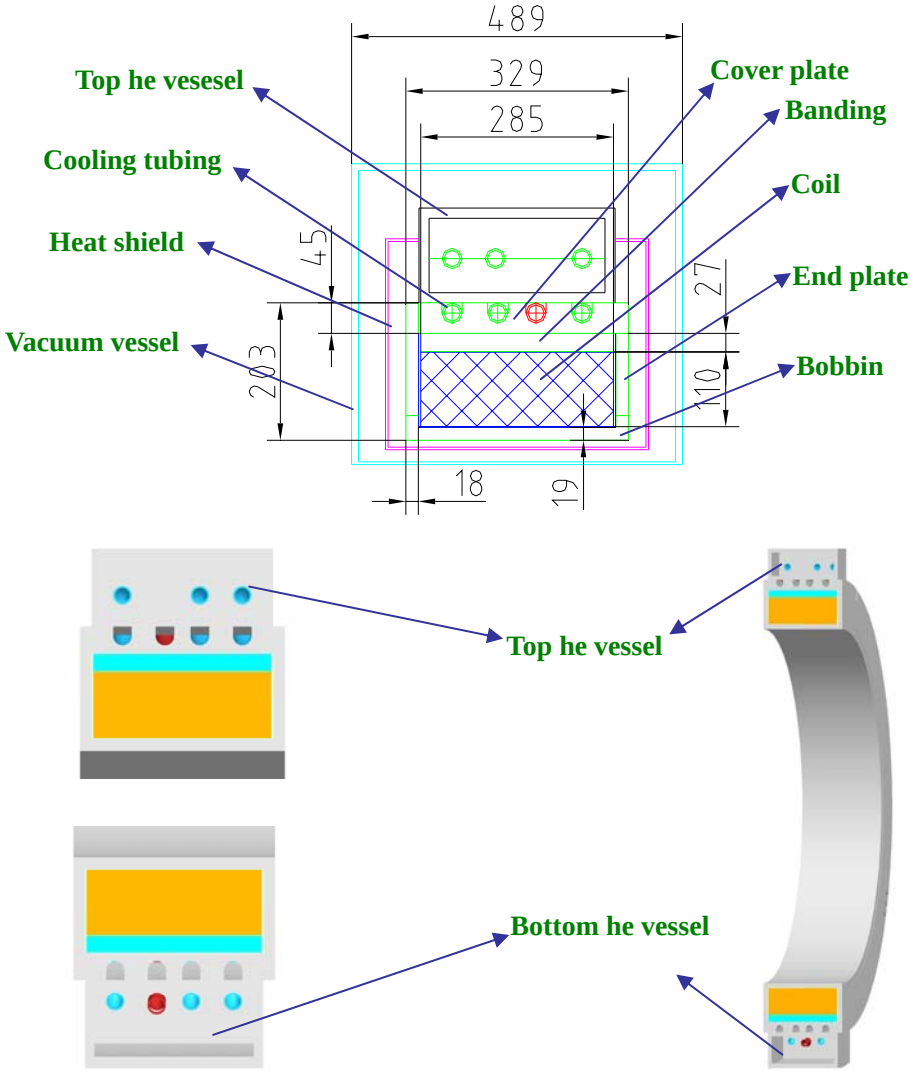

Fig. 2-5 Cross-section of the coil assembly

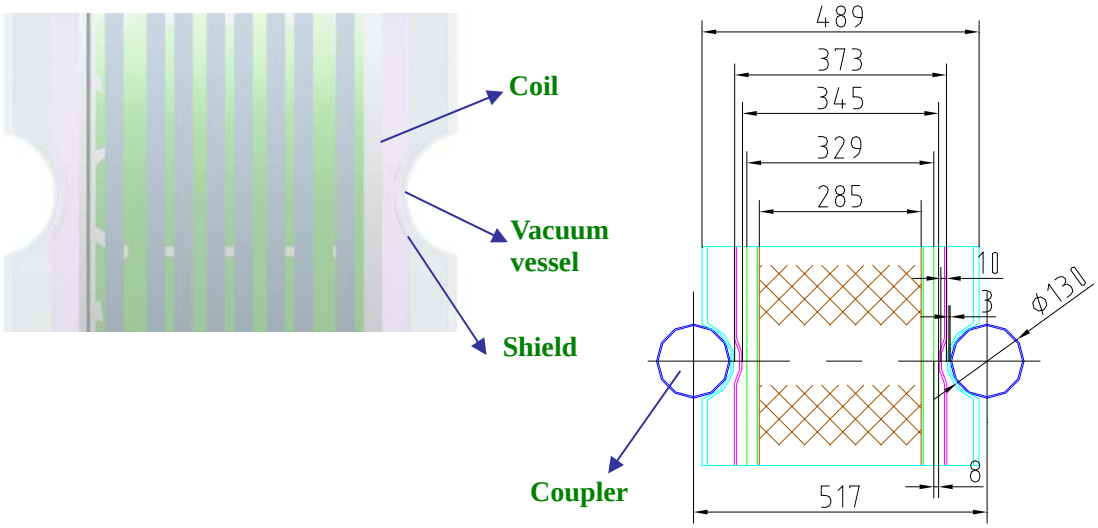

Fig.2-5 Coupling coil cross-section looking into the RFCC vessel

3 MICE Coupling Coil Assembly Design

3.1 Magnetic fields

The magnetic fields for the MICE cooling channel were calculated in an axially symmetric finite element using ANSYS. The magnetic field distribution along the axis of the channel is obtained, as well as the field around the coupling coil.

3.1.1 Physical parameters

Table 3-1-1 and Table 3-1-2 show the physical locations and current densities for MICE coils at flip mode and solenoid mode respectively. These current densities are calculated based on the coil warm positions and dimensions. If the coil cold positions and dimensions are used, the current densities go up from 0.8 to 1.5 percent. As a result, the calculated forces go up as much as 3%.

Table 3-1-1 Physical locations and current densities for MICE coils at flip mode

	MICE Coil	z_0 (m)	r1(m)	r2(m)	b(m)	J(Amm^{-2})	
						200MeV/c	240Mev/c
1	Spectrometer End Coil #2	7.3260	0.258	0.324	0.0553	-135.18	-135.18
2	Spectrometer Centre Coil	6.5761	0.258	0.2793	0.65715	-152.44	-152.44
3	Spectrometer End Coil #1	5.8260	0.258	0.3176	0.0553	-127.37	-127.37
4	Match Coil #2	5.4261	0.258	0.2878	0.09975	-137.13	-150.52
5	Match Coil #1	4.9860	0.258	0.3027	0.1006	-118.56	-142.48
6	Focus Coil #3	4.3300	0.263	0.347	0.105	-113.95	-136.74
7	Focus Coil #2	3.9200	0.263	0.347	0.105	+113.95	+136.74
8	Coupling Coil	**2.7500**	**0.750**	**0.860**	**0.1425**	**+89.02**	**+106.85**
9	Focus Coil #1	1.5800	0.263	0.347	0.105	+113.95	+136.74
10	Focus Coil #1	1.1700	0.263	0.347	0.105	-113.95	-136.74
11	Coupling Coil	**0.0000**	**0.750**	**0.860**	**0.1425**	**-89.02**	**-106.85**
12	Focus Coil #2	-1.1700	0.263	0.347	0.105	-113.95	-136.74
13	Focus Coil #3	-1.5800	0.263	0.347	0.105	+113.95	+136.74
14	Match Coil #1	-2.2360	0.258	0.3027	0.1006	+118.56	+142.48
15	Match Coil #2	-2.6761	0.258	0.2878	0.09975	+137.13	+150.52
16	Spectrometer End Coil #1	-3.0760	0.258	0.3176	0.0553	+127.37	+127.37
17	Spectrometer Centre Coil	-3.8261	0.258	0.2793	0.65715	+152.44	+152.44
18	Spectrometer End Coil #2	-4.5760	0.258	0.324	0.0553	+135.18	+135.18

Notes: 1) 2b is the coil length; 2) r_1 is the coil inner radius; 3) r_2-r_1 is the coil thickness.

Table 3-1-2 Physical locations and current densities for MICE coils at solenoid mode

	MICE Coil	z0 (m)	r1(m)	r2(m)	b(m)	J(Amm-2)	
						200MeV/c	240Mev/c
1	Spectrometer End Coil #2	7.3260	0.258	0.324	0.0553	+137.48	+137.48
2	Spectrometer Centre Coil	6.5761	0.258	0.2793	0.65715	+150.15	+150.15
3	Spectrometer End Coil #1	5.8260	0.258	0.3176	0.0553	+132.46	+127.37
4	Match Coil #2	5.4261	0.258	0.2878	0.09975	+114.88	+137.50
5	Match Coil #1	4.9860	0.258	0.3027	0.1006	+130.96	+151.11
6	Focus Coil #3	4.3300	0.263	0.347	0.105	+59.52	+71.42
7	Focus Coil #2	3.9200	0.263	0.347	0.105	+59.52	+71.42
8	Coupling Coil	**2.7500**	**0.750**	**0.860**	**0.1425**	**+83.97**	**+100.76**
9	Focus Coil #1	1.5800	0.263	0.347	0.105	+59.52	+71.42
10	Focus Coil #1	1.1700	0.263	0.347	0.105	+59.52	+71.42
11	Coupling Coil	**0.0000**	**0.750**	**0.860**	**0.1425**	**+83.97**	**+100.76**
12	Focus Coil #2	-1.1700	0.263	0.347	0.105	+59.52	+71.42
13	Focus Coil #3	-1.5800	0.263	0.347	0.105	+59.52	+71.42
14	Match Coil #1	-2.2360	0.258	0.3027	0.1006	+130.96	+151.11
15	Match Coil #2	-2.6761	0.258	0.2878	0.09975	+114.88	+137.50
16	Spectrometer End Coil #1	-3.0760	0.258	0.3176	0.0553	+132.46	+127.37
17	Spectrometer Centre Coil	-3.8261	0.258	0.2793	0.65715	+150.15	+150.15
18	Spectrometer End Coil #2	-4.5760	0.258	0.324	0.0553	+137.48	+137.48

Notes: 1) 2b is the coil length; 2) r_1 is the coil inner radius; 3) r_2-r_1 is the coil thickness.

3.1.2 Magnetic field on the axis of the MICE cooling channel

Fig. 3-1-1 and Fig. 3-1-2 show the magnetic field along the axis of the MICE cooling channel at various operating cases based on the parameters in Table 3-1-1 and Table 3-1-2. At solenoid mode for 200MeV/c, the central field of the coupling coil is 2.19T, and for 240 MeV/c, the central field of the coupling coil is 2.62T. At flip mode for 200MeV/c, the central field of the coupling coil is 2.17T, and for 240 MeV/c, the central field is 2.60T.

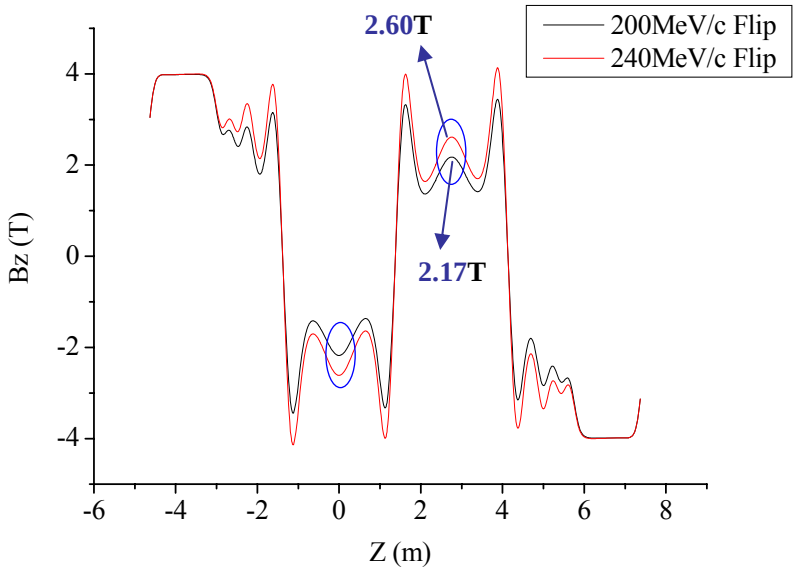

Fig. 3-1-1 Magnetic field on the axis of MICE cooling channel at flip mode

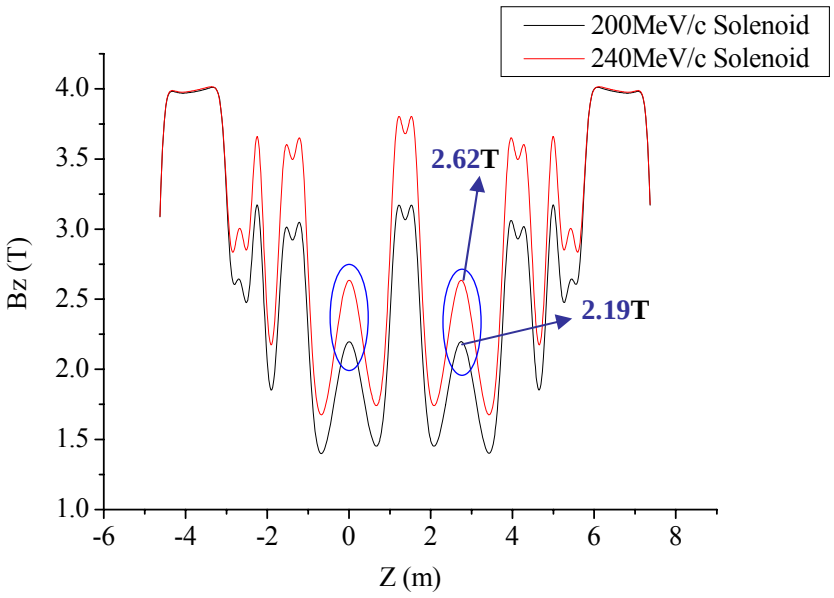

Fig. 3-1-2 Magnetic field on the axis of MICE cooling channel at solenoid mode

3.1.3 Effects of the other coils in the channel on the magnetic field of coupling coil

Because the coupling coil will be operated along with the other coils in the MICE channel, the effects of the other coils on the magnetic field of the coupling coil were studied. Table 3-1-3 and Table 3-1-4 show the magnetic field at various operation modes for only coupling coil and for the coupling coil in the channel. The other coils in the channel can increase or decrease the magnitude of magnetic field generated by only coupling coil and the effect is less than 1.0 percent at the peak field point and the minimum surface field point. The effects of the other coils on the magnetic field

of the coupling coil are small so that they can be neglected in design analysis.

Table 3-1-3 Magnetic fields on the coupling coil at flip mode

	Coil	Peak field (T)	Minimum surface field (T)
200MeV/c	MICE channel	R=0.750, Z=0, B= 6.08	R=0.860,Z=0, B= 3.56
	Coupling coil*	R=0.750, Z=0, B=6.10	R=0.860,Z=0, B= 3.52
240MeV/c	MICE channel	R=0.750, Z=0, B= 7.29	R=0.860,Z=0, B= 4.27
	Coupling coil*	R=0.750, Z=0, B= 7.32	R=0.860,Z=0, B= 4.22

*The magnetic field is only generated by coupling coil.

Table 3-1-4 Magnetic fields on the coupling coil at solenoid mode

	Coil	Peak field	Minimum surface field
200MeV/c	MICE channel	R=0.750, Z=0, B= 5.85	R=0.860,Z=0, B= 3.24
	Coupling coil*	R=0.750, Z=0, B= 5.75	R=0.860,Z=0, B= 3.32
240MeV/c	MICE channel	R=0.750, Z=0, B= 7.02	R=0.860,Z=0, B= 3.89
	Coupling coil*	R=0.750, Z=0, B= 6.90	R=0.860,Z=0, B= 3.98

* The magnetic field is only generated by coupling coil.

3.1.4 Magnet field around the coupling coil in the channel

According to the parameters in Table 2-3, both for the 200MeV/c case and for the 240MeV/c case, the coupling coil current at flip mode are higher than that at solenoid mode, and flip mode is the worse case for design. The magnetic field distribution around the two coupling coils is the same. Fig. 3-1-3 shows the magnetic field on the axis of the coupling coil in the channel at flip mode, for 200 MeV/c the central field is 2.17T, and for 240 MeV/c that is 2.60T. Fig. 3-1-4 shows the magnetic field along the radial direction of the coupling coil in the channel at flip mode, for 200 MeV/c the peak field is 6.08T at R=0.750m and for 240 MeV/c that is 7.29T at R=0.750m.

The magnetic field distribution around the coupling coil is nearly symmetric for each coil. Fig. 3-1-5 shows the magnetic field around the coupling coil at 210A. The cold diodes is in a field from 1.5 to 2.5T, the warm end of HTS leads is in a field from 0.3T to 0.4T and the cold end is 0.6 to 0.7T, the valve motor of the cooler is in a field from 0.15 to 0.20T, and the PTR cooler second stage cold head is in a field from 0.5 to 0.6T. The effects of the magnetic field on performance of these components will be studied in detail in the following sections of this report.

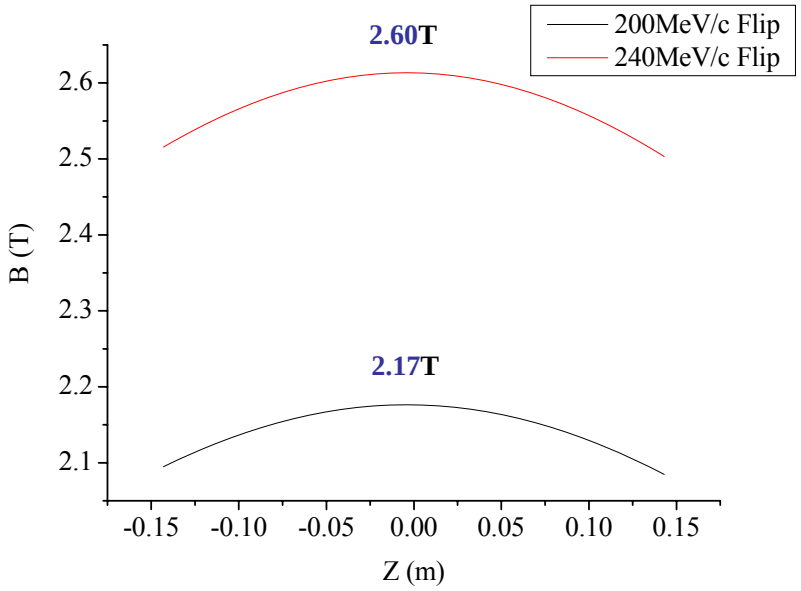

Fig. 3-1-3 Magnetic field on the axis of coupling coil in the channel at flip mode

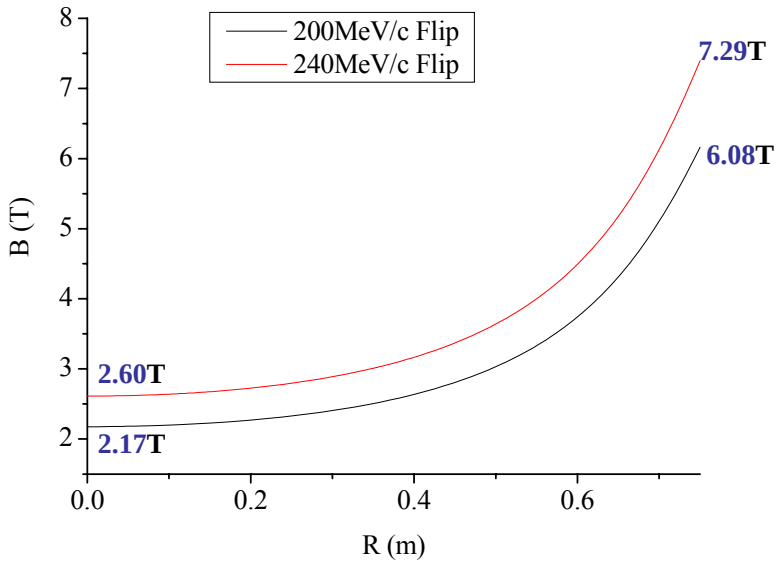

Fig. 3-1-4 Magnetic field on the radial of coupling coil in the channel at flip mode (z=0m)

3.1.5 Stray magnetic field around the coupling coil

Fig. 3-1-6 shows the stray magnetic field around the coupling coil when the current is 210A. For safely operating the coupling coil, operators and metals should work at the field below 0.03T, better below 0.008T. Fig. 3-1-6 shows the field of 0.03T is away from the coil center about 3.4m in radius, and that of 0.008T is about 5.0m in radius.

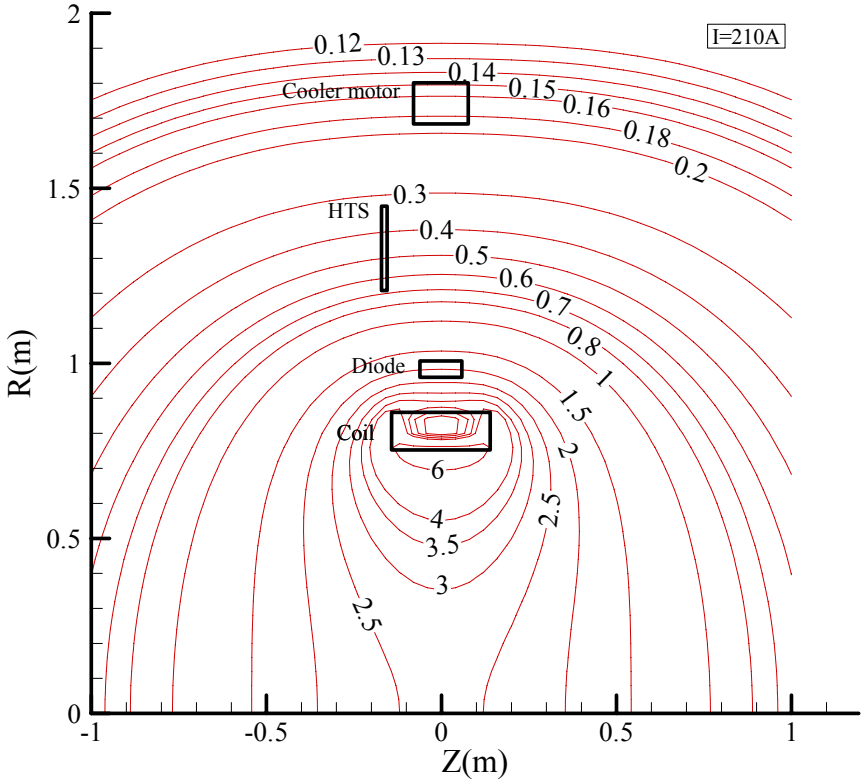

Fig. 3-1-5 Magnetic field around the coupling coil (T)

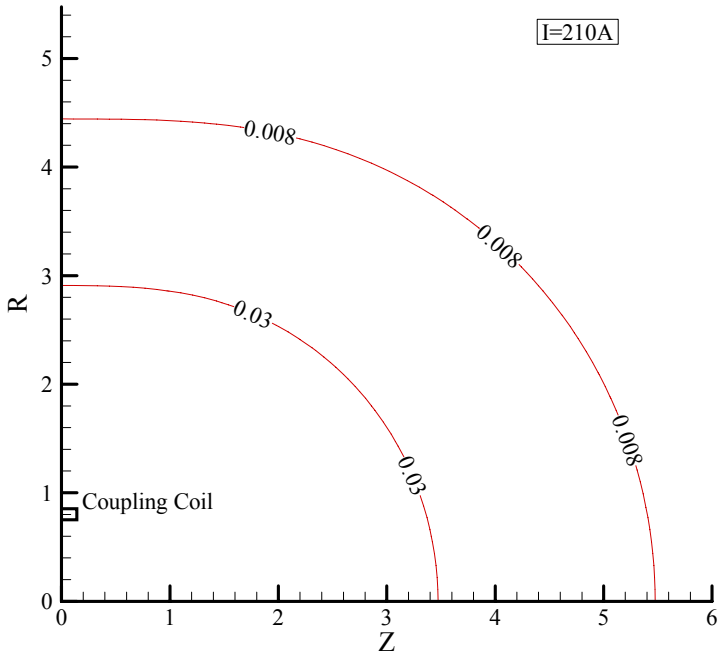

Fig. 3-1-6 Stray magnetic field around the coupling coil at 210A

3.2 Magnetic forces on coupling coil

The peak longitudinal force on the coupling magnet is calculated by ANSYS considering the effects of all the coils in the MICE cooling channel. For all the coils in the cooling channel, if their centers are aligned on the same axis, the magnetic forces on the coupling coils are always in the longitudinal direction. This peak longitudinal force determines the longitudinal design load for the cold mass supports of the coupling coil. The dominant radial force on the coupling coil is due to gravity and MICE magnets misalignment.

The parameters used in the calculations by ANSYS are shown in Table 3-1-1 and 3-1-2. The coils in three AFC modules are connected in series to form circuit F. Coupling coils C1 and C2 are individually powered. The end coils and center coil of tracker spectrometer magnet are connected in series and in series with the same coils at the other end of the channel forming circuit S. Each match coil in the tracker solenoid is connected in series with the corresponding match coil in the tracker module at the opposite end of the MICE channel forming circuits M1 and M2.

Since there are no iron shields to shield the flux lines of the coils, the eighteen MICE coils are coupled together magnetically. The inductive coupling between coils causes the forces between various modules in MICE. The magnetic force on a magnet coil is proportional to the magnetic induction on the coil from the currents in the other coils and the total current in the coil.

When all the coils in MICE channel work well (no quench happens), the magnetic forces on the coupling coils are listed in Table 3-2-1. RFCC1 is the left coupling coil ($z<0$) in MICE channel, and RFCC2 is the right coupling coil ($z>0$). In normal operation, the longitudinal forces are higher in the flip mode case at p = 240MeV/c and β= 420 mm, because the currents in most of the coils are higher.

The cold support forces of coupling magnets for various quench are shown in Table 3-2-2. The calculation assumes that one coil or one group of coils can quench without inducing any other coils in MICE channel to go normal. Once one AFC magnet quenches, it will bring about quench of three AFC magnets because they are connected in series. A coil in one tracker magnet quench will quench all coils in the tracker magnet because they have the same Al bobbin, and furthermore both tracker magnets will quench for they are in series. The peak force on a coupling magnet during a quench is 338.1 kN, away form the channel center, which occurs when both tracker magnets quench at 240MeV/c and β =420mm in flip mode.

Table 3-2-3 shows the coupling coil cold support forces when the current leads of hooking coils reversal. The longitudinal forces due to lead reversal on most coils' circuits are lower than that due to quench of both tracker magnets, except when the leads are reversed on one coupling coil. And the peak value is 416.4 kN, towards the channel center.

Table 3-2-1 Longitudinal force (kN) on coupling magnet

Case		RFCC1	RFCC2
Flip	200Mev/C	170.7	170.7
	240Mev/C	253.2	253.2
Non-Flip	200Mev/C	-160.4	-160.4
	240Mev/C	-237.3	-237.3

Note: A negative force is toward the channel center, and a positive force is away from the channel center.

Table 3-2-2 Longitudinal Forces (kN) on coupling magnet for various quench modes at 240MeV/C

Case		All Focus magnets normal	Both detector magnets normal	RFCC1 normal	RFCC2 normal
Non-flip	RFCC1	-228.3	-307.1	0	60.6
	RFCC2	-228.2	-307.1	60.6	0
Flip	RFCC1	249.7	338.1	0	-81.6
	RFCC2	249.8	338.1	-81.6	0

Note: A negative force is toward the channel center, and a positive force is away from the channel center.

Table 3-2-3 Longitudinal Forces (kN) on coupling magnet for lead reversal modes in flip mode at 240Mev/C

Module	RFCC1	RFCC2
AFC Reversed	246.3	246.3
Coil C1 Reversed	-253.5	-416.4
Coil C1 and Coil C1 Reversed	416.1	416.2
Coil M1 Reversed	331.2	331.2
Coil M2 Reversed	281.4	281.5
Spectrometer Reversed	316.0	316.0

Note: A negative force is toward the channel center, and a positive force is away from the channel center.

From Table 3-2-1, 3-2-2, and 3-2-3, one can see that the peak longitudinal force happens when one coupling coil's leads reversal, and the peak value is **416.4 kN**, towards the channel center. Therefore, the design longitudinal load for the cold mass supports is set as **500 kN** considering the contingence.

3.3 Finite element analyses on stress and deflection in coupling coil assembly

The stresses in the MICE coupling coil during the processes of winding, cool down and charging should be studied in order to predict the proper value of pre-tension force for winding the coil, and to check the stress and strain condition in the coil assembly and verify the structural design for the coil mandrel. The stress and strain in MICE coupling coil assembly is analyzed using FEA method. The coil, ground insulations, mandrel, banding and cover plate, are combined together in the FEA model.

3.3.1 Material Properties

The material proposed for the coil mandrel and cover plate is 6061-T6 aluminum alloy. The coupling coil consists of epoxy resin, fiber glass cloth and conductors fabricated from the NbTi superconductor embedded in a copper matrix (NbTi:Cu=1:4), which is considered as the composite material. Herein we assume the coil is elastic and orthotropic. The material of banding is 5356 Al wire. The material of ground electrical insulation is G-10. The properties used for simulation are shown in the following tables.

Table 3-3-1 Mechanical properties of 6061-T6 Aluminum

Temperature (K)	Young's Modulus（GPa）	Shear Modulus(GPa)	Poisson's Ratio
295	70.1	26.4	0.338
77	77.2	29.1	0.328
4	77.7	29.2	0.327

Table 3-3-2 Material properties for coupling coil

Material	Young's Modulus(GPa)
Electrical insulation E2	20
Conductor E1	120
Coil radial direction ER	50
Coil longitudinal direction EZ	70
Coil winding direction Eθ	90

Notes: The Poisson ratio of coupling coil PrθZ=0.3. For PrθR, PrZR, we assume they are also 0.3. And we get the shear modulus of coupling coil GθZ, GθR, GZR using G=E/2*(1+Pr)

Table 3-3-3 Mechanical properties of G-10

Temperature(K)	Young's Modulus（GPa）	Shear Modulus(GPa)	Poisson's Ratio
4	22	-	0.2

Note: Assumed G-10 is isotropic material.

Table 3-3-4 Mechanical properties of banding

Material	Temperature (K)	Young's Modulus（GPa）	Shear Modulus(GPa)	Poisson's Ratio
5356 Al	295	70	26.4	0.32
304 S.S	295	200	77.3	0.29
	77	200	83.8	0.278

	4	214	82	0.279
Brass H65	285	97	36.2	0.34

Table 3-3-5 Mean integral thermal expansion coefficient used in the FEA

Material	Mean integral thermal expansion coefficient from 300K to 4K (K^{-1})
6061-T6	$1.4189*10^{-5}$
Coupling coil	$1.1486*10^{-5}$
5356 Al	$1.4189*10^{-5}$
304S.S	$1.05*10^{-5}$
Brass H65	$1.38*10^{-5}$

Note: The mean integral thermal expansion coefficient of G-10 is orthotropic, αn: normal direction, 2.57*10-5, αw: wrap direction, 0.84*10-5, αf: fill direction, 0.97*10-5

Table 3-3-6 Allowable stress of materials

Material	Temperature (K)	Tensile Strength (MPa)	The allowable stress (MPa)
6061-T6	295	309	100
	77	405	135
	4	485	161
304S.S	295	660	220
	77	1460	486
	4	1590	530
5356 Al	4	309	100
Coupling coil	4	500	167
Brass H65	4	390	130

3.3.2 Operating conditions and Assumptions

3.3.2.1 Assumptions

- To neglect the effect from the other coils in MICE cooling channel
- To neglect the effect of 500 kN axial magnetic force;
- To assume the coil and its mandrel at uniform temperature T=4.2K;
- To assume the current centre in the Z direction expected to locate at original position;
- To neglect the effect from cold mass supports;
- To assume the uniform current in the coupling coil;
- To assume the across area of cooling tube is square;
- To neglect the effect of the cooling tube number;
- To neglect the effect of the pressure in cooling tube.

3.3.2.2 Operating conditions

- The coil and its mandrel is cooled down from 300K to 4.2K;
- The coil is energized at J=110.8A/mm^2, i.e. at the worst case, p=240MeV/c, β=42cm and full-flip mode; (magnetic stress induced by coupling coil itself)

3.3.3 FE model

The inner diameter of coil winding is 1500 mm, the G-10 insulation between the coil and its bobbin is 1 mm thick. The SC conductors are wound layer by layer onto the 6061-T6 Al mandrel under certain appropriate constant pre-tension, and the outmost layer insulated by G-10 is the Al or brass banding wound under certain pre-tension. The 6061-T6 Al cover plate is mounted onto the mandrel finally.

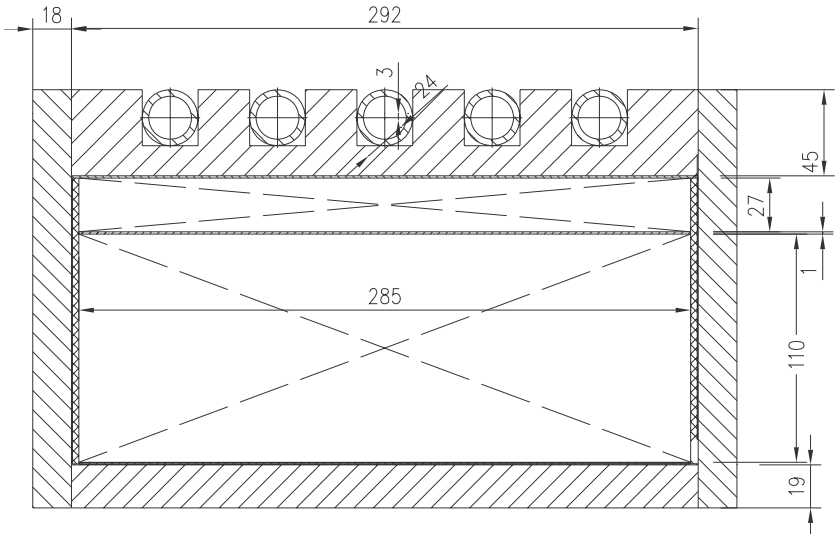

Fig. 3-3-1 The coupling coil assembly

A 2-D axisymmetric model is used. The model includes the coil, mandrel, banding, G-10 insulations and cover plate with or without slip planes. The coupling coil has 96 layers. In order to simulate the pre-stress in the coupling coil exactly, we sub-divide the coil into 96 layers and than banding into 6 layers in the radial direction. For the model without slip planes, all of theses parts are glued together in the simulation. For the model with slip planes, the contact elements were used.

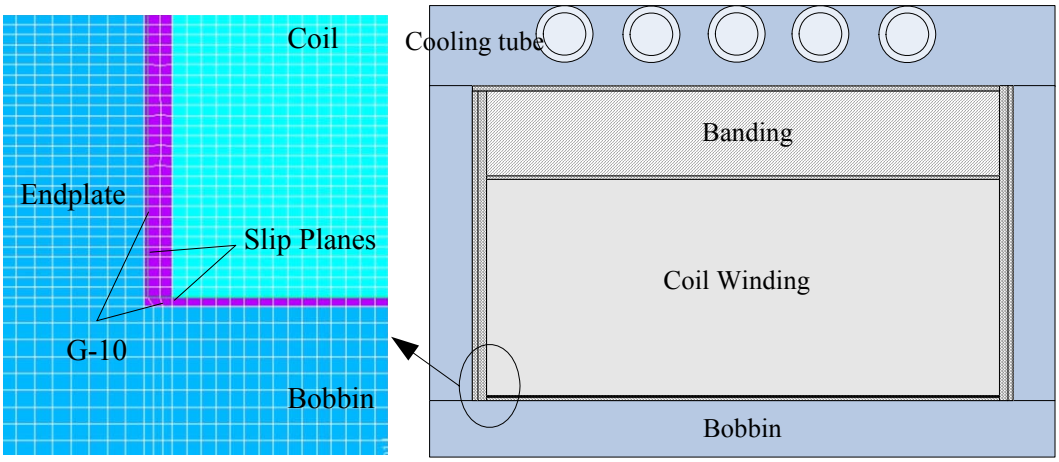

Fig. 3-3-2 FEA Model of coupling coil assembly

During normal operation, the magnet is first cooled down from 300K to 4.2K, and then charged

to a full current of 210A at the worst case. The simulation involves all the processes of the coil winding, the banding winding, cooling down and charging the coil to a full current.

3.3.4 Simulation and analyses

3.3.4.1 Results with slip planes

The FE simulation was done by ANSYS with the optimized dimensions as shown in Fig 3-3-1, and the pre-tension applied to the conductor during winding is 60 MPa, the pre-tension to the banding is 60 MPa as well.

Because of the interaction of magnets in MICE channel, the coupling coil will suffer a magnetic force up to 500 kN from the other coils. If there is slip planes between the coil winding and the mandrel, the epoxy between banding and cover plate will be stressed. It will suffer shear stress and moment, but the peak shear stress is about 0.2 MPa and the peak tensile stress due to moment is 12MPa, both of which are in the range of allowable stress of epoxy. Because of the little influence, we ignored the axial force effect in the simulation.

1) Radial Stress (Pa)

From Fig.3-3-3, the radial stress in inner coil winding is negative, which means this region is compressed either during cooling down or charging. The radial stress in the inner side bobbin is also negative either during cooling down or charging, which means the bobbin is hold by coil winding, and there is no gap between the coil and the bobbin.

2) Hoop Stress (Pa)

The peak hoop stress in the coil is 96.6 MPa after charging, which happened in the outer corner of the coil and close to the banding and the side G-10 sheet. The hoop stress in bobbin is always negative, which means bobbin is compressed by the coil during winding, cooling and charging.

3) Axial Stress (Pa)

The two sides of the coil are under compressive axial pressure, but the value is near zero, which means there is no gap generated between the coil and the end plate, but the contact is not tight.

4) Shear Stress (Pa)

The peak shear stress in the coil is about 25.2 MPa only due to cool down, which happened in the g-10 around the coil bottom corners.

5) Von Mises stress with slip planes (Pa)

The peak stress in the mandrel is about 140 MPa after winding the banding, which appears in the middle of the bobbin. The peak stress in the coil is about 78 MPa after winding the banding, which appears in the middle of inner layer. The peak stress on stress concentration point is about 301 MPa in the coil assembly only due to cool down, which appears in the bottom corner of G-10. The stress in the middle of bobbin is 142 MPa after cool down and 87.1 MPa after charging. The stress in the banding is about 151 MPa less than the allowable stress of 5356 aluminum. The peak stress in the coil is about 114 MPa during cool down, which appears in the middle of inner layer. The peak stress is 117 MPa due to magnetic force, which appears in the middle of outer layer. The

stress concentration may be due to sharp angle effect, and the peak value is always on one node. The results of stress linearization along two stress classification lines show that the actual stress in this point is not so high which is less than 180MPa.

6) Radial and axial deflections (m)

The maximum inward radial deflection of the coil is about 4.2 mm during cool down. The maximum inward radial deflection is 3.599 mm during charging. The average inward radial deflection of the coil during cooling down is 3.922 mm, and the deflection rate is 0.487%. The average inward radial deflection of coil during charging is 3.311 mm, and the deflection rate is 0.411%. The maximum inward axial deflection of the coil assembly is about 0.9 mm during cool down, which-happened in the cover plate. The maximum inward axial deflection is 0.95 mm during charging, which-also-happened in the cover plate.

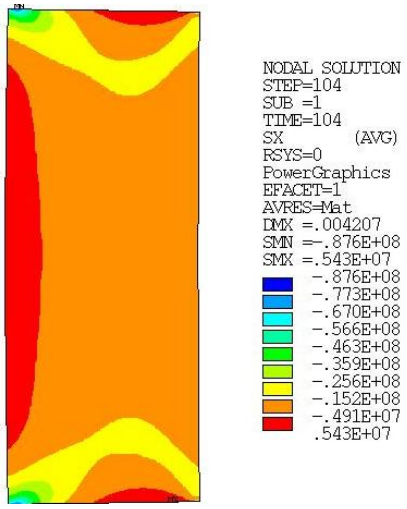

Fig.3-3-3a Radial stress in coil after cooling

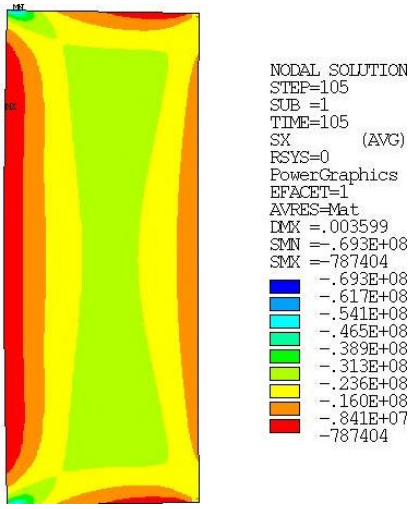

Fig.3-3-3b Radial stress in coil after charging

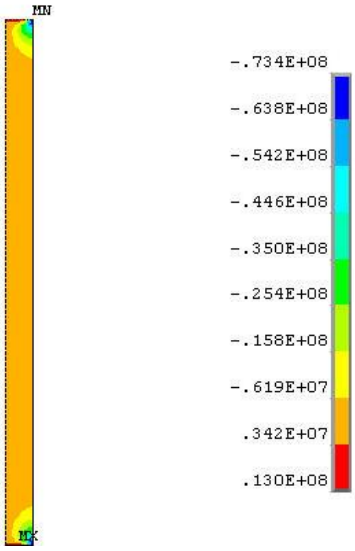

Fig.3-3-3c Radial stress in bobbin after cooling

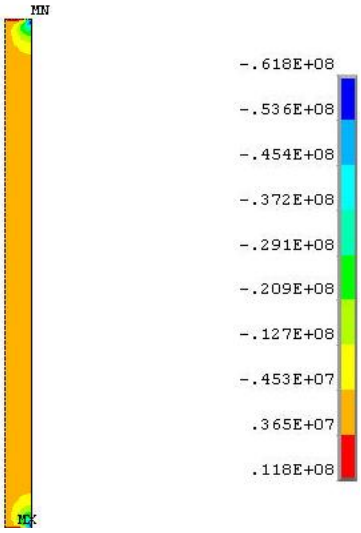

Fig. 3-3-3d Radial stress in bobbin after charging

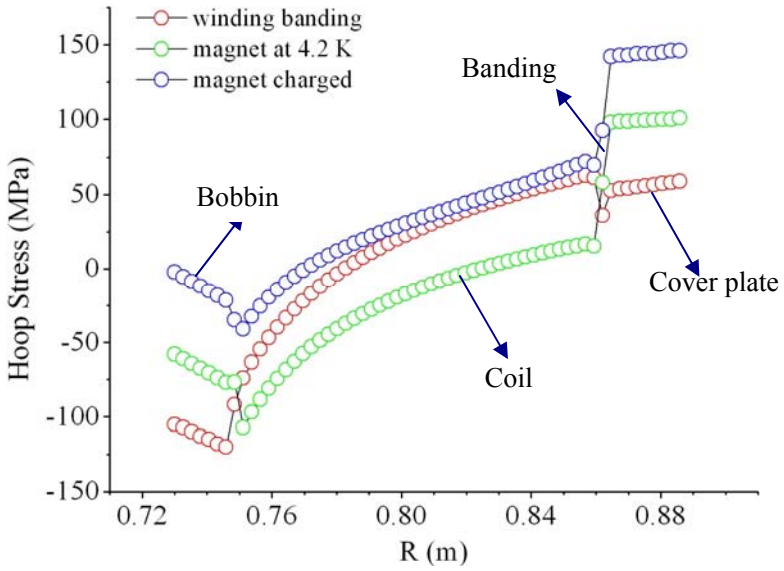

Fig.3-3-4a Hoop stress in coil assembly

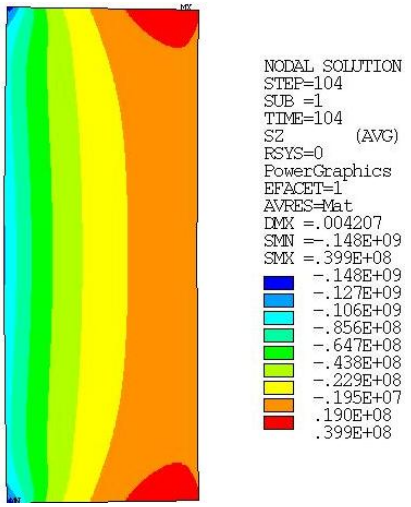

Fig.3-3-4b Hoop stress in coil after cooling

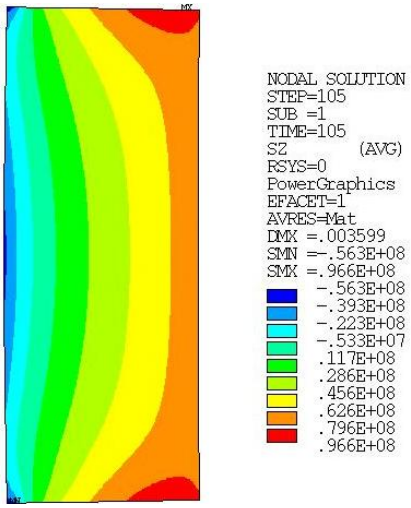

Fig.3-3-4c Hoop stress in coil after charging

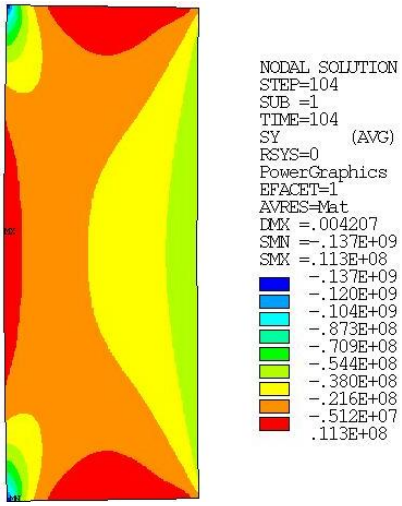

Fig.3-3-5a Axial stress in coil after cooling

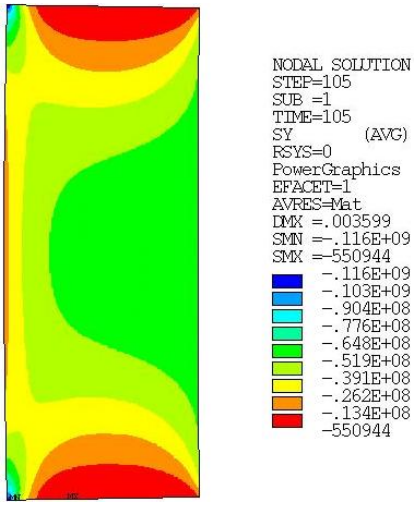

Fig.3-3-5b Axial stress in coil after charging

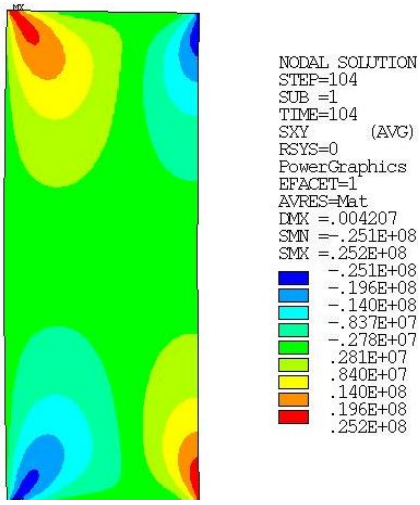

Fig.3-3-6a Shear Stress in coil after cooling

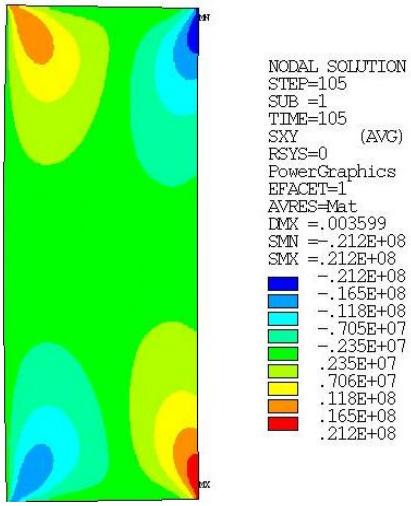

Fig.3-3-6b Shear Stress in coil after charging

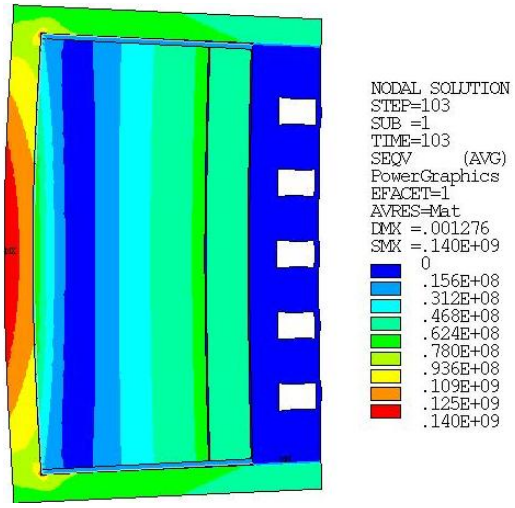

Fig.3-3-7a Von Mises Stress in coil assembly after winding

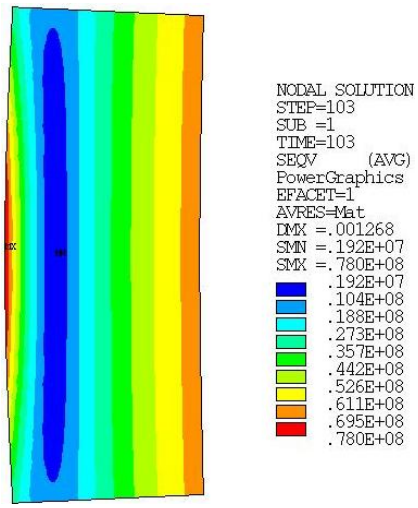

Fig.3-3-7b Von Mises Stress in coil after winding

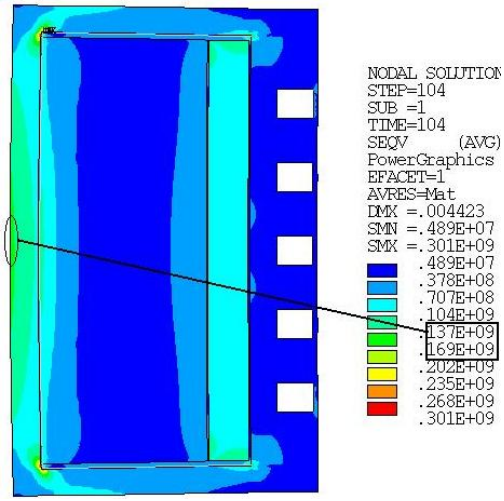

Fig.3-3-7c Von Mises Stress in coil assembly after cooling

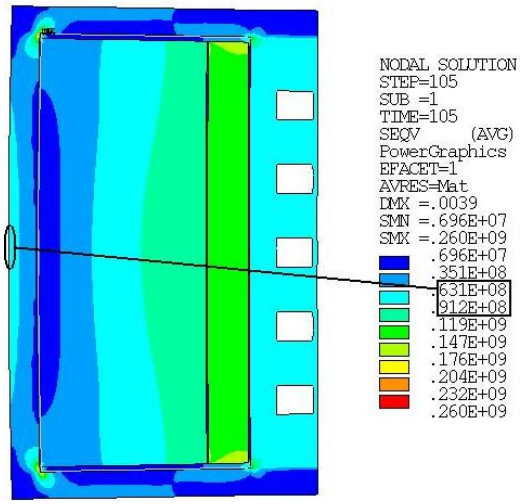

Fig.3-3-7d Von Mises Stress in coil assembly after charging

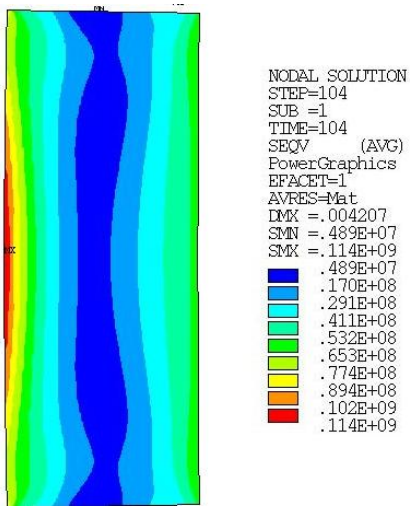

Fig.3-3-7e Von Mises Stress in coil after cooling

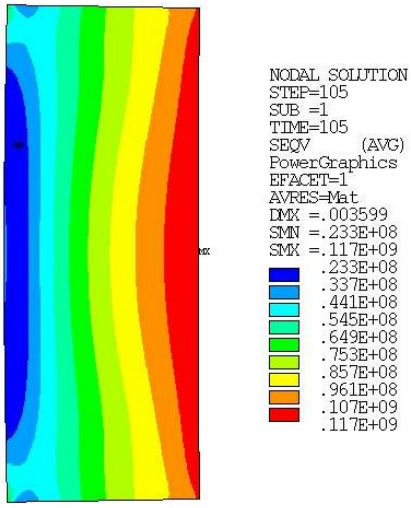

Fig.3-3-7f Von Mises Stress in coil after charging

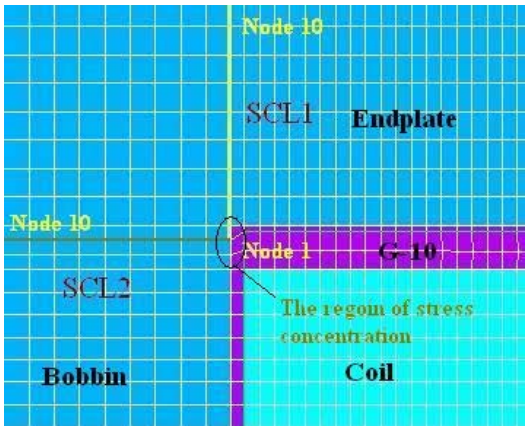

Fig.3-3-8a Stress classification lines

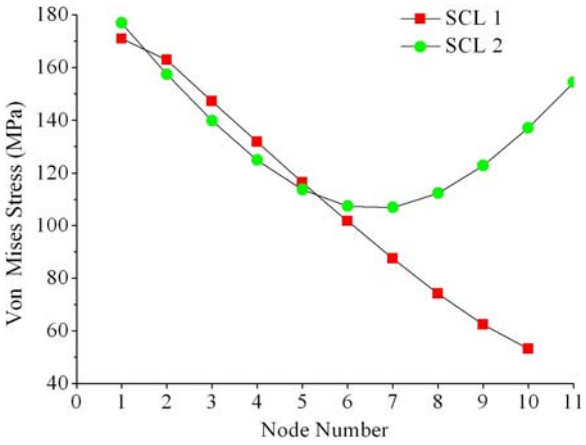

Fig.3-3-8b Linearized stress with the nodes

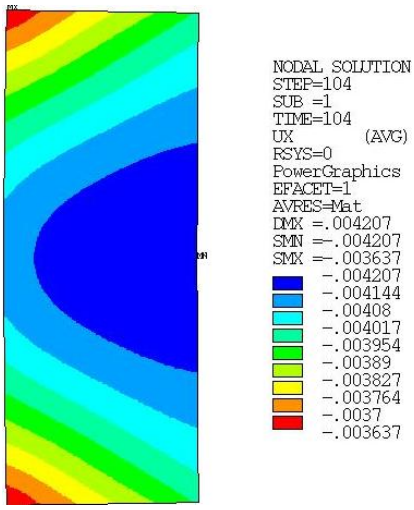

Fig.3-3-9a Radial deflection in coil after cooling

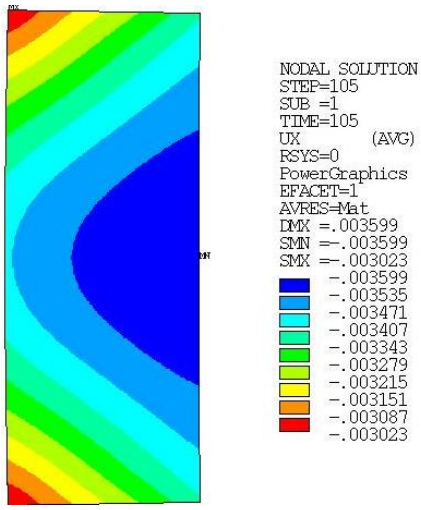

Fig.3-3-9b Radial deflection in coil after charging

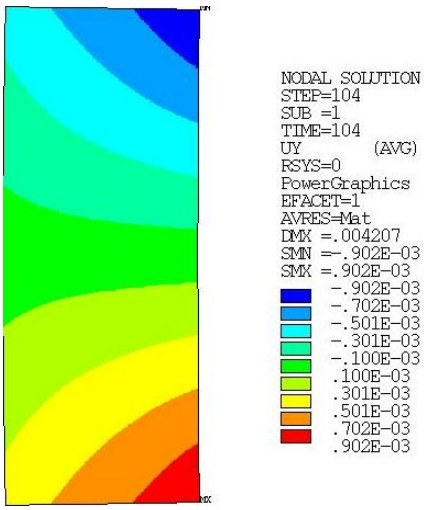

Fig.3-3-9c Axial deflection in coil after cooling

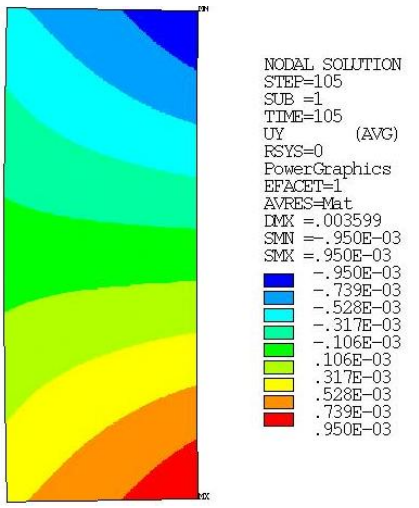

Fig.3-3-9d Axial deflection in coil after charging

3.3.4.2 Results without slip planes

From Fig 3-3-10 to 3-3-, the radial stress in the inner coil is negative, which means this region is compressed either during cooling down or charging. The peak tensile hoop stress in the coil is 92

MPa due to magnetic force, which is in the outer layers. The peak shear stress in coil winding is about 57.3 MPa only due to cool down, which happened in the g-10 around the bottom corners.

The peak von Mises stress in the mandrel is about 137 MPa after winding the banding, which appears in the middle of the bobbin. The peak von Mises stress in the coil is about 71.8 MPa after winding the banding, which appears in the middle of the inner layer and the outer layer. The peak von Mises stress is about 164 MPa in the coil assembly only due to cool down, which appears in the middle of the bobbin. The peak von Mises stress in the coil is about 110 MPa during charging, which appears in the middle of outer layer. The stress in the banding is about 151 MPa less than the allowable stress of 5356 aluminum.

The maximum inward radial deflection of the coil is about 4.173mm during cool down. The maximum inward radial deflection is 3.569mm during charging. The average inward radial deflection of the coil during cooling down is 3.909 mm, and the deflection rate is 0.485%. The average inward radial deflection of the coil during charging is 3.299 mm, and the deflection rate is 0.409%. The maximum inward axial deflection of the coil assembly is about 0.9 mm during cool down, which-happened in the cover plate. The maximum inward axial deflection is 0.95 mm during charging, which-also-happened in the cover plate.

3.3.5 Conclusion

By comparison of the stress simulation results with and without slip planes, slip planes may decrease the stress in the coil assembly, in particular, decrease the shear stress obviously, but it introduces the stress concentration in inner corners of the mandrel. If there are no slip planes, the shear stress in the coil is relatively high up to 58 MPa, which is more than the allowable shear strength of 30 MPa (based on Dr.Mike Green's suggestion). But because the coil assembly is glued together, the stress situation in the corner is better than the one with slip planes.

For the MICE coupling coil winding, according to practical experience from the professionals, in order to avoid more often quench due to high shear stress inside the coil, the slip planes will be applied.

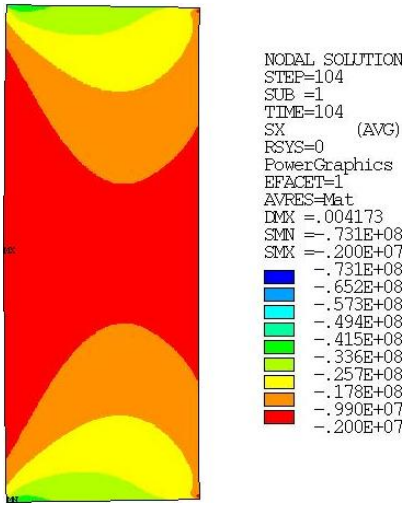

Fig. 3-3-10a Radial stress in coil after cooling

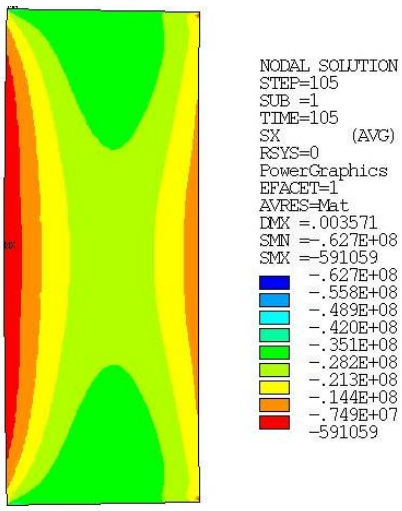

Fig. 3-3-10b Radial Stress in coil after charging

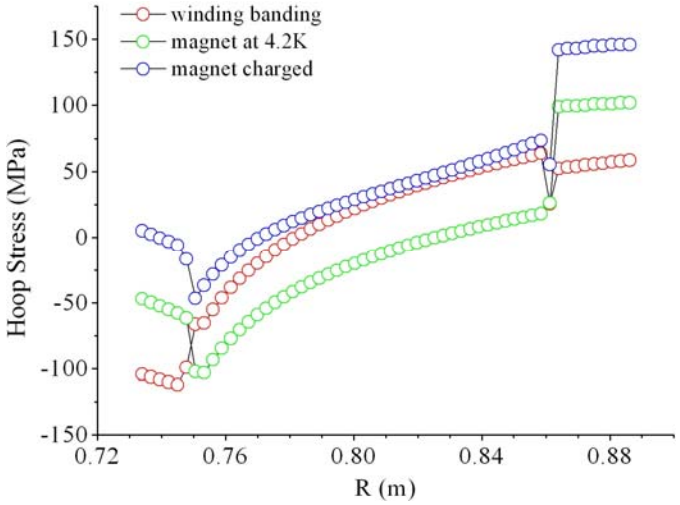

Fig. 3-3-11a Hoop stress in coil assembly

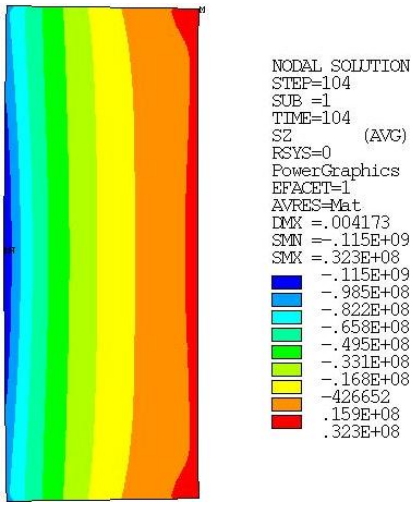

Fig. 3-3-11b Hoop stress in coil after cooling

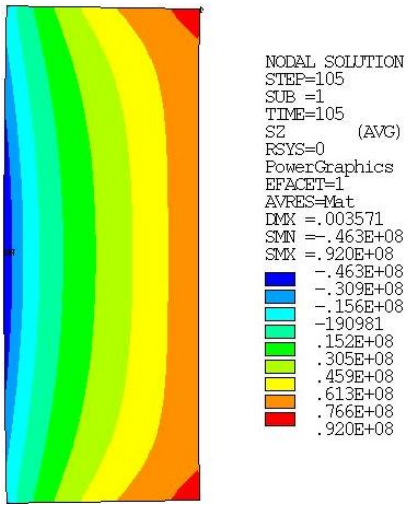

Fig. 3-1-11c Hoop stress in coil after charging

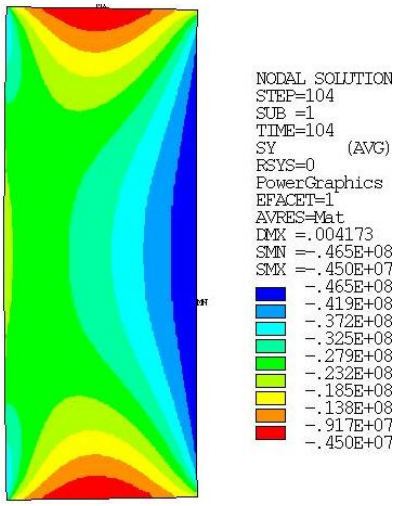

Fig. 3-11-12a Axial Stress in coil after cooling

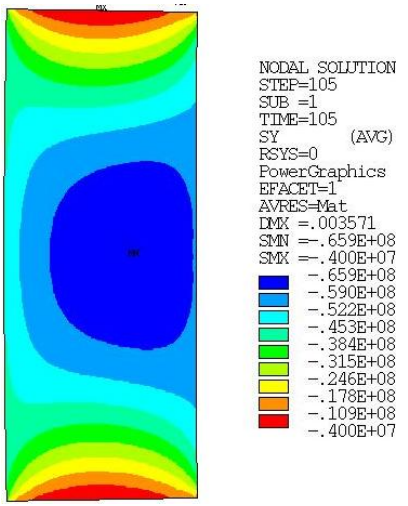

Fig. 3-11-12b Axial Stress in coil after charging

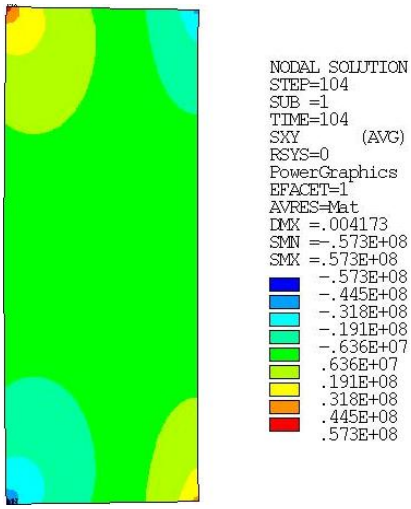

Fig. 3-11-13a Shear stress in coil after cooling

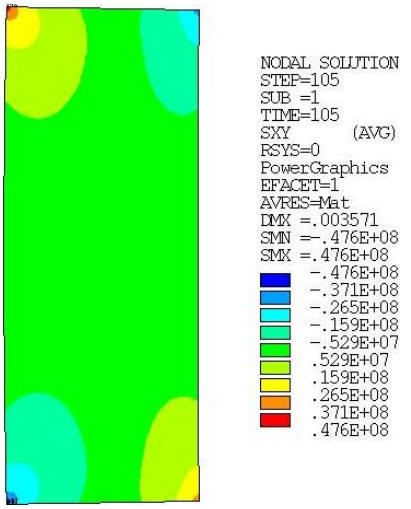

Fig. 3-11-13b Shear stress in coil after charging

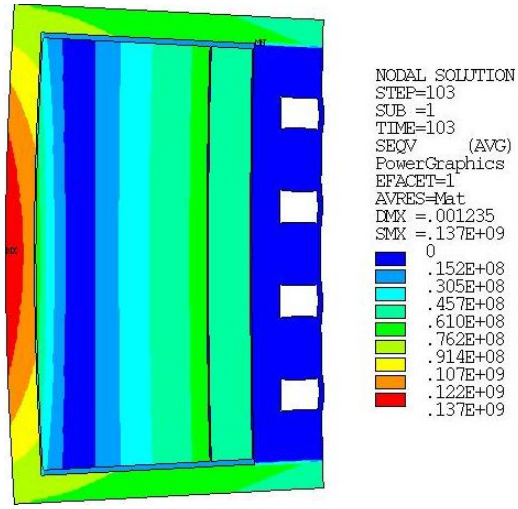

Fig. 3-3-14a Von Mises Stress in cold mass assembly after winding

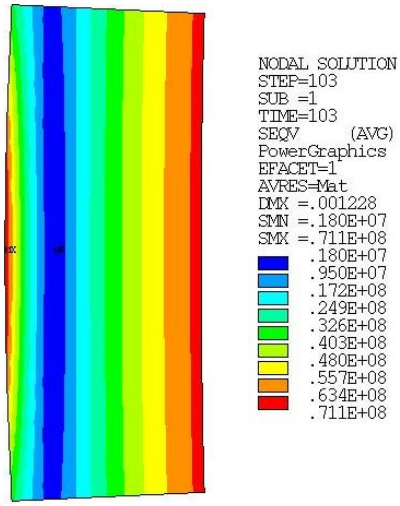

Fig. 3-3-14b Von Mises Stress in coil after winding

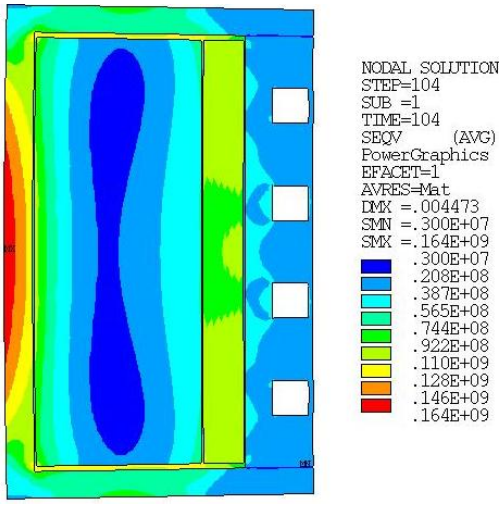

Fig. 3-3-14c Von Mises Stress in coil assembly after cooling

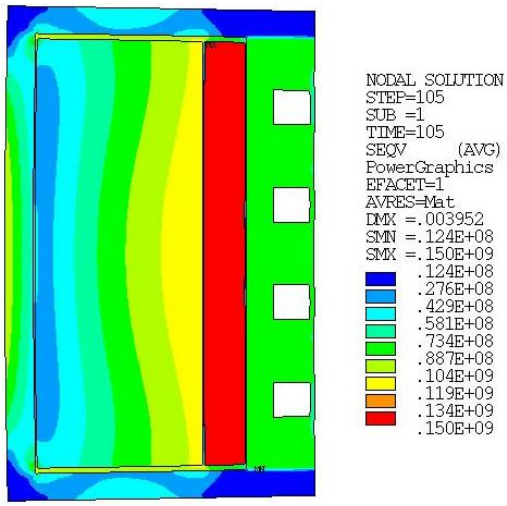

Fig. 3-3-14d Von Mises Stress in coil assembly after charging

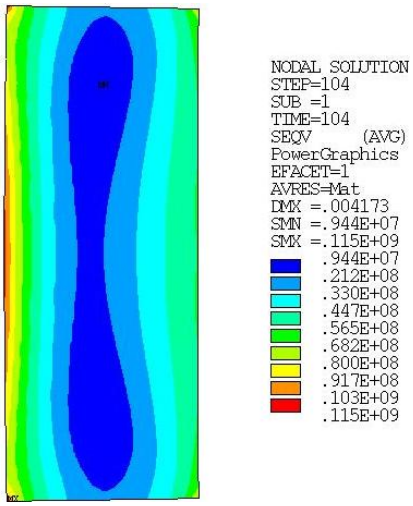

Fig. 3-3-14e Von Mises Stress in coil after cooling

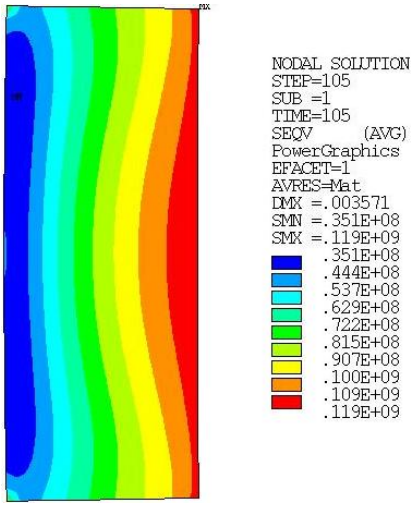

Fig. 3-3-14f Von Mises Stress in coil after charging

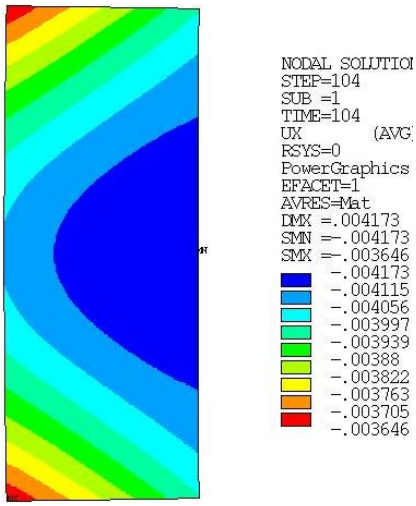

Fig. 3-3-15a Radial deflection in coil after cooling

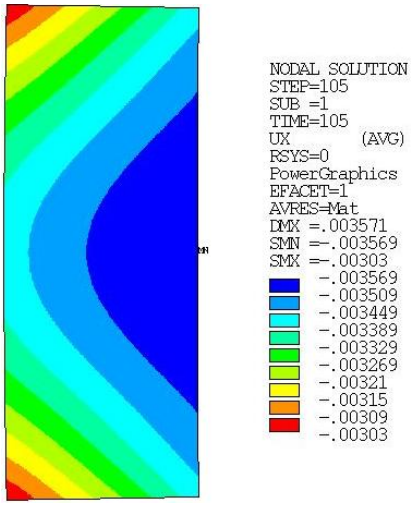

Fig.3-3-15b Radial deflection in coil after charging

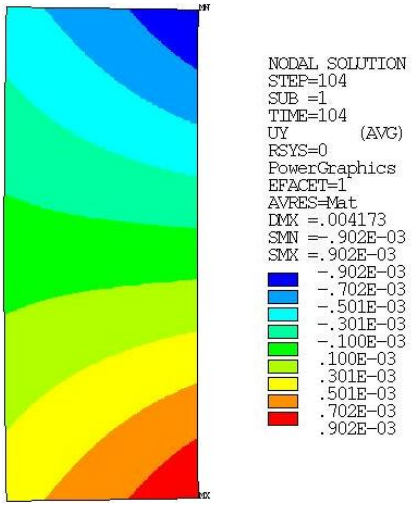

Fig. 3-3-15c Axial deflection in coil after cooling

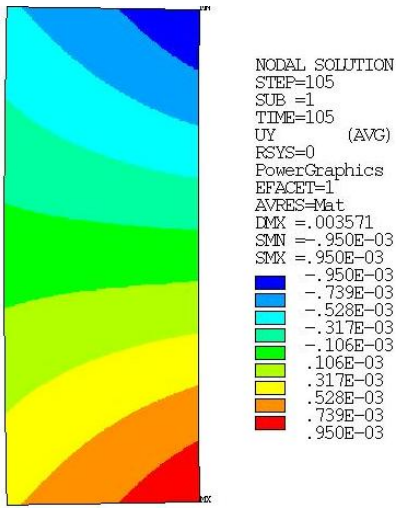

Fig. 3-3-15d Axial deflection in coil after charging

3.4 Quench process and passive quench protection

The design principle of passive quench protection has been specified by LBNL. Because of larger self-inductance and more stored energy, the technology of subdivision protection and quench back is adopted in order to reduce the internal voltage and the hot-spot temperature. The coil is designed to be divided into 8 sections by a pair of back-to-back R620 cold diodes and a pair of resistors across each subdivision as shown in Fig.3-4-1. A unipolar 330A/0-20V power supply will be used to charge and discharge the magnet by using a single pair of binary current leads composed of a copper lead and a HTS lead. A rapid discharge system consisting of pairs of diodes in each direction mounted on a cooling plate will be applied to the coupling coil. Resistors of 200 ohms connected with voltage taps are used to avoid accidentally destroying instruments. The coil mandrel and the coil banding act as the shorted secondary circuit coupled with each coil subdivision.

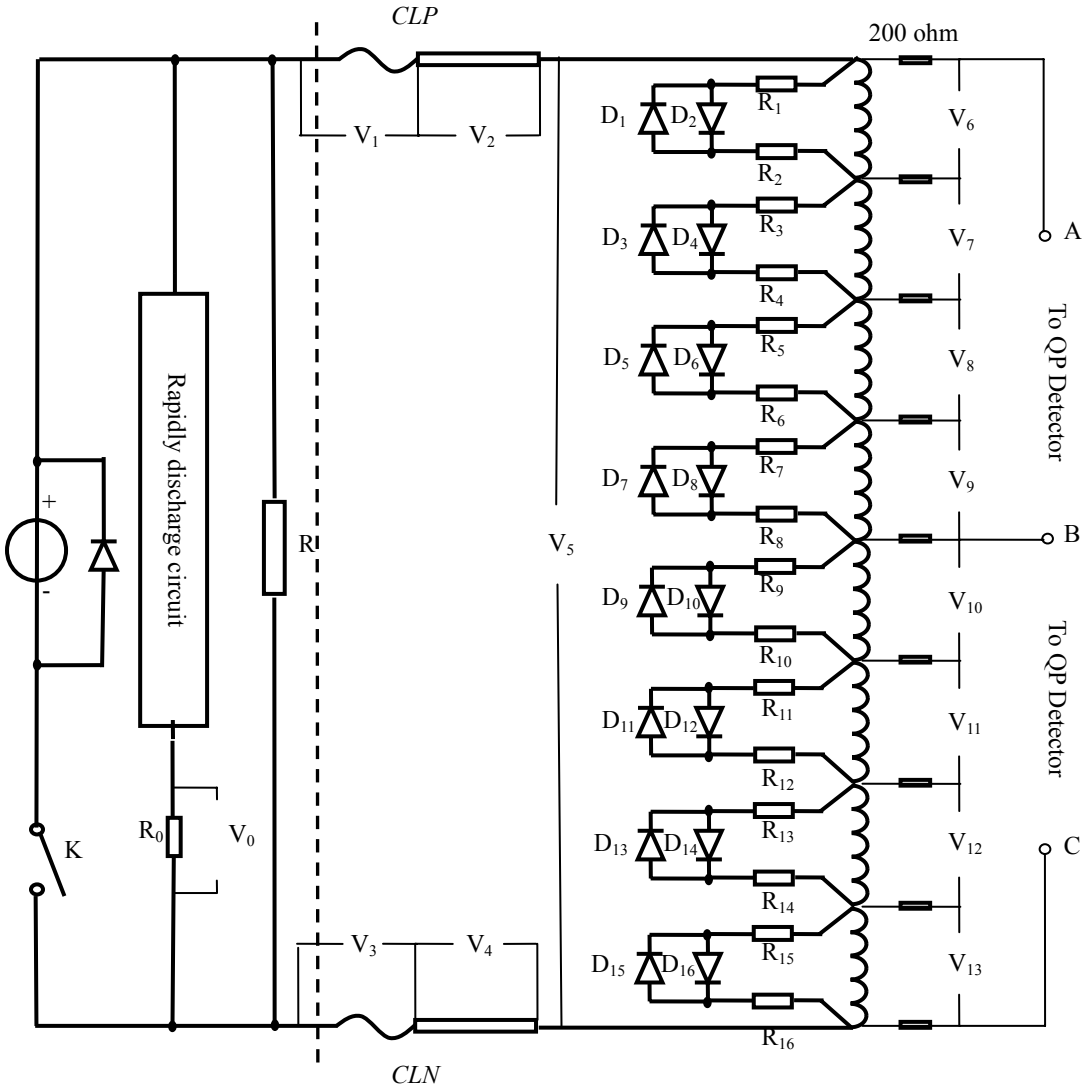

Fig.3-4-1 Quench protection circuit and power supply for coupling magnet

Magnet subdivision is a passive quench protection method normally used in MRI magnets. Subdivision reduces both the voltage to ground and the hot spot temperature. Back-to-back cold diodes allow the magnet to be safely quenched at either magnet polarity. In the other hand, the high forward voltage (the forward voltage of each cold diode is about 3~4V at liquid helium temperature) across the diodes prevents the current form bypassing the magnet coil during a magnet charge or discharge at its design charging and discharging voltage.

The coil mandrel and the banding are inductively coupled to all of the coil subdivisions. They will act as a shorted secondary circuit and absorb energy form the magnet during quench. During the quench process, the mandrel and the banding will be heated by the induced current, which will eventually heat up the adjacent coil subdivisions and induce new normal zone. This process is called quench back. Quench back will speed up the quench process, and thus reduce the hot spot temperature.

3.4.1 Simulation and analyses on quench process

The cross sectional structure and parameters of the coupling coil used for quench process simulation and analyses are shown in Fig. 3-4-2 and Table 3-4-1.

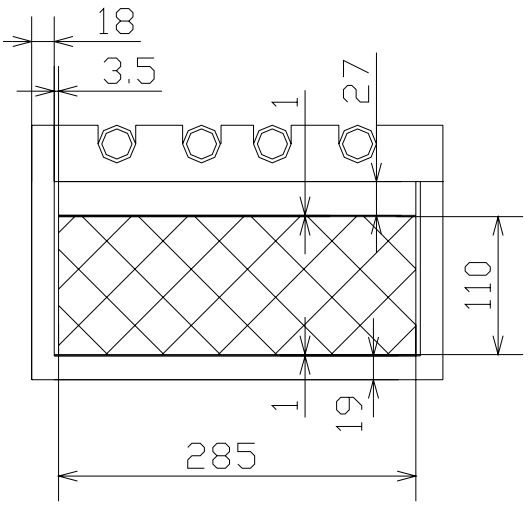

Fig 3-4-2 Cross section of coil assembly

Parameters	Coupling Coil
Coil Length (mm)	285
Coil Inner Radius (mm)	750
Coil Thickness (mm)	110
Number of Layers	96
No. Turns per Layer	166
Magnet Current (A)	210
Self Inductance (H)	591.8
Stored Energy (MJ)	13.0

Table 3-4-1 Parameters of coupling coil

3.4.1.1 Simulation method

A semi-empirical quench model considering both the subdivision and quench back has been developed. Fig.3-4-3 shows the quench propagating model. A quench is initiated in the mid-plane and starts to expand in three directions with velocities v_ϕ (longitudinal propagation along the wound conductor), v_r (radial propagation) and v_z (axial propagation). The normal zone shape is assumed to be an ellipsoid. In the model, the average constant quench propagation velocities in three directions are used during quench process. The calculation proceeds at time step of Δt. At each step another layer is added to the surface of the normal zone like the skin of an onion. After the quench back from the mandrel happens, new normal zone will be induced near the mandrel, and the normal zone

will propagate as shown in Fig.3-4-3b. After a time step, the current will decay. The calculation ends until the current of each coil subdivision is less than the 1 percent of the initiating current. In this simulation, the helium cooling is ignored.

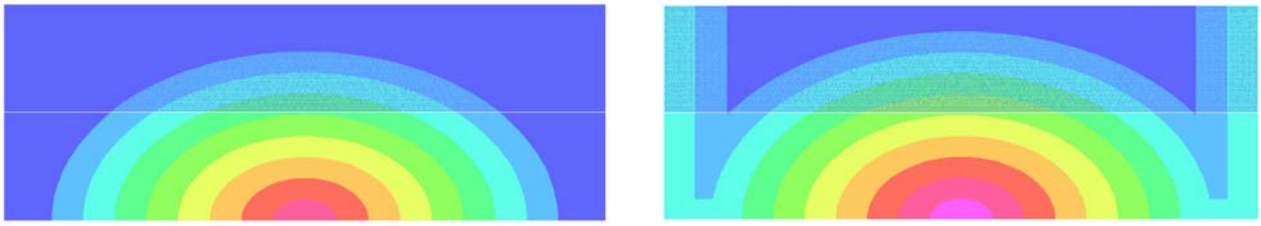

a) Normal zone before quench back happens b) Normal zone after quench back happens

Fig 3-4-3 Cross section of the normal zone growth

For the thermal characteristic, assuming local adiabatic, at each time step, the temperature of successive quenching volume T is determined by the joule heating in the volume, and T can be decided by the following equation (1),

$$(C \cdot \gamma)_{av} \frac{dT}{dt} = J^2 \rho_{av} \tag{1}$$

where $(\gamma C)_{av}$ is the coil average volumetric specific heat, t is time, J is the average current density, ρ_{av} is the coil average resistivity. The hot spot temperature in each subdivision is the temperature of the start point in the subdivision. During the quench process, we assume the switch opens once the quench happen and rapid discharge diodes do not turn on. Since the cold diode resistance changes greatly with its temperature and the current through it, the cold diode effect on the quench process is assumed to be equivalent to the effect of a 10mΩ resistor (the average current through the diode during quench is about 100A and the forward voltage is around 1V.). The current I_j (j=1…8) in each coil section, I_9 in the mandrel and I_{10} in the banding can be calculated by the following equation (2).

$$[L]\frac{dI_j}{dt} + [R_{Qj} + R_j + R_d]I_j = 0 \qquad (j = 1...10) \tag{2}$$

where L is the inductance matrix of the coil sections, the mandrel and the banding, R_j is the protection resistor at each section, R_d is the 10mΩ equivalent resistance of the cold diode, R_{Qj} is the normal zone resistance at each section, R_{Q9} and R_{Q10} is the resistance of the mandrel and the banding respectively, R_9=0Ω, R_{10}=0Ω. The voltages to ground (internal voltages) U_{Qj} are estimated by the voltage drop through the normal zone resistance at each coil section as shown in the following equation (3).

$$U_{Qj} = I \cdot R_{Qj} \tag{3}$$

For the quench back modeling, the key parameter is the time when new normal zone induced by the heat from the mandrel and the banding appears. This time is the sum of two time periods. The first time period is the time when the mandrel or the banding is heated up to around 10 K. It is associated with the shift current from the superconducting coil to the mandrel or the banding. The second time period is the time when heat flows from the mandrel or the banding to the

superconductor. It is a function of the thickness of the insulation between the coil and mandrel or the banding. Usually it has a value of 0.03-0.04s when the insulation thickness between the superconductor and the mandrel is 0.5mm. When the insulation thickness increases by 1.0mm, it increases by 0.08-0.10s. After quench back happens, the normal zone is the integration of both the normal zone induced by the quench propagation and the normal zone induce by the quench back.

Table 3-4-2 shows the average propagation velocities used in the simulation. The velocities are based on a quench propagation measurement experiment correlation in LBNL in the 1970's. According to this correlation, the propagation velocity is dependent only on the current density in the conductor cross-subdivision and the magnetic induction the conductor sees.

Table 3-4-2 Average propagation velocities

Parameters	**Coupling Coil**
Curret (A)	210
Bave (T)	2.5
v_ϕ (m/s)	3.477
v_r (m/s)	0.057
v_z (m/s)	0.085

Table 3-4-3 shows the coupling coil subdividing parameters. The coupling coil is divided to 8-section with 12 layers in each section.

Table 3-4-3 Coupling coil 4-section subdividing parameter

Parameter	Sec 1	Sec 2	Sec 3	Sec 4	Sec 5	Sec 6	Sec 7	Sec 8
Number of layers per sec	12	12	12	12	12	12	12	12
Number of turns per layer	166	166	166	166	166	166	166	166

3.4.1.2 Simulation results and analyses

Fig.3-4-4 shows typical simulation results with the protection resistor of 20mΩ and a 304 stainless steel banding. After about 16.1s, all currents in the coil decay to below 0.01 of the initial current, and this time is named quench time in this report. The quench time indicates the current decay velocity. The hot spot temperature is about 130 K and the maximum internal voltage is about 2611 V. The layer-to-layer voltage can be estimated by this maximum voltage and layer number, and the layer-to-layer voltage is about 435 V.

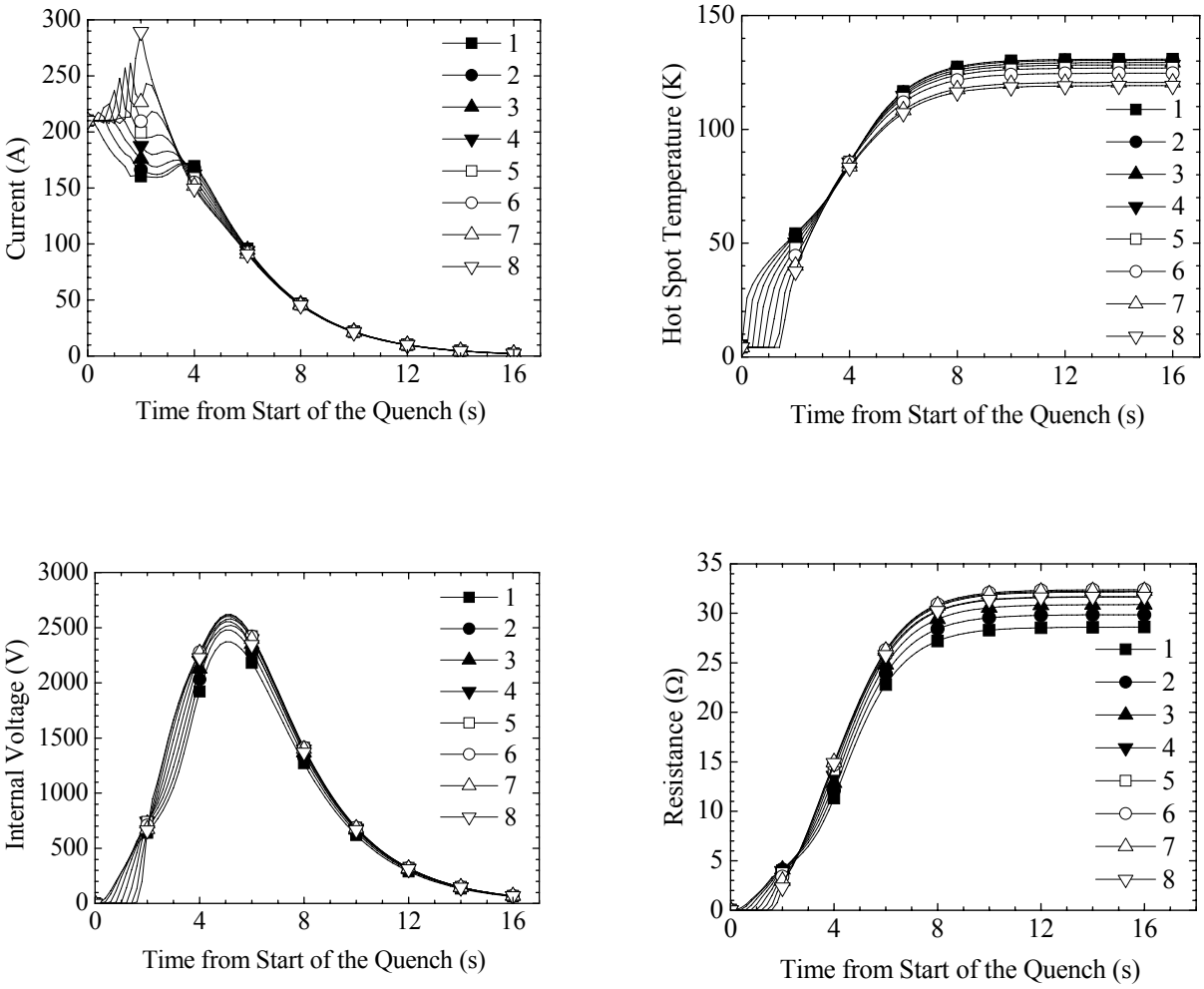

Fig 3-4-4 Coupling coil quench simulation results, R_p=20mΩ, SS304 banding, 8-section

Table 3-4-4 shows the summary of coupling coil quench simulation results with different section numbers at a 20mΩ protection resistor and a SS304 banding. It is found that the section numbers have great effect on the hot spot temperature and the voltage-to-ground. It is mainly because the temperature and the voltage in the coil will be distributed more uniform with the section number increasing. The energy dumped on resistors and diodes will increase with the section number increasing. The section number's effects on the other quench parameters are small.

Table 3-4-4 Summary of simulation results with different section numbers at R_p=20mΩ and a SS304 banding

Parameters	2-subs	4-subs	6-subs	8-subs
Quench Time (s)	16.1	16.1	16.1	16.1
Hot Spot Temperature (K)	147	136	132	130
Voltage-to-Ground (V)	10337	5226	3484	2611
Layer-to-Layer Voltage (V)	431	436	436	435
Energy on Mandrel (kJ)	631.7	630.5	630.9	630.1

Energy on Banding (kJ)	13.4	12.5	12.6	12.7
Energy on Resistor and Didoes (kJ)	12.1	24.2	36.4	48.5
Energy on Coil (kJ)	12401.7	12391.8	12379.1	12367.6

Table 3-4-5 shows the summary of coupling coil quench simulation results with different protection resistance. The coil hot spot temperature will decrease as the protection resistance increases, because more energy is dumped on the resistor and diode. The voltage-to-ground will decrease as the protection resistance increases, because a larger resistance induces faster current decay, and the voltage drop on the normal zone resistance will decrease. The quench time increases a little with the protection resistance increases, because during the later phase of quench process, the coil normal zone resistance at 20mΩ case is larger than that at 1Ω case.

Table 3-4-5 Simulation results with different protection resistances, SS304 banding, 8-section

Parameters	0mΩ	20mΩ	1Ω
Quench Time (s)	16.1	16.1	16.5
Hot Spot Temperature (K)	131	130	124
Voltage-to-Ground (K)	2618	2611	2279
Layer-to-Layer Voltage (K)	436	435	380
Energy on Mandrel (kJ)	631.4	630.1	580.9
Energy on Banding (kJ)	12.8	12.7	11.6
Energy on Resistor and Diodes (kJ)	16.2	48.5	1481.8
Energy on Coil (kJ)	12398.569	12367.6	10984.6

Table 3-4-6 shows the summary of coupling coil quench simulation results with different banding material. Table 3-4-7 shows the resistivity of different banding materials. A lower resistivity material banding (6061-T6Al) can absorb more energy during the quench. The hot spot temperature and the voltage to ground with an Al banding are lower than that with a SS one. But the effect of different banding materials (304 stainless steel, Brass, 6061-T6 aluminum) on the quench parameters is negligible, because the energy absorbed by banding is so small. The quench time increase a little with the banding material resitivity increase, because during the later phase of quench process, the coil normal zone resistance with 304 stainless steel is larger than that with 6061-T6 Al.

Table 3-4-6 Simulation results with different banding materials, R_p=20mΩ, 8-section

Parameters	304 Stainless Steel	Brass	6061-T6 AL
Quench Time (s)	16.1	16.3	16.9
Hot Spot Temperature(K)	130	130	129
Voltage-to-Ground (K)	2611	2568	2475
Lay-to-Lay Voltage (K)	435	428	413
Energy dumped on mandrel (kJ)	630.1	620.2	598.9

Energy on banding (kJ)	12.7	136.1	402.6
Energy on Resistor and Diodes (kJ)	48.5	48.2	47.9
Energy on Coil (kJ)	12367.6	12254.4	12009.5

Table 3-4-7 Resistivity of different banding material (nΩm)

Temperature	304 Stainless Steel	Brass	6061-T6 AL
4K	490	44.8	13.8
77K	527	49.3	16.7
300K	720	72.1	42.5

Table 3-4-8 shows the summary of coupling coil quench simulation results with and without quench back. The simulation results show the quench back's effect on the quench parameters is small. It is because the coil is thicker and shorter, the protection velocities are relatively fast, so the quench back's effect of speeding up the quench process is small and negligible. According to the simulation results, the quench back happen time is 1.6s, the time when the coil becomes total normal with quench back is 2.28s, the time when the coil becomes total normal without quench back is 2.64s.

Table 3-4-8 Simulation results with and without quench back, R_p=20mΩ, 8-section, SS304 banding

Parameters	With quench back	Without quench back
Quench Time (s)	16.1	16.1
Hot Spot Temperature(K)	130	130
Voltage-to-Ground (K)	2611	2611
Lay-to-Lay Voltage (K)	435	435
Energy dumped on mandrel (kJ)	630.1	630.0
Energy on banding (kJ)	12.7	12.7
Energy on Resistor and Diodes (kJ)	48.5	48.5
Energy on Coil (kJ)	12367.6	12367.7

3.4.1.3 Conclusion

The temperature and voltage distribution in the coil will be more uniform with larger section number, the 8-sectioned coupling coil has hot spot temperate of 130K and voltage-to-ground of 2611V. The hot spot temperature and voltage-to-ground will decrease with the protection resistor increasing. Considering the resistor's heat capacity to handle the worst case quench currents safely and the space limitation, a 20mΩ resistance is adopted. The resistor in series with the diode is also required to charge the section if the diode across the coil section is broken. The mandrel's effect in absorbing energy during quench process is small, and the aluminum mandrel material is to be adopted. The quench back can speed up the coil quench process, but its effect on the quench parameters is so small and negligible.

3.4.2 Quench protection assembly design

The quench protection assembly will be mounted on the outer surface of the coil cover plate and is kept cooled lower than 4.8K by heat conduction during normal operation as shown in Fig. 3-4-5. It is divided into two groups, and each group is spread at one side of the helium tank. Each group is composed of a cold diode assembly and a resistor assembly.

As shown in Fig.3-4-1, three voltage taps marked as A, B, C are to detect quench and to transfer quench signal to the power supply. Two pairs of voltage taps are used to monitor the voltage drops along each current lead. They may also be used as quench detection signals, which are more reliable and rapid than temperature signals. The voltage signal marked as V5 is used to monitor various operational situations of the magnet.

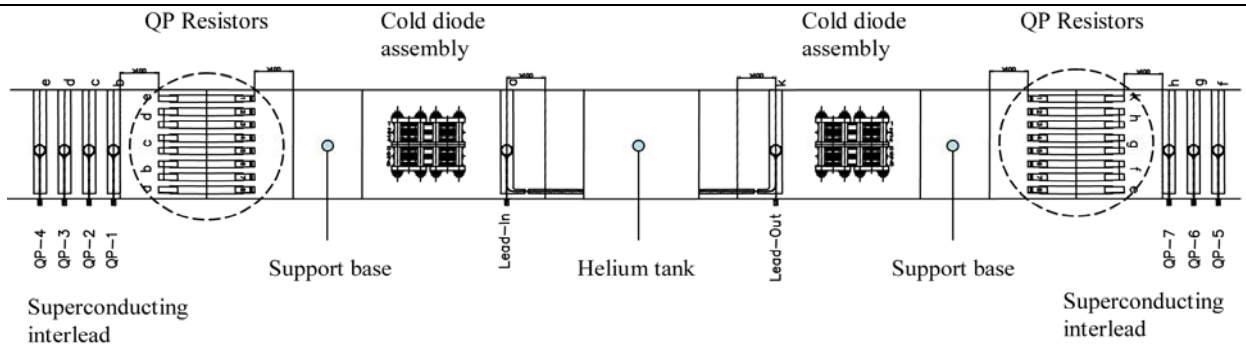

Fig. 3-4-5 Top view of passive quench protection assembly

3.4.2.1 Cold diode assembly

Each cold diode assembly is composed of 4 pairs of back-to-back diodes as shown in Fig. 3-4-6, which are R620 “hockey puck” high current rectifiers with industry grade. This kind of diode has been successfully applied in the cryogenic temperature. The forward voltage of the quench diode is very sensitive to the diode temperature, external magnetic field and its direction. The field around the diode is about 1.5~2.5T. Before mounting, the diodes should be tested at low temperature (e.g. 4.2K) for verifying the quality and measuring the forward threshold voltage drop, forward and reverse leak current.

The diode assembly is designed as a sandwich-like structure in order to meet the demands on heat conduction, electrical conduction and elec-insulation simultaneously. As shown in Fig. 3-4-6, each pair of diodes is clamped between 2 copper plates with thickness of 4mm, which are used as both thermal sink and electrical connection for cold diodes. The G10 sheets with thickness of 1mm are used for electrical insulation among diode pairs and copper pieces. A stack of Bellville washers are to be used to maintain the clamping force with pressure of 1000-1400 lbs even at 4K so as to keep good electrical contact of diode assemblies. The Aluminum plates are used as fixture as well as thermal sink and cooling conduction. The G-10 washers and G-10 tubes are used to insulate bolt assembly with copper plates. 5kV Hi-pot test should be performed for the diode assembly. The clear path between copper poles and the aluminum plate will be more than 10mm.

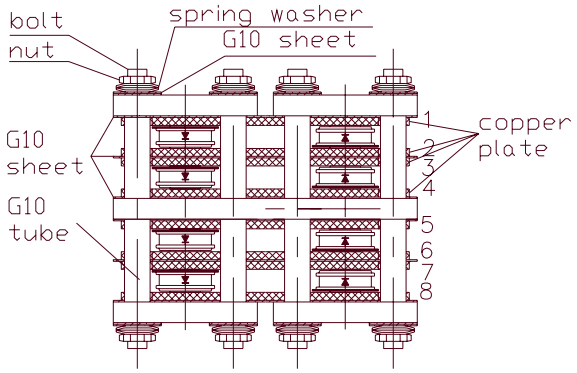

Fig. 3-4-6 Top view of cold diode assembly

3.4.2.2 Resistor assembly

Each resistor assembly is composed of 8 resistors made of stainless steel strips with brazed copper at both ends and mounted on a G-10 plate to be attached to the coil cover plate. The G-10 plate is used for electrical insulation between the resistors and the coil assembly. Each resistor has a cross section area of 40mm^2, length of about 800mm, and the resistance of around 10 mΩ at 4.2K. The total resistance for each quench protection section is about 20 mΩ at 4.2K. The resistor assembly is designed to be kept lower than 150K during quench.

3.4.2.3 Wiring design

The wiring diagram between the cold diode assembly and quench protection resistors is shown in Fig. 3-4-7. The terminals with the same marking number will be connected together using square copper wires. The copper square wires will be soldered onto the copper plates of the diode assembly and the copper ends of resistors.

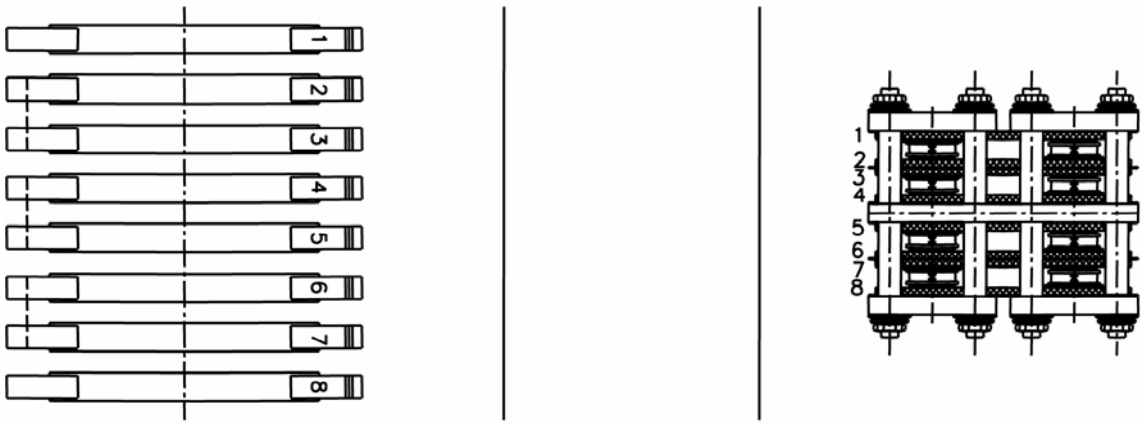

Fig. 3-4-7 Wiring diagram of diode assembly and resistor assembly

3.5 Coil assembly design

The coil assembly comprises the coupling coil and the coil case as shown in Fig. 3-5-1. The coupling coil is composed of electrical insulations, epoxy resin, and conductors fabricated from the NbTi superconductor embedded in a copper matrix (NbTi:Cu=1:4). The coil case includes the mandrel, the cover plate and the banding, which are mostly made of 6061T6 aluminum. The coil mandrel consists of the inner bobbin and end plates.

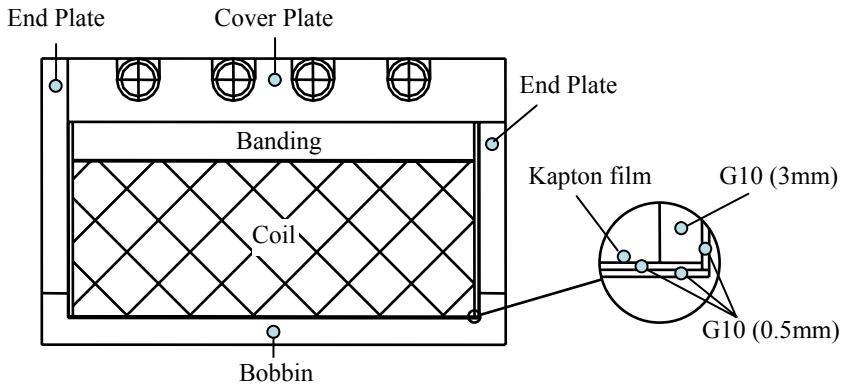

Fig. 3-5-1 Cross section of coupling coil assembly

3.5.1 Coil mandrel

As shown in Fig. 3-5-1, the coil mandrel is made of welded 6061-T6 aluminum plates. The inner diameter of the coil bobbin is 1461 mm, and its thickness is 19 mm. The thickness of the end plate is 18 mm, and the outer diameter of the left plate is 1867 mm, that of the right plate is 1777 mm. The length of the mandrel is 329 mm. All the 6061-T6 aluminum plates should have chemical composition analyses and heat treatment certification, and after welding and machining, it must be inspected for dimensional tolerance and for surface finish, deburring, and for cleanness.

3.5.2 Insulation of conductor, turn-to-turn, layer-to-layer, and coil-to-ground

3.5.2.1 Conductor insulation

The superconducting composite per *LBNL-MICE Superconductor Specification* would be insulated with formvar (0.025 mm thick) per NEMA standard MW-1000 section 18-C poly-viny1 formal resin /class 10J)/ heavy build. The insulated overall dimension of conductor is 1.00 mm by 1.65 mm, with corner radius in the range of 0.2 mm to 0.475 mm.

3.5.2.2 Turn-to-turn Insulation

The turn-to-turn insulation includes the gap of 0.040~0.065 mm that would be filled with StyCast epoxy, except 0.050 mm thick formvar.

3.5.2.3 Layer-to-Layer insulation

The layer-to-layer insulation is made of 0.100 mm thick fiberglass cloth (E glass) wetted with

epoxy, as well as 0.050 mm formvar. The layer-to-layer thickness will reach up to 0.15mm considering thickness of epoxy according to experience from winding large prototype coil.

3.5.2.4 Coil-to-ground insulation

Coil to mandrel insulation is shown in Fig. 3-5-1. The coil to be wound onto the bobbin will be insulated with 2 layers of 0.5 mm G-10, plus 2 layers of 50 micrometer Kapton films which can be used as slip plane at the same time. The insulations between the coil and end plates will be realized using a 0.5mm G-10 sheet and a 3mm G-10 plate. The side slip plane is between the two G-10 plates. In the corner, the insulation will be designed as Fig. 3-5-1 shows, and an additional layer of Kapton tape may be attached to the inner side. Except slip planes, the other contact surfaces will be glued to the mandrel or coil by epoxy.

The insulations will be test to satisfy 5 kV by Hi-pot test and 200μA leakage current requirement.

3.5.3 Coil banding and coil-to-banding insulation

The outermost layer of the coil will be insulated with two layers of G-10 sheets totally at least 1 mm thick. The contact surface will be glued by epoxy. An additional layer of Kapton tape may be attached in the inner corner in order to ensure the electrical insulation of coil to ground. This insulation will be test to satisfy the requirement of 5 kV by Hi-pot test.

The banding is to be wound on the outside of the coil and combined with the cover plate of the coil case to provide some hoop force support on the coil. The high strength 6061-T6 or 5083 aluminum alloy banding with thickness of 27 mm is preferred to be used for banding the coil, which will ensure coil is tightly packed when it is cooled down as well as increase the distance from welding spot of cover plate to the superconducting coil.

3.5.4 Coil winding pack design

3.5.4.1 Winding density control

During each layer winding, winding density (# of turn per cm) will be controlled to assure turn-to-turn uniformity.

3.5.4.2 Coil layer and potting epoxy

The 0.1mm thick fiber glass cloth will be used for layer to layer insulation. The StyCast 2850 FT with Catalyst 24LV will be used to wet each coil layer. It should penetrate into any gap and aperture in the coil.

3.5.4.3 Conductor joints and voltage taps

Conductor joints, which are to be wound into the coil and soldered in up-down manner, are placed at the end of a certain layer separately. Since they will generate Joule heating to 4.2K, it is important to minimize the number of joints and to reduce resistance of each joint.

Due to the required length of the conductor is rather long (about 80000 meters per coil), at least 12 conductor joints will exist in each coil. The Lapping joints will be longer than 1m. All the joints will be carefully insulated with 25 μm thick adhesive-backed Kapton tape. The total thickness of a conductor joint is 2×0.95+0.1+2×0.025=2.05mm, corresponding to thickness of 2 coil layers of 2×1+0.15=2.15mm.

The 1.0 m overlapping SC joint made by ICST was tested to have a resistance of 10^{-10} Ω order even at 4.2K and 5T magnetic field, which will generate heat loss much lower than 1mW for the maximum current of 210 A.

In order to ensure the layer of conductor joint evenly, no voltage taps are attached onto the joints.

3.5.4.4 Superconducting leads

Superconducting leads include 2 coil leads (in and out leads) and 7 superconducting inter-leads for quench protection circuit. Each inter-lead first goes out along a G-10 groove, and then goes back along the same groove. A G-10 groove for inter-leads is shown in Fig. 3-5-2, which is composed of approach groove, round corner and radial groove. The round radius will be greater than 15mm in order not to decrease the performance of the superconducting wire.

All leads should be brought to the same side of the coil. Fig. 3-5-3~5 shows how to bring out each lead onto the cover plate. Each lead corresponds to a groove, which is machined on the mandrel end plate. Each bend radius of a superconducting lead will be greater than 15mm. The minimum gap of 3mm between the superconducting wire and the mandrel will be satisfied in the insulation overlapping position, where insulation materials are bonded each other. As shown in Fig. 3-6-4, QP-7 superconducting inter-lead will interfere with the banding, so the insulation between the superconducting wire and the banding should be paid more attention.

All the leads will be soldered into flexible copper plates of 1mm thick on the cover plate surface and each bend radius of the lead should be greater than 15mm at the end. After each lead is fixed, 5 kV Hi-pot test will be performed and satisfy 200 μ A leakage current requirement.

Voltage taps will be attached to all the superconducting leads in order to monitor magnet performance. All leading conductors will be insulated with adhesive-backed Kapton, carefully supported and cooled on the cold mass surface.

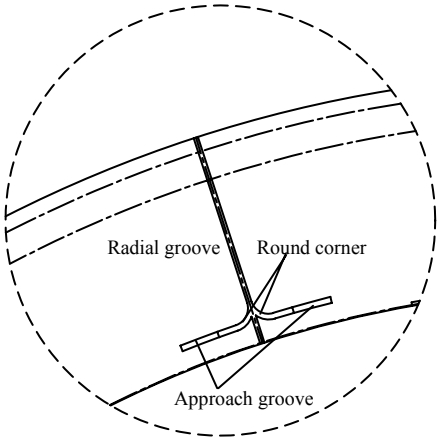

Fig. 3-5-2 A G-10 groove for SC inter-lead

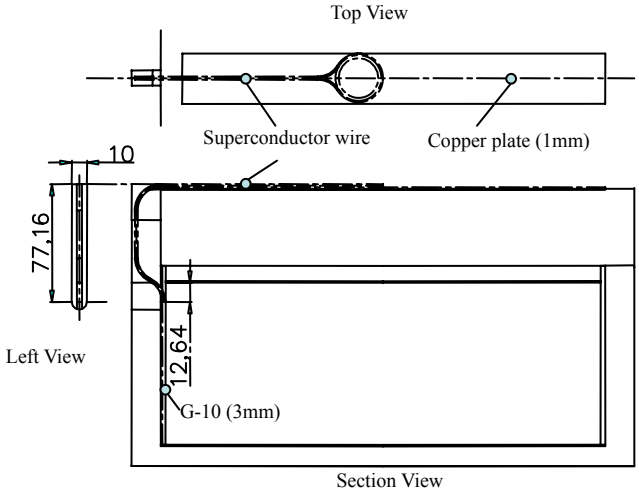

Fig. 3-5-3 Lead-In and QP-1~6 superconducting inter-leads

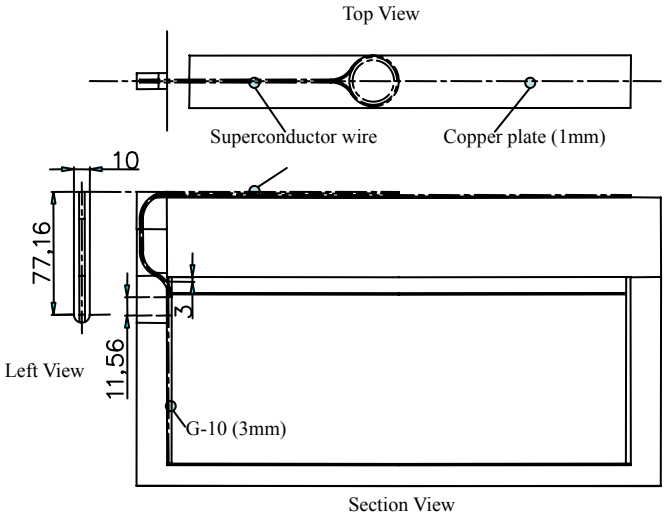

Fig. 3-5-4 QP-7 superconducting inter-lead

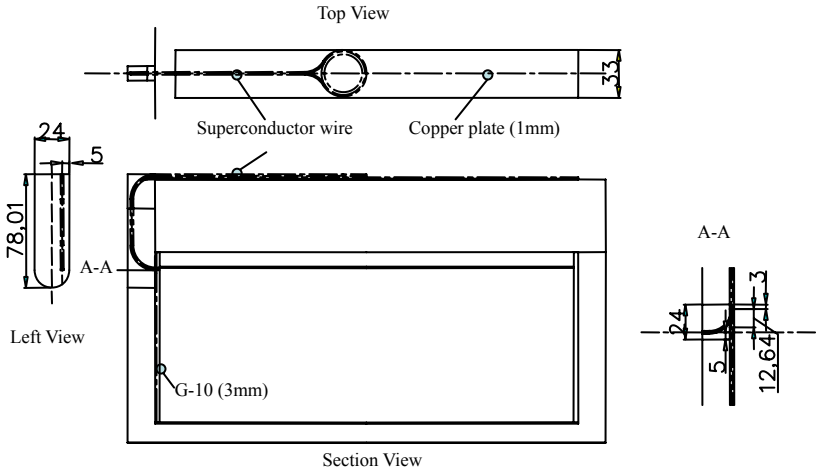

Fig. 3-5-5 Lead-out

3.5.4.5 The inner coil radius (R1)

The inner coil radius of the coil will be 750 mm.

3.5.4.6 The turn-to-turn width

The turn-to turn width should be 1.695~1.715mm considering the gap between turns.

3.5.4.7 The layer-to-layer thickness

The layer-to-layer thick should be 1.0mm+0.1mm+0.05mm = 1.15mm considering the fiber glass cloth between layers.

3.5.5 Coil winding and short checking for turn-to-turn, layer-to-layer and coil-to-ground

Table 3-5-1 is the sample of the winding instruction with number of turns per layer and the dimensional quality control after each layer of coil winding. The 4-wire method will be used to measure the total resistance of coil and storage spool. Any change of coil resistance due to turn-to-turn short or layer-to-layer short will be indirectly monitored before and after each coil layer winding. In order to sensitive enough to check loss of fractional turn, two DMM e.g. Agilent 34401A and one current-constant DC power supply (0-300mA, 0-300V) should be used. Epoxy curing and ambient temperature are factors affecting the small change of coil resistance. One must investigate and understand any decrease in coil resistance assisted by theoretical calculation.

During the winding of each layer, the length of each of about 50 turns must be measured to make sure that turn density is kept constant and the number of turns per layer is maintained according to the coil design.

Epoxy dosage should be planed carefully; the recording form of the weight of all epoxies used will be needed.

3.5.6 Connection of SC conductors to HTS leads

The coil leads (in and out) on the cover plate surface is shown in Fig. 3-5-6, a copper strip of 33mm width will be connected with quench protection circuit. Another copper strip with section area of 6mm×3mm as shown in Fig. 3-5-7 will be connected to the HTS lead. As shown in Fig. 3-5-7, the top surface of the strip will be soldered into the HTS Lead with Sn60Pb40 solder, the joint length is 25mm according to the HTS lead specification.

Theoretically, the conservative joint resistance should be less than 1.924×10^{-7} ohm and the Joule heating is 0.012 watt. Assuming the temperature of cold mass is 4.2K, the distance of coil lead from the cold mass to the HTS lead joint should be less than 0.133m in order to keeping the temperature difference less than 1K.

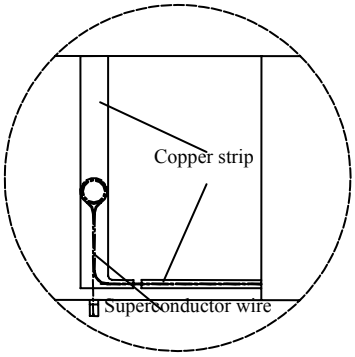

Fig. 3-5-6 Coil lead on cover plate surface

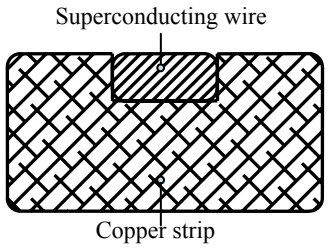

Fig. 3-5-7 Section view of a coil lead brought to HTS lead

4 Cryostat Assembly Design

4.1 Cold mass support assembly design

The purpose of the cold mass support system for the coupling magnet is to transmit both the cold mass and electromagnetic load from the 4.2K package to the vacuum vessel of the cryostat at 300K. It has to ensure the precise and rigid suspension of the cold mass inside the vacuum tank. It should be designed: 1) First, it should withstand shipping loads at room temperature. 2) Second, after the magnet is cooled down and fully charged, it should withstand the forces put on the magnet during a quench or a fault as well as when the MICE channel is normally operated besides its weight. The cold support system for the coupling coil is designed to carry a longitudinal force up to 500 kN in either direction, and the radial force of 50 kN.

A self-centering tension band support system is designed for the coupling magnet, which has the characteristic that the physical center of the magnet does not change as the magnet is cooled from 300 K to 4 K.

4.1.1 Requirements for MICE coupling magnet cold mass support system

4.1.1.1 Position precision and rigid requirement

The performance of the MICE channel requires that the magnets be accurately centered over the beam. The relative longitudinal position of the coil current center must be the same as design within ±1 mm. The coupling solenoid cold mass central axis shall be co-axial with the cryostat vacuum vessel axis within ±0.3 mm. The maximum allowable tilt of the cold mass axis (the magnetic axis) with respect to the axis of the warm bore tube shall be less than ±0.001 radian (±0.057 degree).

4.1.1.2 Thermal requirement

The limited cooling capacity of coolers used for the MICE coupling magnet requires that the cold mass support system must have low heat leak less than 0.25 W at 4 K. It shall be designed so that the temperature of the cold mass support intercepts does not exceed 70 K.

4.1.1.3 Strength requirement

According to the ANSYS magnetic analysis results (see section 3.2), the peak longitudinal load on the coupling magnets is 416.4kN, towards the channel center. The radial forces and torques due to MICE magnet misalignment are less than the forces that must be carried during shipping. Considering the contingence, so the design longitudinal force is set as 500kN, and the design radial force is set as 50 kN. The longitudinal and radial spring constants for the cold mass supports shall be greater than 2x10^8N·m^-1. Each cold mass support assembly shall be held at a force of 1.25 times its design force for 24 hours before the assembly is installed on the magnet.

4.1.1.4 Shipping requirement

The cold mass support system is required to withstand shipping loads. The coupling magnet is to be shipped in a horizontal orientation (with the solenoid axis oriented vertically) at warm condition. And the transmitted loads from the shipping container exterior to the magnet must be less than 2 g along the beam-line (z), lateral(x), and vertical (y) axes for the NCT and normal handling. The transmitted shock load to the magnet during the worst hypothetical accident condition HAC event must be limited to 3 g. So, the support system is designed to withstand accelerations of 2.5 g in any direction. Since the cold mass of the coupling magnet is of the order of 1500 kg, its support system must carry a minimum force in any direction of about 37kN.

4.1.2 Forces imposing on the cold mass support system

The force loads on the cold mass support system at different stages are summarized in Table 4-1-1.

Table 4-1-1 The cold mass support system loads at different cases

Case	**Force loads on the support system**
After assembled at room temperature	Cold mass gravity in vertical direction: 14.7 kN (1500kg)
Warm transportation	Inertial force in any direction 37 kN (accelerations of 2.5g)
Normal operation in flip mode at 200Mev/C	Radial direction: Cold mass gravity in vertical direction 14.7kN (1500kg); The magnet force due to misalignment 37 kN（<2.5g） Longitudinal direction: The magnet force from other MICE magnets 170.7kN
Failure mode	Radial direction: Cold mass gravity in vertical direction 14.7kN (1500kg); The magnet force due to misalignment 37 kN（<2.5g） Longitudinal direction: The magnet force from other MICE magnets 416.4 kN

4.1.3 Design parameters for the cold mass support system

The self-centering cold mass support system proposed for the coupling magnet consists of eight support strap assemblies (four at each end of the magnet). Each support strap assembly consists of four glass fiberglass epoxy (E-Glass) support bands (a double-band scheme) with attachment hardware at each end and an intermediate temperature intercept between the bands. The intermediate temperature intercept is connected to the thermal shield for cooling through a copper bridge. The intermediate temperature is expected to be less than 70 K. The warm ends of the cold mass supports will be near the vacuum vessel at azimuthal angles of 45, 135, 225, and 315 degrees. The cold ends will be at the same angles but off by plus or minus several degrees toward the mid-plane.

Fig.4-1-1 shows the 3-D view of the support strap assemblies. The cold mass support cold

clevis and base plate will be fabricated from 304 or 316 stainless steel or Inconel, and bolted to the outer surface of the cold mass. The thermal intercept section between the support bands will be fabricated from 304 or 316 stainless steel. The room temperature end of the support system will be mounted on the vacuum vessel through a stainless steel sleeve.Each band assembly consists of four glass fiberglass epoxy support bands that are 40 mm wide and 8.0 mm thick and one stainless steel thermal intercept. The two fiberglass bands at one side and the stainless steel intercept are linked together through stainless steel pins, which form a pivot in the support.

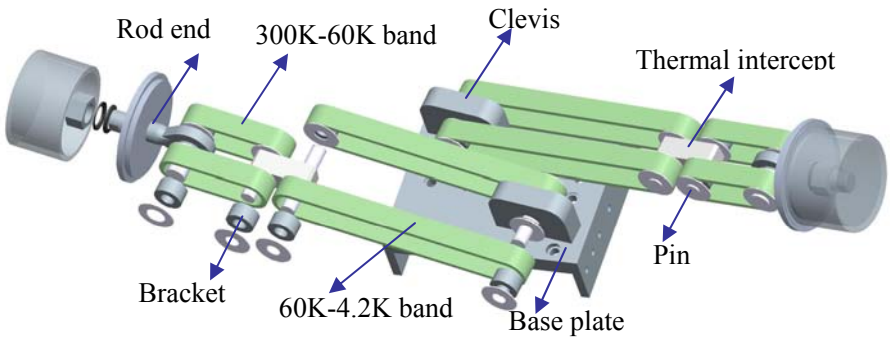

Fig.4-1-1 A 3D view of coupling magnet cold mass support assembly

The positions of the cold end and the warm end for MICE coupling magnet support system are show in Table 4-1-2. The warm ends of the cold mass supports will be near the vacuum vessel ends at azimuthal angles of 45, 135, 225, and 315 degrees. The cold ends will be at the same angles but off by plus or minus five degrees toward the mid-plane. The support system is configured so that it provides rotational restraint. When the magnet is cooled down from 300K to 4K and fully charged, the position changes of support cold ends are obtained by FEA method, which are shown in Table 4-1-2. The position changes of support ends are closely associated with the pre-stress value in bands.

Table 4-1-2 The support ends' positions for MICE coupling coil at different phases

Warm End angle (degree)	45
Warm End R (mm)	1036.225
Warm End Z (mm)	582.0
Cold End Angle (degree)	50
300K Cold End R (mm)	956.5
300K Cold End Z (mm)	-125.5
4.2K Cold End R (mm)	952.96
4.2K Cold End Z (mm)	-125.04
4.2K & Charged Cold End R (mm)	953.53
4.2K & Charged Cold End Z (mm)	-125.02

4.1.3.1 Effect of magnet transportation on pre-stress

The support system will be sealed by a welded cap at the warm end after the final alignment.

Adjustment of the cold mass supports will no longer be possible. Magnet transport scheme will affect the pre-stress level needed in bands at 300 K and affect the band pre-stress after cool-down and charging. When the coupling magnet is shipped cold, the support system must withstand a dynamic shipping 3-g load at 4.2 K, and when the coupling magnet is shipped warm, the support system should withstand a dynamic shipping load of 2.5 g at room temperature depending on the transportation conditions. Table 4-1-3 shows the behavior of the support system as a function of transportation schemes. In the calculations, the band cross-section area is 1280 mm^2, the lengths of 60~300 K and 4.2~60 K bands are 250 mm and 289 mm respectively. The table shows that reducing the shipping load is helpful for the support system design.

Table 4-1-3 Design Parameters for various transportation modes

	Transportation Schemes		
	3-g warm ship	**3-g cold ship**	**2.5-g warm ship**
300K Band stress (MPa)	87.9	43.0	65.2
4.2K Band stress (MPa)	174.0	111.1	151.2
4.2K& Charged Band stress (MPa)	164.9	102.0	142.2
Band Cross-section Area (mm^2)	1280	1280	1280
b x h (mm^2)	40x8x2	40x8x2	40x8x2
Heat leak at 60Kx 8 (W)	6.30	6.30	6.30
Heat leak at 4.2K x 8(W)	0.464	0.464	0.464
Support Spring Constant (N.m^-1)	9.61x10^7	9.61x10^7	9.61x10^7
300K Resonant Frequency (Hz)	40.2	40.2	40.2
Stress in bands considering longitudinal load (MPa)	213.7	150.1	191.3
Stress in bands considering bending stress (MPa)	303.7	240.1	281.3

When a 500 kN longitudinal load is applied on the support system, the tensions in four support assemblies on one side increase, and those in the other four assemblies on the other side reduce at the same value. The pre-stress provided at room temperature is to assure no any relaxation happens on the support straps under the additional magnetic force from the MICE channel.

The bending stress on the band near the pin is proportional to the band thickness and inversely proportional to the bending radius, but almost independent of tension force in band. The thickness of the bands used in the calculation is 8 mm and the bending radius is 50 mm. So the bending stress on the band is about 90 MPa acceptable.

4.1.3.2 Effect of band length ratio and material on the support system

In order to reduce the heat leak at 4.2 K region, the length ratio between 4.2~60 K band and 60~300 K band is increased to 3 from 1.156 with keeping the total length of tension bands constant.

The changed lengths of 60~300 K and 4.2~60 K bands are 410 mm and 135 mm respectively. The behaviors of the support system as a function of band length ratio and material (using the properties of G-10 or estimated E-glass) are summarized in the Table 4-1-4. The thermal contraction coefficient of tension band (E glass) is about half of that for G-10. The thermal conduction coefficient of tension band (E glass) is about two third of that for G-10.

Table 4-1-4 Design Parameters for different band length ratio and material

	Length ratio and material		
	1.156	**3:1 (G-10)**	**3:1(E-Glass)**
300K Band stress (MPa)	65.2	65.2	65.6
4.2K Band stress (MPa)	151.2	163.4	115.9
4.2K& Charged Band stress (MPa)	142.2	154.3	106.9
Band Cross-section Area (mm^2)	1280	1280	1280
bxh (mm^2)	40x8x2	40x8x2	40x8x2
Heat leak at 60Kx8 (W)	6.30	11.70	7.808
Heat leak at 4.2K x8(W)	0.464	0.332	0.219
Support Spring Constant (N.m^-1)	9.61x10^7	9.61x10^7	9.61x10^7
300K Resonant Frequency (Hz)	40.2	40.3	40.3
Stress in bands considering longitudinal load (MPa)	191.3	203.1	155.8
Stress in bands considering bending stress (MPa)	281.3	293.1	245.8

The cold mass support system design parameters are shown in Table 4-1-5 to afford 2.5-g shipment load at 300 K and 50 kN radial load, 500 kN longitudinal force at 4.2 K after fully charged.

Table 4-1-5 Design Parameters for MICE coupling magnet cold mass support system

Material	E-glass
300K Band stress (MPa)	43.8
4.2K Band stress (MPa)	91.9
4.2K& Charged Band stress (MPa)	82.8
Band Cross-section Area (mm^2)	1280
bxh (mm^2)	40x8x2
Heat leak at 60Kx8 (W)	7.808
Heat leak at 4.2K x8(W)	0.219
Support Spring Constant (N.m^-1)	9.61x10^7
300K Resonant Frequency (Hz)	40.3
Stress in bands considering longitudinal load (MPa)	149.8
Stress in bands considering bending stress (MPa)	239.8

4.1.4 Thermal and stress analyses of the support assembly

The FEA model of the support assembly without clevis is shown in Fig 4-1-2. The brackets and thermal intercept are made of 304SS. The pin and the rod end are made of inconel. To assume the mechanical properties of oriented glass fiber bands are isotropic and don't vary with temperature. The mechanical properties used in the calculation are listed in Table 4-1-6.

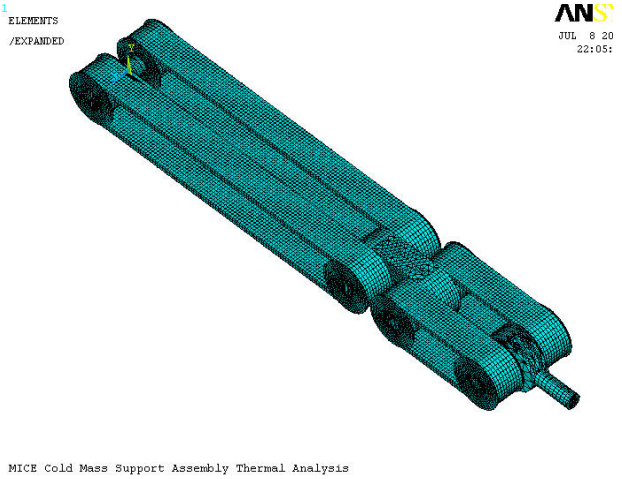

Fig.4-1-2 The FEA model of MICE coupling magnet support assembly

Table 4-1-6 Mechanical properties of materials at 300 K

	Material	Young's Modulus（GPa）	Poisson's Ratio	Tensile strength σ_b (MPa)
Band	oriented glass fiber	41	0.3	>820
Interrupt and bracket	SS304	214	0.29	570
Pin and rod end	Inconel (20K)	220	0.3	1280

4.1.4.1 Thermal analysis of support assembly

The heat leak along the cold mass support is simulated by ANSYS. The applied boundary conditions are set as 4.2 K at the support cold end, 300 K at the support warm end and 60 K at thermal interception. In this analysis, we assumed that the bands only contact with the outer faces of brackets, which is consistent with actual situation. The temperature distribution along the bands is shown in Fig. 4-1-3.

The calculated heat leak (based on the properties of G-10 due to lack of E-glass thermal properties) for one cold mass support from 60 K to 4.2 K is 38.84 mW, and the total heat leak down the eight cold mass supports is about 0.31 W . The calculated heat leak for one cold mass support from 300K to 60K is 1.19 W, and the total heat leak down the eight cold mass supports is about 9.58 W. The thermal conductivity integral of the oriented fiberglass support band is about two thirds of the thermal conductivity of G-10. So the heat leak down the cold mass support system can satisfy the requirement is specification, which is 0.25 W at 4 K.

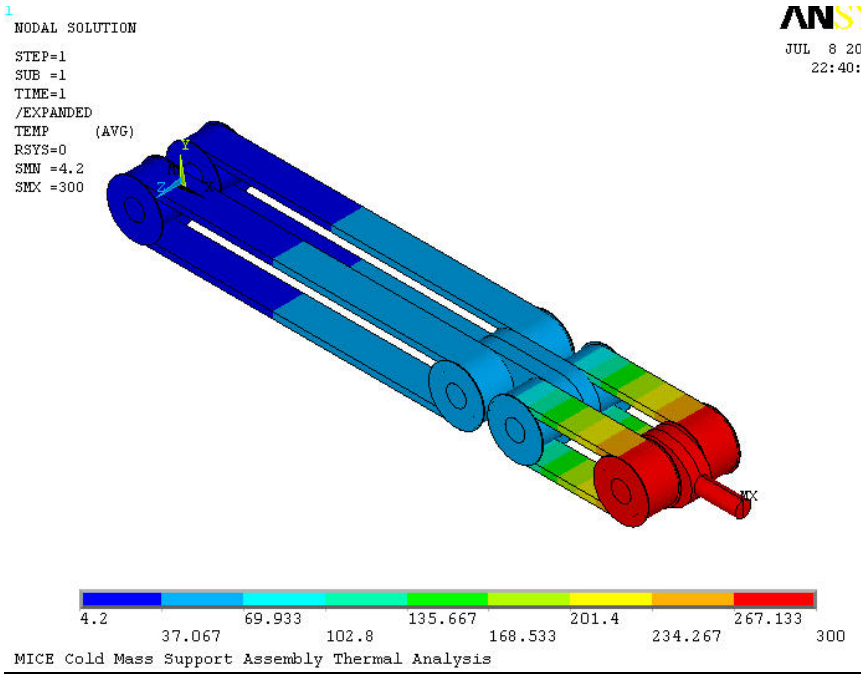

Fig.4-1-3 Temperature profile along the cold mass support assembly

4.1.4.2 Structural analysis of the support assembly

The peak tension applied on the support assembly will be less than 200 kN considering 2.5g warm shippable load, 500kN of longitudinal magnetic force as well as the cold mass weight, and the peak Von Mises stress on the support band will be about 240 MPa due to both tension and bending force as listed in Table 4-1-5. Because the cross-section areas of the rod end and the thermal intercept are quite smaller than the support bands, so the stresses induced on these components are quite high. The stress analyses are carried out under the band peak tension of 200kN. For on-site operation, without considering the 2.5g shipment load, the peak tension is about 170kN.

4.1.4.2.1 Boundary conditions

- The rod end at room temperature is completely constrained,
- To apply symmetry Dofs condition on the symmetry plane,
- To apply the pressure of 131.6 MPa on the area of pin contacting with the cold end bearing, which is corresponding to the peak tension force of 200 kN,
- The fraction coefficient between bands and pins is negligible.

4.1.4.2.2 Spring constant of the support system

The displacement of the cold mass support assembly under 200kN force is shown in Figure 4-1-4. Because the warm end of the support is fixed, the peak displacement happens on the cold end, of which the value is 3.31 mm. The spring constant of the support assembly can be expressed in the following equation:

$$k = \frac{F}{\Delta L} = \frac{200kN}{3.31mm} = 6.04 \times 10^7 N/m$$

The spring constant of the support system is $8k = 4.83 \times 10^8 N/m$, which is greater than the requirement in specification $2 \times 10^8 N/m$.

4.1.4.2.3 Stress of the support system

The Von Mises stress profiles of the cold mass support assembly are presented in the following figures. The stresses of suspicious stress concentration areas are linearized to eliminate the effect of stress concentration. The peak stress happens on the rod end at the interface area between the rod end and the pin, which is shown in Figure 4-1-6. After stress linearization, the total membrane and bending stress is 380.4 MPa, which is lower than $\sigma_b/3$ of Inconel at 300 K.

Figure 4-1-7 shows the stress on the tension band between 60 K and 4.2 K. The average von Mises stress in the support band is 156 MPa, and the peak stress is 213 MPa occurred on the inner surface of the band around the support pin due to tension and bending of band. Along with the peak stress, there is a force gradient across the band. Along with this force gradient is a shear stress about 13 MPa. In order to reduce the bending stress and shear stress, the thickness of the band relative to its bend radius has to be reduced as thin as possible. The band thickness is 8 mm, and the width is 40 mm.

The tension band between 300 K and 60 K is identical with that between 60 K and 4 K, except for the band length. Figure 4-1-8 shows the stress on it. The average von Mises stress in the band is 156 MPa, and the peak stress is 223 MPa occurred on the inner surface of the bend around the support pin due to tension and bending of band.

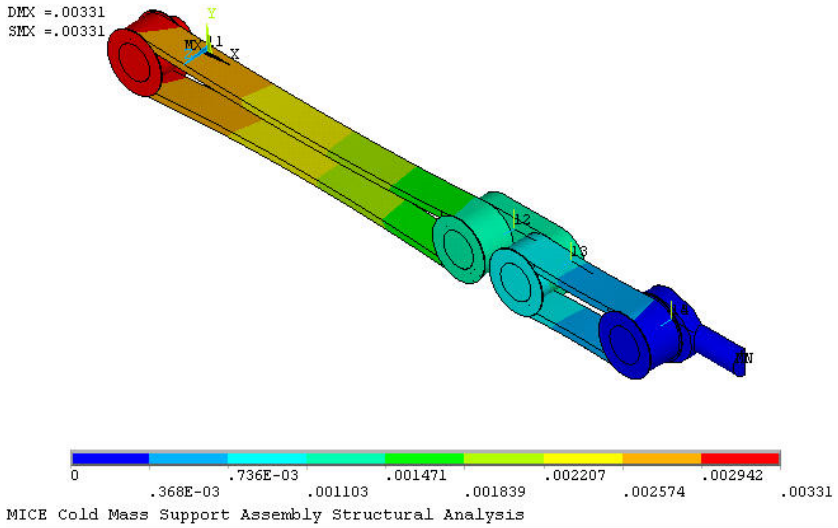

Fig.4-1-4 Displacement profile of the support assembly

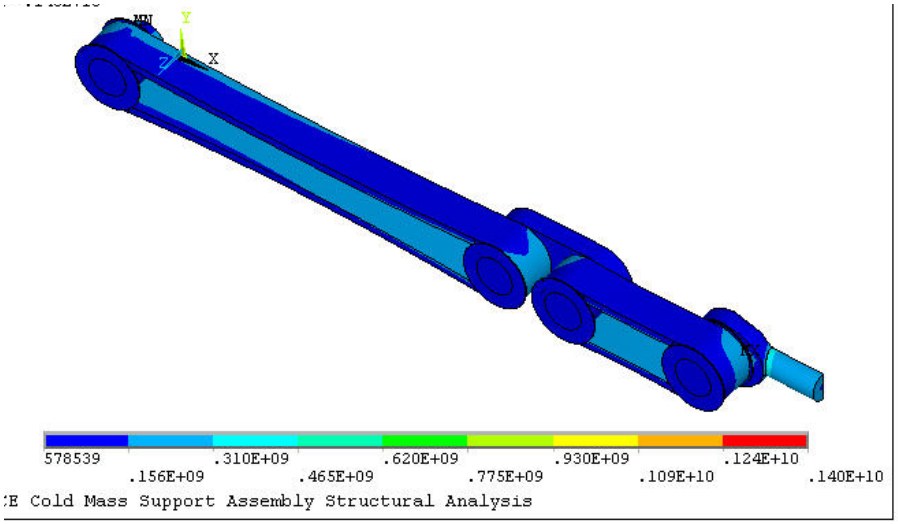

Fig.4-1-5 Von Mises stress of the support assembly

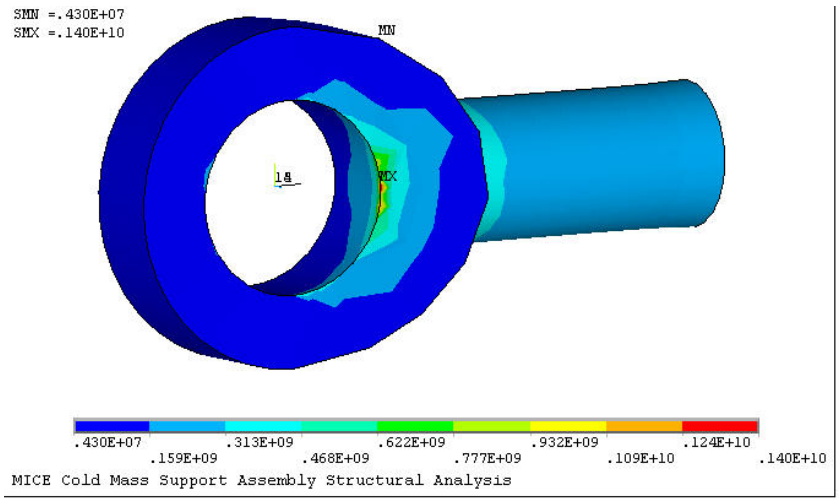

Fig.4-1-6 Von Mises stress of the rod end

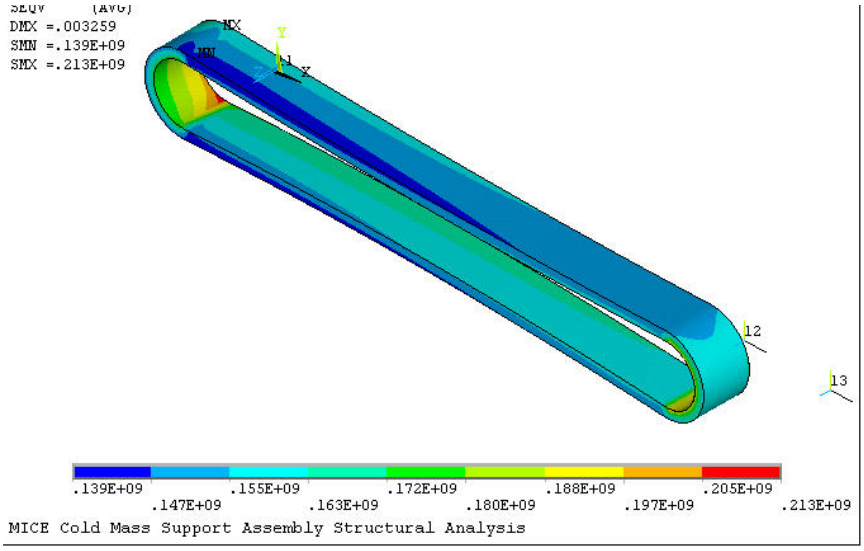

Fig.4-1-7 Von Mises stress of the 4~60K tension band

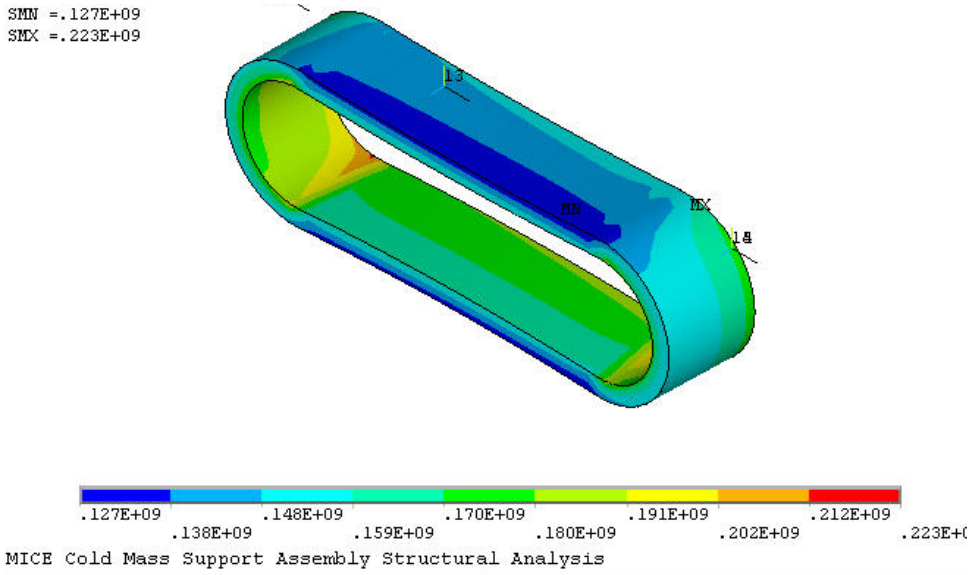

Fig.4-1-8 Von Mises stress of the 60~300K tension band

4.2 Current leads design

The coupling magnet is to be cooled by using cryocoolers at 4.2K. In order to reduce the heat leakage induced to the 4.2K cold mass from high temperature, a pair of binary current leads composed of conventional copper leads and high temperature superconductor (HTS) leads are to be employed in electrical connection for the magnet to a unipolar 300A/0-20V power supply. The binary leads are to be conduction-cooled by two two-stage cryocoolers. The copper lead is optimized at a current of 220 A, but capable of carrying a current up to 250 A. The HTS lead with a nominal current of 220A is capable of carrying 500 A when the high-temperature end of the lead is nominally at 64 K and at 0.5 T.

As shown in Fig.4-2-1, the upper warm end of HTS lead is connected to the cold end of copper lead. The cold end of HTS lead is flexibly connected to niobium titanium pigtail lead from the coupling coil. Most of heat leak from the copper leads is taken away by the first stage cold heads of cryocoolers which are connected to both the cold end of copper leads and the warm end of HTS leads through copper thermal links. Only a little heat flows into 4K temperature region along the HTS leads by conduction. Because the coupling magnet is not shielded, there is stray magnetic field on the HTS leads. The performance of the HTS lead is affected by the HTS material, the magnetic field on it and the temperature at the warm end of HTS leads.

This section presents the optimization of conventional conduction-cooled metal leads for the coupling magnet, effect analyses of the magnetic field on the performance of the HTS leads and cooling of HTS leads in case of power failure during rapid discharge of the magnet.

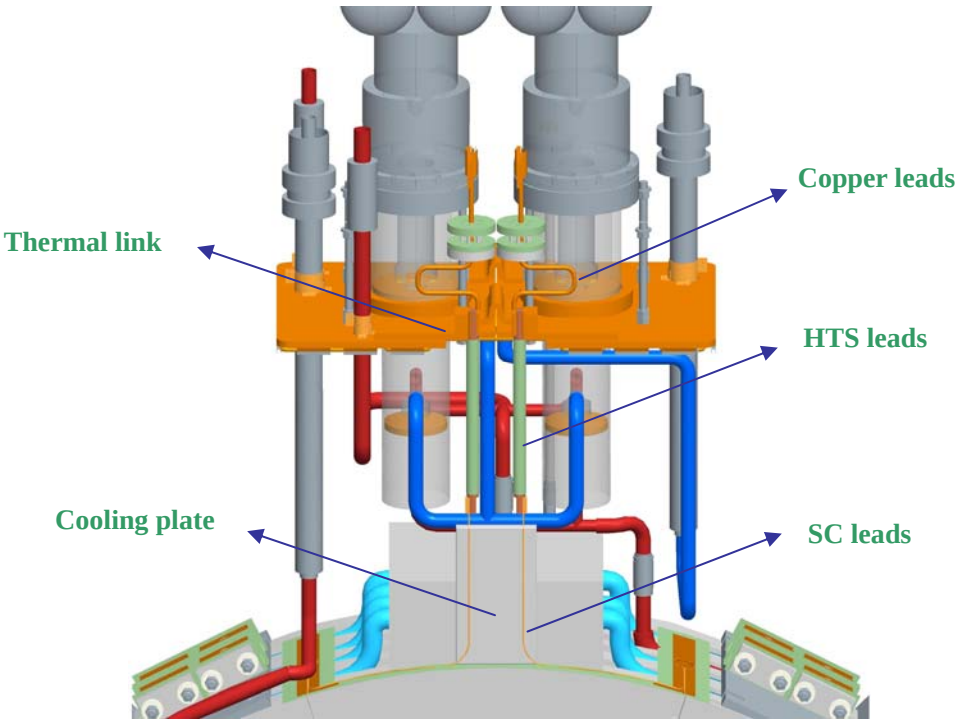

Fig. 4-2-1 A 3D view of current leads for coupling magnet

4.2.1 Copper leads

Generally, pure copper is used as the material of conventional metal current leads since its thermal and electrical conduction is well. Heat leakage down the copper lead during operation comes from two sources: conducted heat from room temperature and joule heat generated within the lead. The Fourier rate equation shows that conduction heat is proportional to the conduction area and inversely related to the length. The effect of area and length on the joule heat is totally different from the conduction heat. For a given current and the material, there is an optimal relationship for length and area which makes the heat leak minimum.

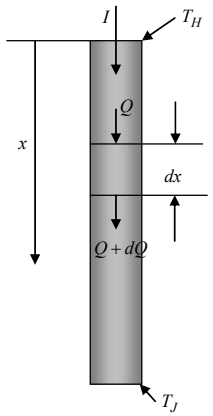

Fig. 4-2-2 Schematic of one conduction copper lead

Figure 4-2-2 shows a single conduction-cooled copper lead. The lead carries a current I. The top and bottom of lead are kept at higher temperature TH and lower temperature TL. Combine the Fourier rate equation for one dimensional steady heat transfer and energy conservation of principle. The minimum heat leak Qopt at the cold end of lead and the shape factor (IL/A)opt under optimal operation can be described as follows:

$$\frac{Q_{opt}}{I}=\sqrt{2\int_{T_L}^{T_H}k(T)\rho(T)\mathrm{d}T} \tag{1}$$

$$\left(\frac{IL}{A}\right)_{opt}=\int_{T_J}^{T_H}\frac{k(T)\,\mathrm{d}T}{\sqrt{2\int_{T}^{T_H}k(T)\rho(T)\,\mathrm{d}T}} \tag{2}$$

Where: A is the cross-sectional area, L is the length of lead, k(T) is temperature dependent thermal conductivity of material, and ρ(T) is temperature dependent electrical resistance of material.

Most of pure metals and alloys obey the microscopic Wiedemann-Franz Law (WF) fairly well, i.e. k(T) ρ(T)= LoT, where Lo=2.45×10-8W-Ω/K^2 is the Lorentz constant[5]. To apply the WF on the above expressions, then Eq. (1) and Eq. (2) become:

$$\frac{Q_{opt}}{I}=\sqrt{L_0(T_H^2-T_J^2)} \tag{3}$$

$$\left(\frac{IL}{A}\right)_{opt}=\frac{1}{\sqrt{L_0}}\int_{T_J}^{T_H}\frac{k(T)\,\mathrm{d}T}{\sqrt{T_H^2-T^2}} \tag{4}$$

From Eq. (3), the theoretical minimum heat leak Qopt is almost independent of the materials to be used.

Under the optimal operating condition, the heat leak to the cold end of lead is equal to the joule heat generated in the lead from the energy conservation of principle. Hence, the voltage drop along the lead can be obtained:

$$(\Delta V)_{opt}=Q_{opt}/I \tag{5}$$

The conduction copper lead used for the MICE coupling solenoid can be optimized based on the above equations. The results for the copper lead are listed in Table 4-2-1.

Table 4-2-1. Theoretical optimized results of copper leads for MICE coupling magnet

Optimized current I（A）	220	210A
Temperature range T（K）	300-60	300-60
Material: Copper	*RRR*=10	*RRR*=10
Minimum heat leak Q_{opt}（W）	10.135	9.652
IL/A（10^6A/m）	3.071	3.071
Optimized length L（mm）	384	384
Cross-sectional area A（mm^2）	27.5	26.25
Diameter (mm)	6.0	5.8
Voltage drop ΔV（mV）	46	46

Finite volume method is used to simulate the steady temperature profile of the above 210A current lead. Figure 4-2-3 shows the temperature distributions of the 210A current lead when carrying 0A, 210A and 250A. The corresponding heat leak at the bottom of the lead is 5.638W, 9.074W and 11.069W. The heat leak at a current of 210A is consistent with the theoretical calculated result listed in Table 4-2-1. When the lead carries a current of 250A, the peak temperature on the lead is about 307A. So the lead can carry 250A current safely.

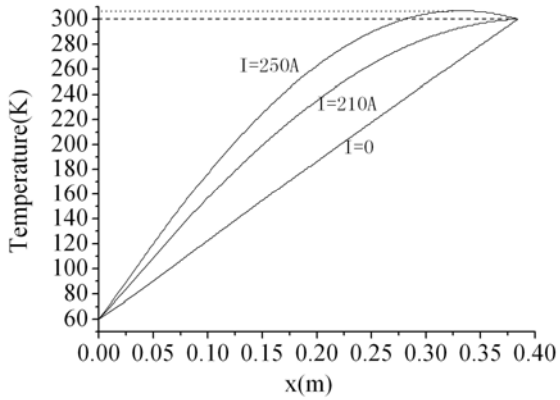

Fig. 4-2-3 Temperature profile of a current lead transferring different currents

The copper lead may be fabricated as a flexible cable or a spiral rod or bar in order to avoid overstressing the HTS leads during cool down process. The upper lead will be connected to the room temperature copper bus by a commercial lead feed through on top of the cryostat.

The burn out time for a copper lead in case of power failure is estimated. If the burnout temperature is set at 300K, to consider current decay and assume adiabatic condition, the calculated time is 4314s. In reality, the burnout temperature is much higher than 300K, so the lead is safe.

4.2.2 HTS leads

The key to be able to operate the MICE superconducting solenoids on small coolers is the application of high temperature superconducting (HTS) leads between the first stage of the cooler and the magnet, which operates at around 4.2 K. Because MICE magnets are not shielded, all of the MICE magnets have a stray magnetic field in the region where the coolers and the HTS leads are located. The performance of the HTS lead is affected by the HTS material, the magnetic field on it and the temperature at warm end of the lead.

The lead made from an oriented piece of HTS material such as the first generation BSSCO magnet conductor has two preferred field directions where the lead can still be superconducting at a higher current. This type of a lead can work in the magnetic field generated from the magnet being powered, such as the MICE magnets.

4.2.2.1 500A HTS-110 leads

The most likely candidate for HTS leads for the coupling coil is shown in Fig. 4-2-4 (made by HTS-110 Ltd., New Zealand). The standard 500A HTS conductor is a composite that places multifilament BSSCO conductor in a low thermal conductivity Ag-Au matrix. The conductor has a very high current density, translating into a small cross-section of conductor and a low heat leak. The conductor put inside the G-10 tubing displays tolerance for strain and thermal cycling. Table 4-2-2 lists dimensions and parameters of the 500A HTS lead. In general, the HTS-110 leads can go above 80 to 85 K before sudden thermal runaway occurs.

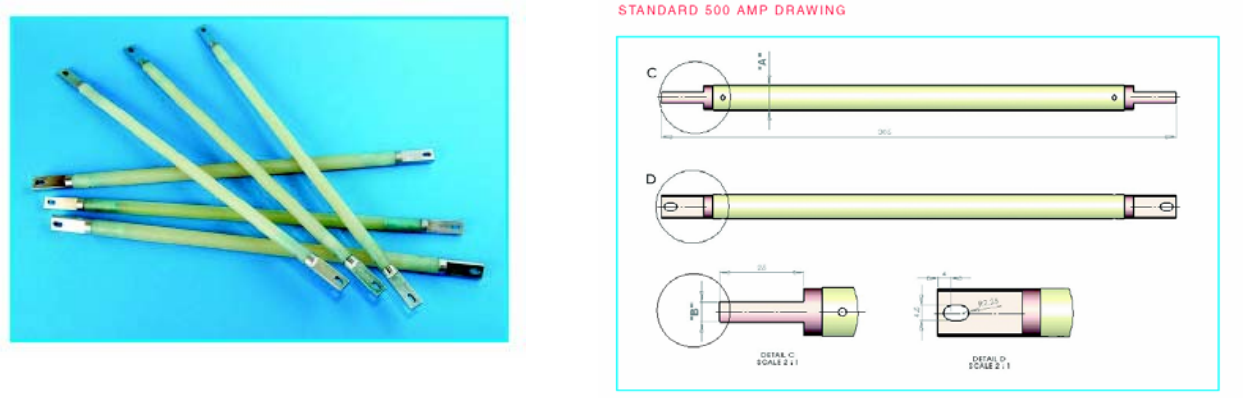

Fig. 4-2-4 HTS leads to be used for coupling magnet

Table 4-2-2. Parameters of a standard 500A HTS-110 lead

Body Diameter A (mm)	14.30
Dimension B (joint thickness) (mm)	6.35
Overall Length (mm)	305
G-10 Sleeve Length (mm)	254
Active Lead Length (mm)	~210

Operating temp. at warm end (K)	64
Operating Current at 64K (A)	500
Conductive Heat Leak at 64K~4.2K (mW)	65

4.2.2.2 Effect of magnetic field on performance of HTS-110 leads

The performance of HTS-110 is determined by the magnetic field and the temperature on the upper end of leads.The position of the HTS leads with respect to the cold mass is determined by MICE worst-case magnetic field at the upper end of the HTS leads. The leads made by HTS-110 are well suited for use in a magnetic field as long as that magnetic field is not above 0.5T. From Figure 4-2-5, it is clear that the HTS-110 leads have two favorable and one unfavorable direction. The favorable directions are along the length of the HTS-110 lead and along the flat face of the conductor when the field is perpendicular to the direction of current flow in the lead. As long as the field is parallel to the flat face of the conductor, the conductor could operate at the highest critical current for a given field and a temperature. In order to make the leads operate with higher performance, the HTS-110 leads should be positioned so that the magnetic field from the coupling magnet runs in the favorable directions.

The self-field from current flowing in the lead will have a component that flows in a direction perpendicular to the flat face of the lead. The worst-case self field from the MICE leads is less than 0.03 T. Thus, self-field even at the lead conductor edge is not an important design factor at 300 A.

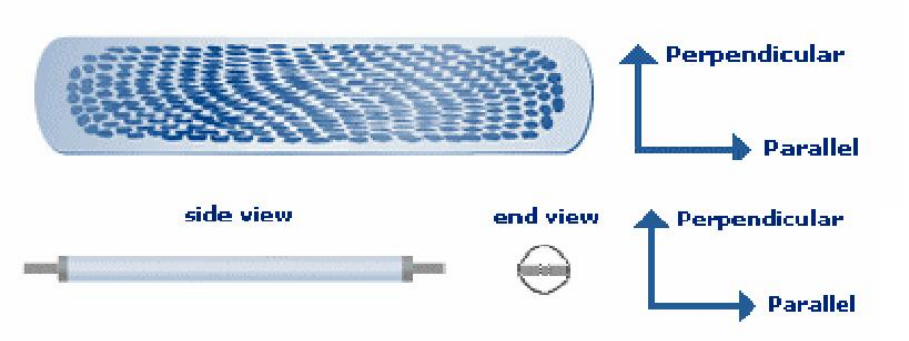

Fig. 4-2-5 Favorable and unfavorable field directions for HTS-110

Fig. 4-2-6 shows the performance factors for the HTS-110 leads. The performance factor of 1 means that the lead will carry the same current as the lead is designed to carry at 64K without magnetic field on the lead. And a performance factor of 0.5 means that the lead will carry half of its design current at 64K and zero field. From Fig. 4-2-6, it is clear that the lower the HTS-110 lead temperature, the better. It is also clear that limiting the magnet field on the lead is desirable. A field that is perpendicular to the lead flat face (i.e. unfavorable direction) is much worse than a magnetic field that is parallel to the flat face (i.e. favorable direction). At a parallel magnetic field of 0.4T, the lead scaling factor is about 0.8 at 64K and 0.5 at 70K. The leads of the coupling solenoid will carry

a current of 210A at worst case. In order to have additional margin, 500A standard HTS-110 leads will be used for the coupling magnet. The disadvantage of using larger leads is that the heat leak into the second stage of cooler is increased. The heat leak down the leads with the upper end temperature at 64K is 90mW for a pair of standard 250A leads and 130mW for a pair of standard 500A leads.

As shown in Fig. 3-1-5, the warm end of HTS leads is in a field less than 0.35T and the cold end is close to 0.7T.

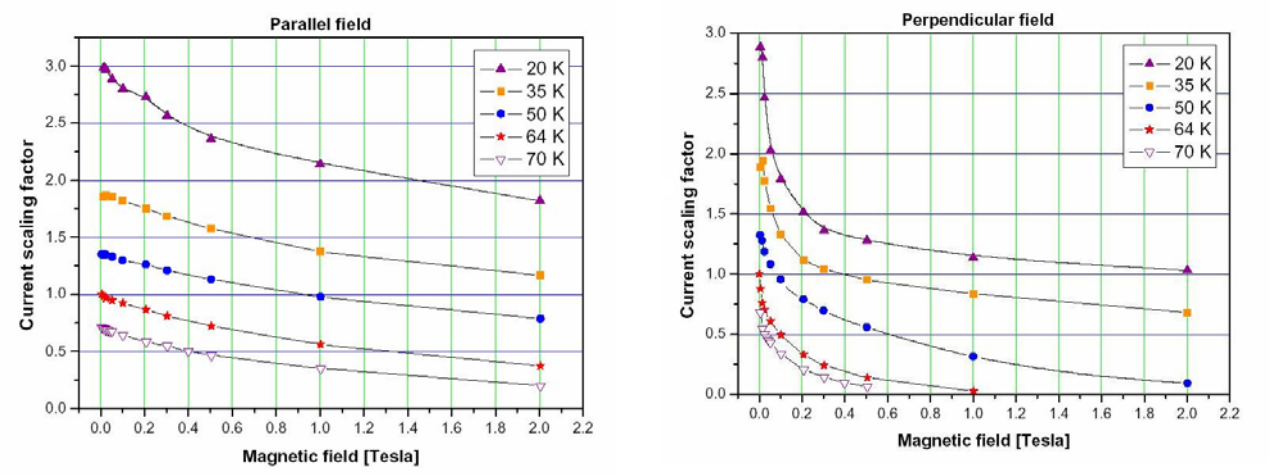

Fig. 4-2-6 HTS-110 current factor vs. B and T

4.2.2.3 Magnetic force along the HTS lead

Ignoring the magnetic force due to self-field of HTS leads. The magnetic force can be calculated using $f_x = B_Z(x) * I$. If the HTS lead operates at 210A, the average magnetic force imposed on the HTS lead can be estimated as 27.49 N for one coupling coil and 30.08 N for all the MICE coils. The magnetic force per length along the HTS lead is shown in Fig.4-2-7.

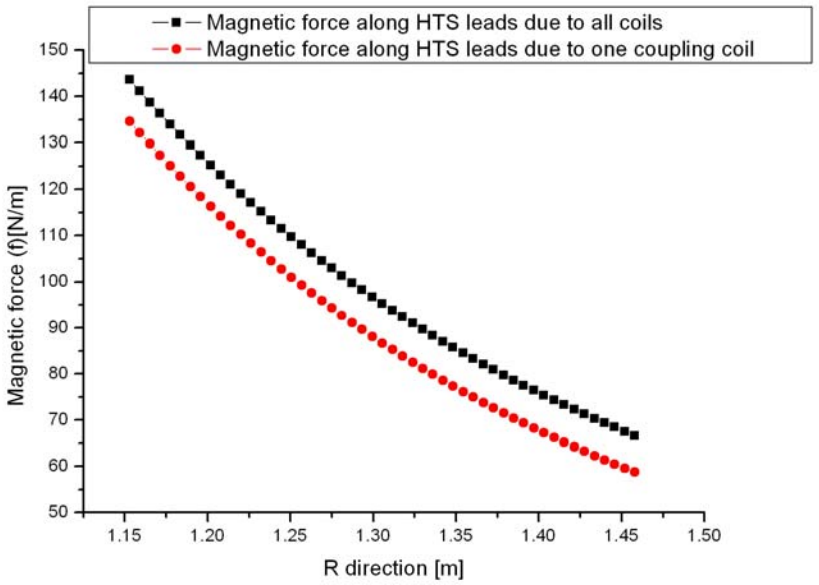

Fig. 4-2-7 Magnetic force along the HTS lead

4.2.2.4 Protection of HTS leads in case of power failure

Lead overheating during a fault is an important consideration for the coupling magnet design. As a matter of the magnet design, the voltage drop along the length of the HTS lead is to be measured. If the voltage drop along one or both magnet leads is too high for some reason, it may finally lead to the magnet quench to protect the leads from burning out. However, once the magnet quenches, the time to recover is quite long.

Some failure modes such as a power failure that causes the cooler to shut off or the malfunction of the cooler can cause the upper end of the HTS lead to overheat. If the upper end of the HTS leads goes to a high temperature, the current from the magnet and its leads must be removed rapidly in order to protect the leads from thermal runaway. In the above scenario, the extra cooling to prevent the HTS leads from going normal and running away has to be provided. There are a couple of ways to provide this extra cooling: 1) Intercept the heat flow down the leads from room temperature with a volume of liquid (or solid) nitrogen held in reserve to prevent the leads from running away and quenching. 2) Have enough solid thermal mass (extra copper or aluminum in the shields) in contact with the leads to prevent them from getting too hot while rapidly discharging the magnet. 3) Use sensible heat of boil off helium from the magnet to cool the HTS leads during a rapid discharge.

For the coupling magnet, considering limited space inside the cryostat, the last two methods were studied for HTS protection cooling.

A block of copper (or aluminum) connected to the first stage of the cooler can be used to ensure that the HTS lead don't burn out during a rapid discharge of the magnet. The rapid discharge of the magnet will not cause the magnets to quench, as long there is liquid helium around the magnet coils. The recommended amount of metals connected to the first stage of the magnet coolers is ~122 kg for copper and 72 kg for Aluminum as shown in Table 4-2-3. The amount of copper

connected to the first stage of the cooler may have to be increased if the copper leads run at higher current densities.

During the rapid discharge process, ~10 liters of liquid helium around the magnet will boil off in terms of AC losses and static heat load at 4.2K. The boiled off helium will go though a coiled heat exchanger attached to the first stage cold heads of the coolers to keep both the shield and the HTS leads cold. The heat exchanger is made of copper tubing of 8mm in inner diameter and 3~4 meter in length. The pressure drop along it is about 100Pa.

Table 4-2-3 An estimated amount of metals needed to keep the upper end of the HTS Leads cold during a fast discharge, when AC Loss and static heat load are considered.

Magnet self inductance (H)	592.5
Number of magnet turns	15744
Average rapid discharge AC loss (W)	2.95
Time for a rapid discharge (s)	5400
Static heat load to cold mass at 4.2 K (W)	2.0
Static heat load to 60 K (W)	61.5
Temperature of copper or Aluminum with cooler cooling (K)	55K
Temperature of copper or Aluminum without cooler cooling (K)	60K
Max. temperature of HTS leads during discharge (K)	64K
Magnet fast discharge voltage (V)	22
Number of quench diode packs	8
Maximum copper lead heat flow (W)	19.3
Heat to copper plate (kJ)	104.22
Copper mass needed w/o cooler cooling (kg)	122.6
Aluminum mass needed w/o cooling (kg)	72

4.2.3 Cooling for current leads

4.2.3.1 Cooling for warm ends of HTS leads

The cold end of the copper lead will be bolted and soldered to the warm end of the HTS lead. The leads are to be conduction cooled by thermal link between them and the first stage cold head of cooler. The thermal link is designed to meet the requirement: 1) to minimize the temperature difference between the cooler cold head and the leads, 2) to provide the electrical insulation between them.

Fig.4-2-8 illustrates the structure of the thermal link for the leads' cooling. The copper plate fulfills the heat conduction and two layers of 25 um kapton film or a thin G-10 sheet with epoxy are used for elec-insulation. The key points for the thermal link design are to reduce ΔT through the elec-insulation due to poor thermal conductivity of kapton or G-10 compared with copper, to enlarge its conduction area and to shorten its conduction length. The related calculation and simulation were carried out.

The calculation results are presented in Fig.4-2-9 and Fig.4-2-10. Fig. 4-2-11 to Fig.4-2-13 shows the simulation results. In the figures, ΔT1 is the temperature difference through two layers of

25 um kapton film with epoxy, ΔT2 is the temperature difference along the copper bracket between the connection spot of leads and the copper plate. The heat flux area in Fig.4-2-9 is conduction area of the copper plate, the area in Fig.4-2-10 is conduction area of the copper bracket.

Assuming the cold head temperature is at 60K, the heat leak from a copper lead is estimated as 9.65W, if the temperature difference ΔT1 is limited within 2K, the heat flow area is no less than 9900 mm^2. If ΔT2 is less than 2K, the length L is 40mm; the width W2 is 40mm; the thickness δ2 is 20mm; the thickness of copper plate δ1 is 10 mm, and the dimensions for the thermal link are summarized in the Table 4-2-3.

Table 4-2-3 Dimensions of thermal link (mm)

L1	W1	δ_1	W2	L	δ_2
140	80	10	40	40	20

From the simulation results, the temperature difference in thermal link is 4.2 K in total. The maximum temperature difference of the elec-insulation is 3.3 K in the neck, and the temperature difference in the rest region is about 1.5~1.8 K.

4.2.3.2 Cooling for cold ends of HTS leads

As shown in Fig. 4-2-1, the two SC leads come from the coil will go along an Al plate attached to the 4.2K cold mass for cooling. The cold ends of the HTS leads are cooled by conduction through the SC leads, which are to be flexibly soldered with the SC leads. The SC leads are to be electrically insulated from the Al plate.

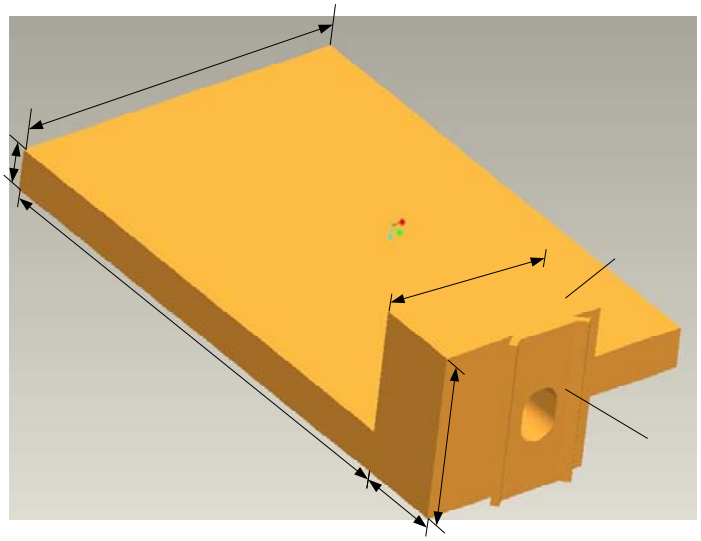

Fig 4-2-8 Thermal link for cooling the warm end of HTS lead

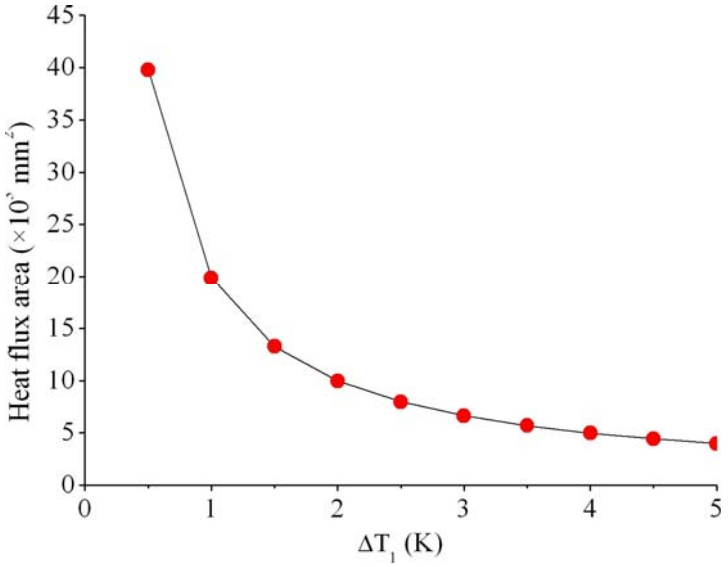

Fig. 4-2-9 Heat flux area with ΔT1

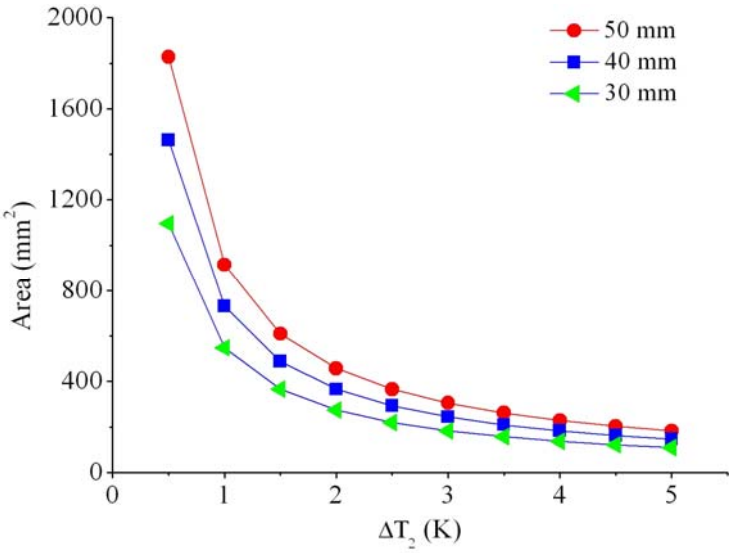

Fig. 4-2-10 Heat flux area with ΔT2

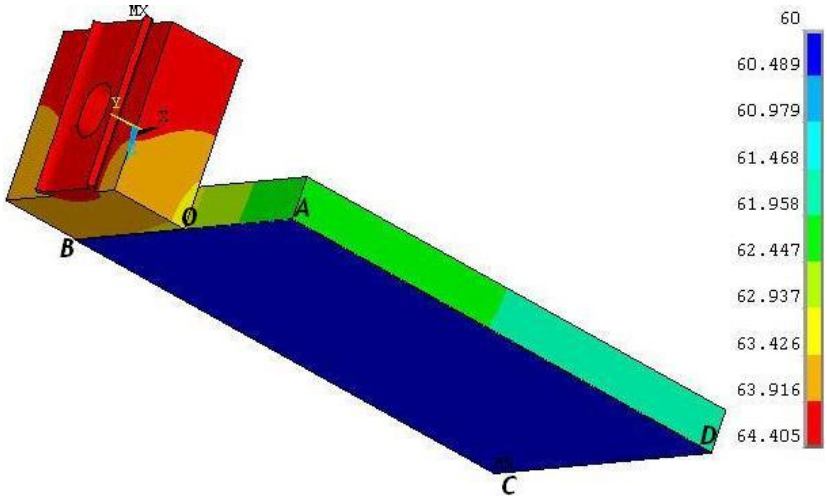

Fig. 4-2-11 Temperature distribution in thermal link

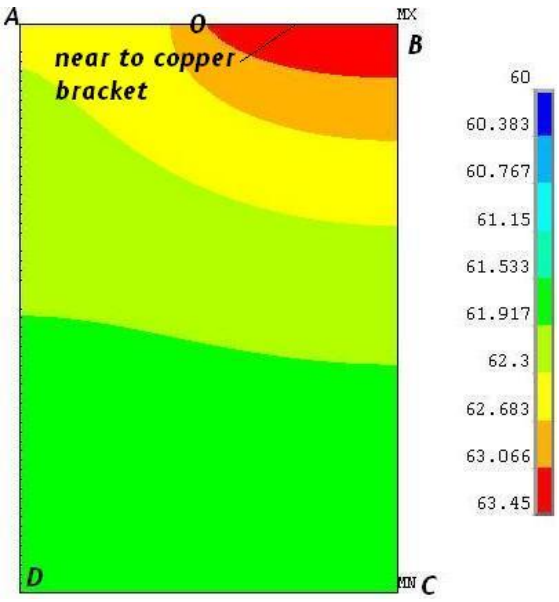

Fig. 4-2-12 Temperature distribution in elec-insulation (top view)

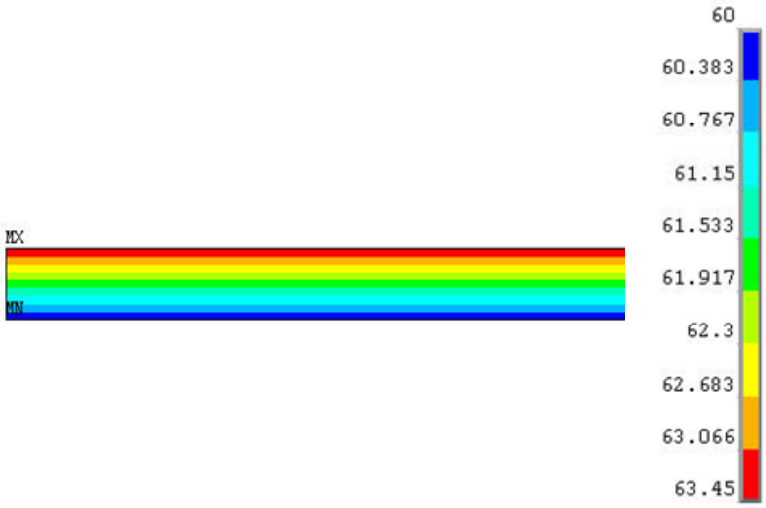

Fig. 4-2-13 Temperature distribution in elec-insulation along thickness

4.3 Cooling system design

4.3.1 Static heat loads and cold mass

4.3.1.1 Heat loads at 60K

Table 4-3-1 Heat loads at 60 K

	Heat load (W)
Copper leads (300K-60K)	19.3
Conduction through 60 K cold mass supports	9.9
Radiation to 60 K shields	8.7
Main shield supports	4.0
Upper neck shield supports	0.62
60K intercepts for neck tubes	4.823
Intercept for instrument wires	1.0
Sub-total	47.343
Contingence	30%
Total	61.5

4.3.1.2 Heat loads at 4.2K

Table 4-3-2 Heat loads at 4.2 K

	Heat load (W)
HTS leads (60K-4.2K)	0.13
Conduction through 4.2 K cold mass supports	0.2
Radiation to 4.2 K cold mass	0.85
4.2K neck tubes	0.212
SC joints	2.64x10^-3
4.2 K instrument wires	0.1
Sub-total	1.492
Contingence	30%
Total	1.94

Based on the above tables, for normal operation, the total heat load at 4.2K including contingence is 1.94 W, and is 61.5 Wat 60K. Considering additional cooling capacity required for the charge and discharge process of the coupling magnet, effect of stray magnetic field on the cooling performance of the coolers with a remote valve (at least 10% deduction), two coolers are necessary to run the coupling magnet.

The cold mass at 60K for the current design is around 122 kg. The total cold mass at 4.2K for the current design is around 1.593 ton.

4.3.2 AC losses during charging, discharging and fast discharging process

The coupling magnet will be charged at constant voltage across a 300A single power supply. The charging voltage of the power supply is 10 V, and the charging time is calculated to be about 13950 seconds (3.9 hours). For normal discharging process, eight diodes are accessed to the

discharging circuit. The maximum voltage across the coupling coil is about 10.1 V, and the normal discharging time is around 13790 seconds (3.8 hours). For fast discharging process, eight diodes are accessed to the discharging circuit. The maximum voltage across the coupling coil is 24.1 V, and the fast discharging time is 5395 seconds (1.9 hours).

AC losses in the coupling magnet come from three sources. The first source is hysteretic AC loss, which is independent of dB/dt in the magnet superconductor per cycle. The second source is coupling loss between filaments in a multi-filament superconductor, which is proportional to dB/dt. The third source is the eddy current loss due to coupling among the superconducting coil, the mandrel and support structure, which is also proportional to dB/dt in the coil. During charging, the AC losses from the mandrel and the support structure are expected to be quite small compared to the hysteretic AC losses. During a rapid discharge of any of the MICE magnets the AC losses from the mandrel and support structure can be expected to be up to 8 times larger than that during magnet charging. The heat load due to AC losses and its effect on the cooling system during charge, discharge and fast discharge are discussed in this section.

4.3.2.1 Charging process

The charging time of the coupling coil is 13950 seconds. Base on the FEA analysis results, the total AC losses in the coupling coil during charge as a function of time is shown in Figure 4-3-1.

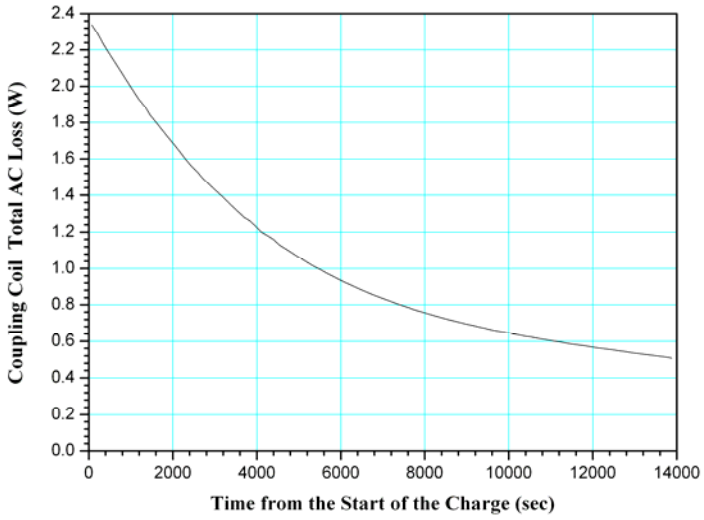

Fig 4-3-1. The total AC loss for the coupling magnet during charging as a function of time

The average hysteretic AC loss is 0.91 W, and the eddy current loss in mandrel and banding is 0.091 W. The superconductor coupling losses have been neglected because they are very low. The total AC losses in the coupling coil during charging are1.01 W. At the beginning of charge, the total AC losses can reach 2.3 W. The total thermal energy released by the coupling magnet due to the AC losses in the coupling coil and the mandrel is 14.3 kJ.

As one can see from Figure 4-3-1, the AC losses can be quite high particularly at the beginning of the charge. Even with penetration effects considered, the coupling magnet AC losses will be above

1 watt early in the charge. This level of AC losses plus the static losses, which are close to 3W, is almost equal to the cooling capacity of two coolers. However, late in the charge process, the margin of the cooling capacity will increase due to the decreasing of AC losses. So a little or even no helium will be vented during charge of the coupling coil with 10 V voltage across the power supply.

4.3.2.2 Discharging process

The discharging time of the coupling coil is 13790 seconds with constant 8 V voltage across the discharging diodes. Base on the FEA analysis results, the total AC losses in the coupling coil during discharge as a function of time is shown in Figure 4-3-2.

The average hysteretic AC loss is 0.91W, and the eddy current loss in mandrel and banding is 0.094 W. The superconductor coupling losses have been neglected because they are very low. The total AC losses in the coupling coil during discharging are about 1.01W. Similar with the process of charge, a little or even no helium will be vented during charge of the coupling coil with 8 V voltage across the power supply.

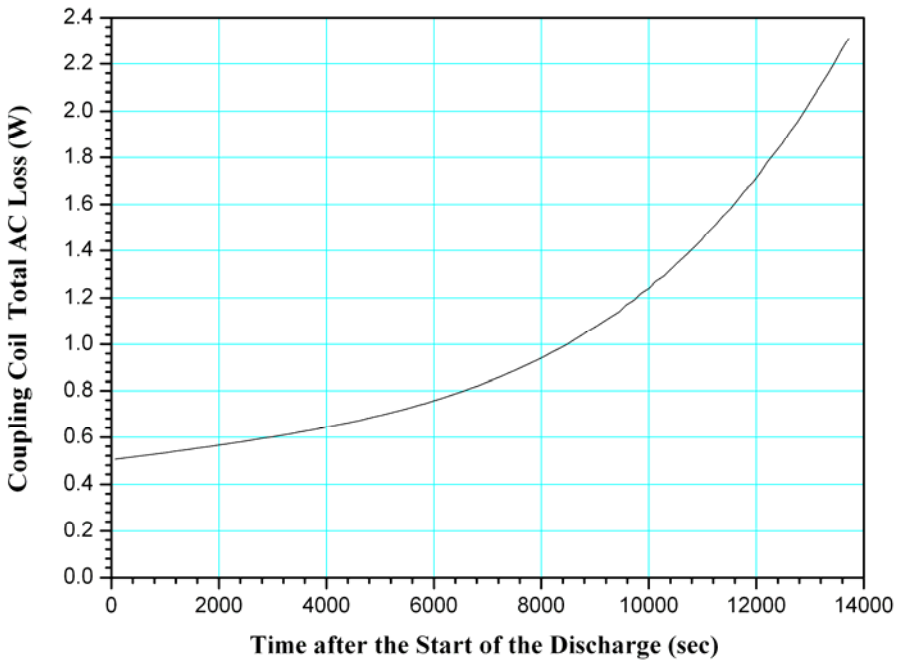

Fig 4-3-2 The total AC loss for the coupling magnet during discharging as a function of time

4.3.2.3 Fast discharging process

It's desirable that one be able to discharge the magnet rapidly, particularly during a power outage or when the tops of the HTS leads get too hot. A fast-discharge will be induced by switch a number of diodes across the coupling coil. This amount of resistance across the coil for a fast discharge is determined by the number of diodes in the quench protection system （using ~4 volts per diode） The voltage of 22 diodes at 300 K (~ 1volt per diode) is too low to trigger the quench protection

diodes and quench the magnet.

The fast discharging time of the coupling coil is 5395 seconds with constant 22 V voltage across the discharging diodes. The hysteretic AC loss in the coupling coil during fast discharging as a function of time is shown in Figure 4-3-3. The average AC loss is 2.95 W during a fast discharge. At the end of fast discharge, the hysteretic AC loss is as large as 6.3 W without considering the effect of penetration. During a fast discharge, the total thermal energy released by the coupling magnet due to the AC losses in the coupling coil and the mandrel is nearly 15.6 kJ. This can only be removed by boiling away about 6.4 liters liquid helium around the magnet. Boiling helium around the magnet is the only option for keeping the magnet cold during a rapid discharge. The sensible heat of the boiled helium can be used to keep the top of HTS leads cold during a rapid discharge, which is discussed in detail later in Section 4.2.

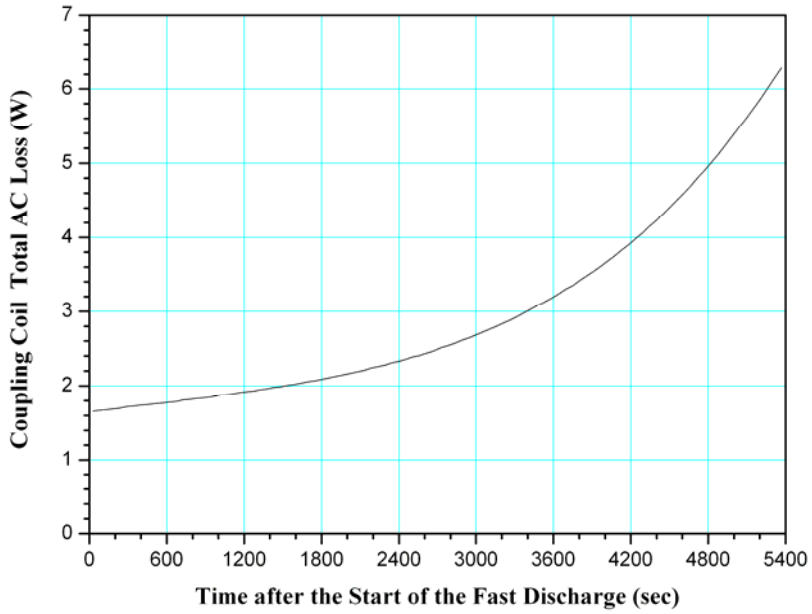

Fig.4-3-3 The total AC loss for the coupling magnet during fast discharging as a function of time

4.3.3 Temperature distribution in the coupling coil

Because the temperature margin in the coupling magnet is relatively low at its maximum design current in the flip mode at p = 240 MeV/c and b = 420 mm, it is important to reduce the temperature drop between the hot spot in the magnet and the inner surface of the cooling tubes. The temperature distribution in the coupling coil was studied for steady operating state (<0.1K). The temperature distribution on the cold mass are shown in Fig. 4-3-4.

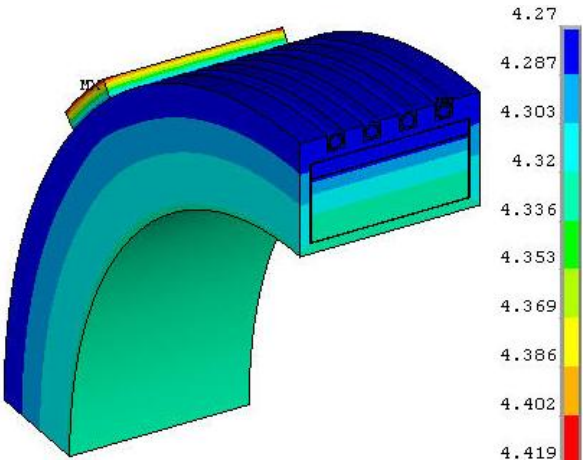

Fig. 4-3-4a Temperature in cold mass

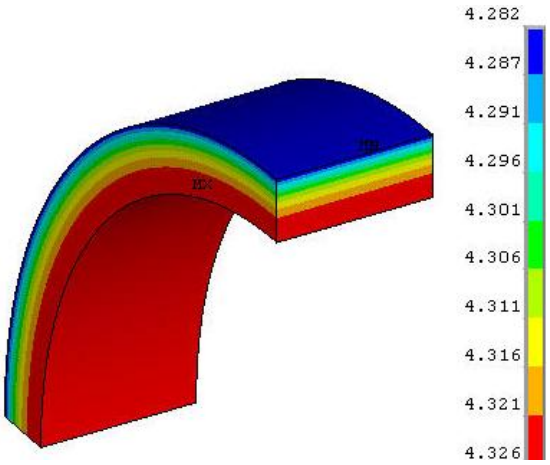

Fig. 4-3-4b Temperature in coil winding

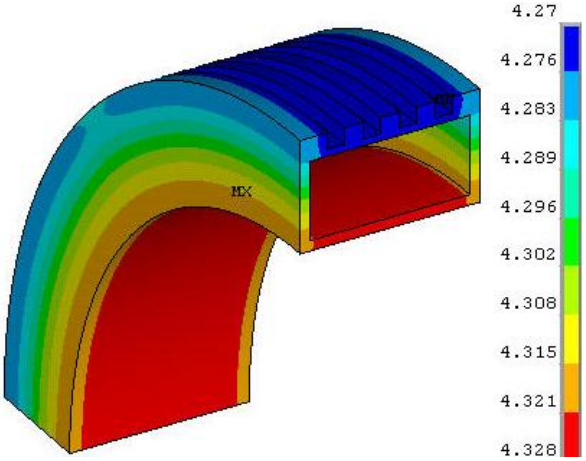

Fig. 4-3-4c Temperature in mandrel

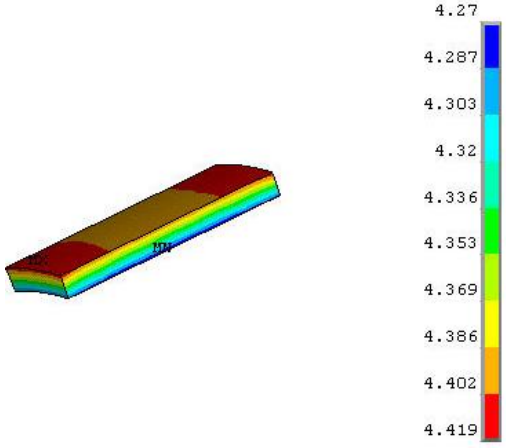

Fig.4-3-4d Temperature in cold base

The peak temperature happens on the upper surface of the cold base for the cold mass support, which is 4.419 K, due to the relatively smaller thermal conductivity of 304 stainless steel compared to 6061T6 aluminum alloy. The peak temperature difference between the hot spot on the coil inner surface where is high field region and the inner surface of the helium tubes is 0.058 K, which is less than 0.1 K according to the specification.

4.3.4 Helium inventory

During normal operation, liquid helium is contained mainly in cooling tubes, a LHe distribution vessel at the bottom of the coil assembly, a LHe collection vessel on the top of the magnet, two cryocooler condensers and LHe supply pipes.

Table 4-3-3. Helium inventory in the cryostat

	Volume (L)
LHe supply pipe	~1.0
Cooling tubes	~8.0
LHe distribution vessel	~11.0

LHe collection vessel	~7.5
Cooler condensers	~1.8
Total	**29.3**

The total volume of LHe in the cryostat during normal operation is about 29 liters. According to the above analyses, during the fast discharge process in the even of power failure, in order to keep the HTS leads from going normal, about 10.4 liters of liquid helium will boil away to keep the warm end of HTS leads and the shield cold by using sensible heat.

4.3.5 Thermosyphon cooling system

The coupling magnet is to be cooled by two-stage cryocoolers. Because the temperature margin in the coupling magnet is relatively low (only 0.8K) at its full design current in the flip mode at p = 240 MeV/c and β= 420 mm, the key for the coil cooling is to minimize the temperature drop between the second stage cold head of cooler and the hot spot in the magnet. The coil cooling circuit must be arranged as a thermal siphon cooling system driven by gravity force, as shown in Fig. 4-3-5. The coupling coil cooling system mainly consists of cryocooler and helium re-condenser, piping system for various operations, liquid helium vessels and safety device.

For each coupling solenoid, two 1.5W cryocoolers (e.g. model PT415 by Cryomech) must be used to provide the cryogen-free refrigeration in terms of heat loads in the magnet and effect of stray magnetic field on the cooler during normal operation. The first stages of the coolers will provide the cooling for radiation shields and their supports, warm ends of HTS leads, and thermal intercepts for cold mass supports, neck tubes and instrumentation wires. The second stages of the coolers will re-liquefy the helium from the magnet after the cooling circuit has been filled with liquid helium.

During normal operation, the liquid helium from the bottom of the cooler condenser flows along a supply pipe with inner diameter of 16 mm, enters a LHe collection vessel of about 11.0 liter at the bottom of the cold mass, and then is delivered into seven tubes with inner diameter of 21 mm each nested into the coil case. The length of each cooling tube is of the order of 2.5 meters. The boil-off helium gas along the cooling passage is collected into a vessel of about 7.5 liter at the top of the cold mass, and then fed back to the condenser pot for re-liquefy through a separated pipe.

For cool down and off normal operations, there are two neck tubes with thermal intercepts connected to the first stage of the cooler. The entrance pipe of 20 mm ID for cryogens is connected to the magnet at the bottom and at one end of the magnet. The exit or vent pipe of 20 mm ID is from the upper side of the helium condenser, and then connected to a coiled heat exchanger attached to the first-stage cold head. The coiled heat exchanger is used for pre-cooling of thermal shields during cool down and cooling of the HTS leads from burning out in the even of power failure. Both of the neck tubes are connected to the outside of the cryostat by two bayonets. The neck tubes are also served as quench vent. The entrance tube will contain a rupture disc as a relief device set between 32 psig and 44 psig. The vent tube is connected to a relief valve set at 29 psig or lower.

The helium tubes are designed at a pressure rating of 20 bar (290 psig), and the design external working pressure is 1 bar (15 psig) for vacuum leak checking. The cooling tube system is to be leak tight to helium at 1 atmosphere at room temperature at the rate of 10^{-10} Pa-m^3/s (10^{-9} mbar-liter/s), and designed in accordance with the ASME Pressure Vessel Code and Chinese Pressure Vessel Code.

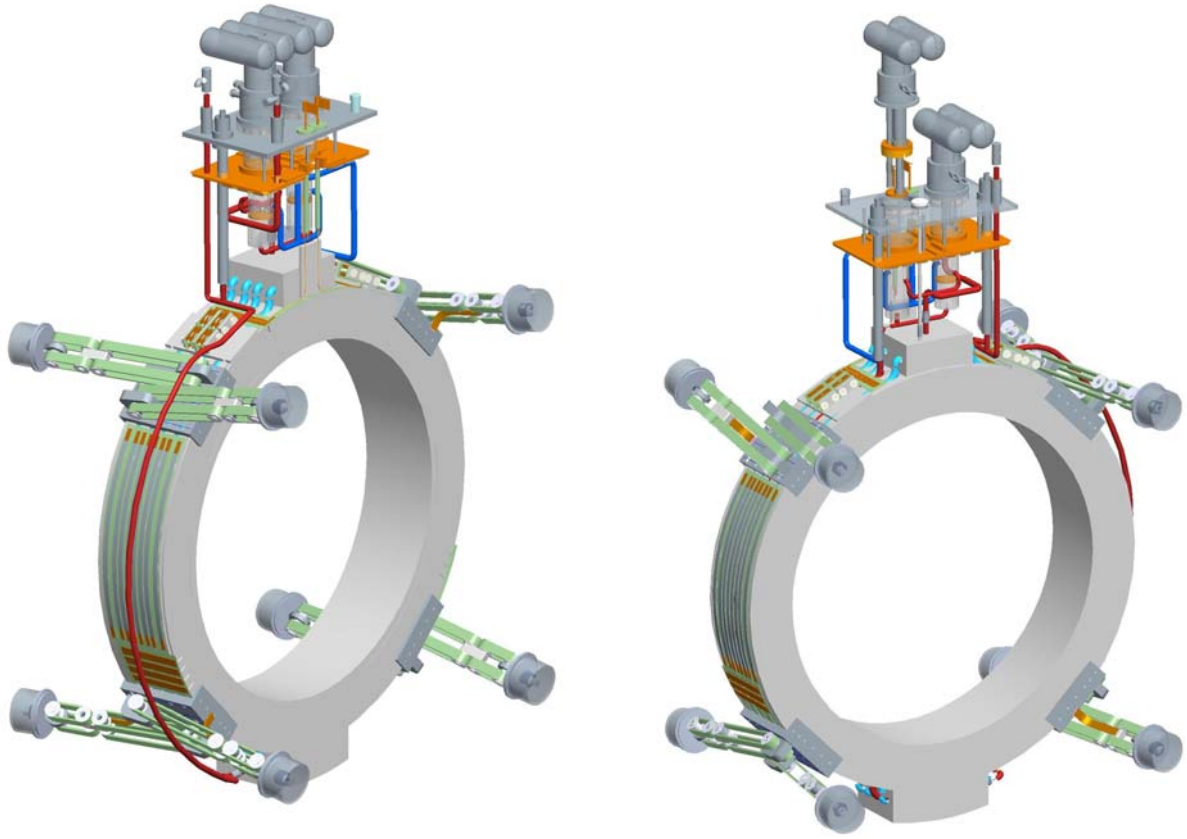

Fig. 4-3-5 Cooling system for coupling magnet

4.3.6 Drop-in cryocooler and re-condenser

There are two types of cryocoolers with cooling capacity of 1.0W to 1.5Wat 4.2K commercially available presently, the G-M type and the PTR type. A pulse tube cooler has the advantages of low vibration, long-term life and less sensitive to magnetic field compared with a GM cooler. The cold heads and GM cooler drive units cannot withstand a magnetic field of more than 0.1 T. The only part of a pulse tube cooler that is sensitive to magnetic field is the drive motor for its rotary slide valve. This motor can be shielded for operation in the field up to 0.5 T or can be moved to a location up to 1-meter from the rest of the cold head assembly, but the cooler capacity is reduced about 10 percent. The 2nd stage regenerator material is affected by the field over about 1.5 T. The cooler capacity is reduced 10 percent at 2 T.

For each coupling solenoid, two 1.5W pulse tube cryocoolers (e.g. model PT415 by Cryomech) must be used to provide the cryogen-free refrigeration in terms of heat loads in the magnet and effect of stray magnetic field on the cooler during normal operation. The combined

refrigeration power will be 3.0W at 4.2K and 110W at 60K (50Hz) or 90W at 50K. The PTR coolers will operate with the cold heads down and be mounted on top of the cryostat vacuum chamber.

There are two ways to mount the PTR coolers into the coupling magnet cryostat. One is to directly place the cooler into the cryostat, and the cooler shares the same vacuum with the cryostat, as shown in Fig. 4-3-6a. The other is to adopt so called drop-in mode, and the cooler is isolated from the cryostat vacuum by thin-wall helium-filled stainless steel sleeve in order to eliminate the additional conduction heat through it, as shown in Figure 4-3-6b and Figure 4-3-7. For the drop-in cooler, the key element is free-convection heat transfer between the cooler tubes (both regenerator and pulse tubes) and the sleeves. The arrangement shown in Figure 4-3-x allows the heat leak down the sleeves to be intercepted by free-convection currents between the sleeves and the cooler tubes. This arrangement allows for the easy removal of the cooler from the magnet cryostat. Considering possible shipment load imposed on the cooler during long-term transportation, it must be demountable from the cryostat to avoid potential damage. So, the drop-in cooler is finally adopted for the couple magnet cooling.

The 1st-stage tapered joint of the drop-in cooler allows heat from the leads, the thermal radiation shield, and the cold mass supports to the cooler 1st stage cold head. The condenser section is the holes in the copper piece that comprises the second-stage of the cooler. The performance of the PT-415 in the drop in configuration was measured this May in USA, and the cooling capacity of only 1.3W was obtained.

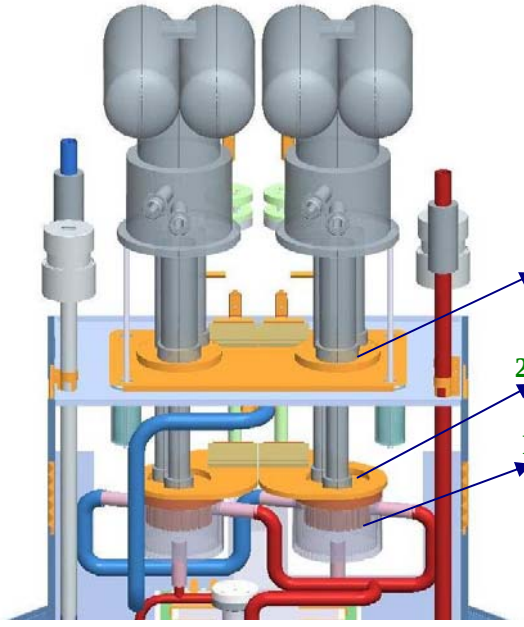

Fig. 4-3-6a PTR cooler and re-condenser

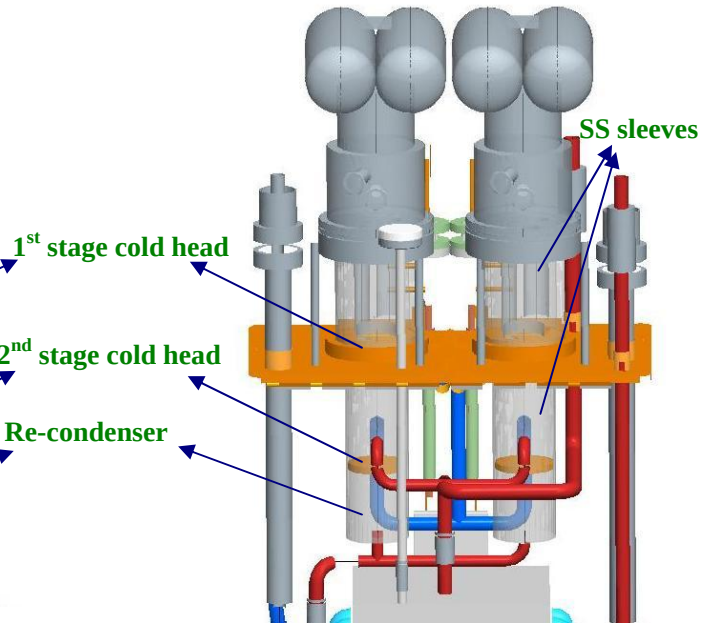

Fig.4-3-6b Drop-in cooler and re-condenser

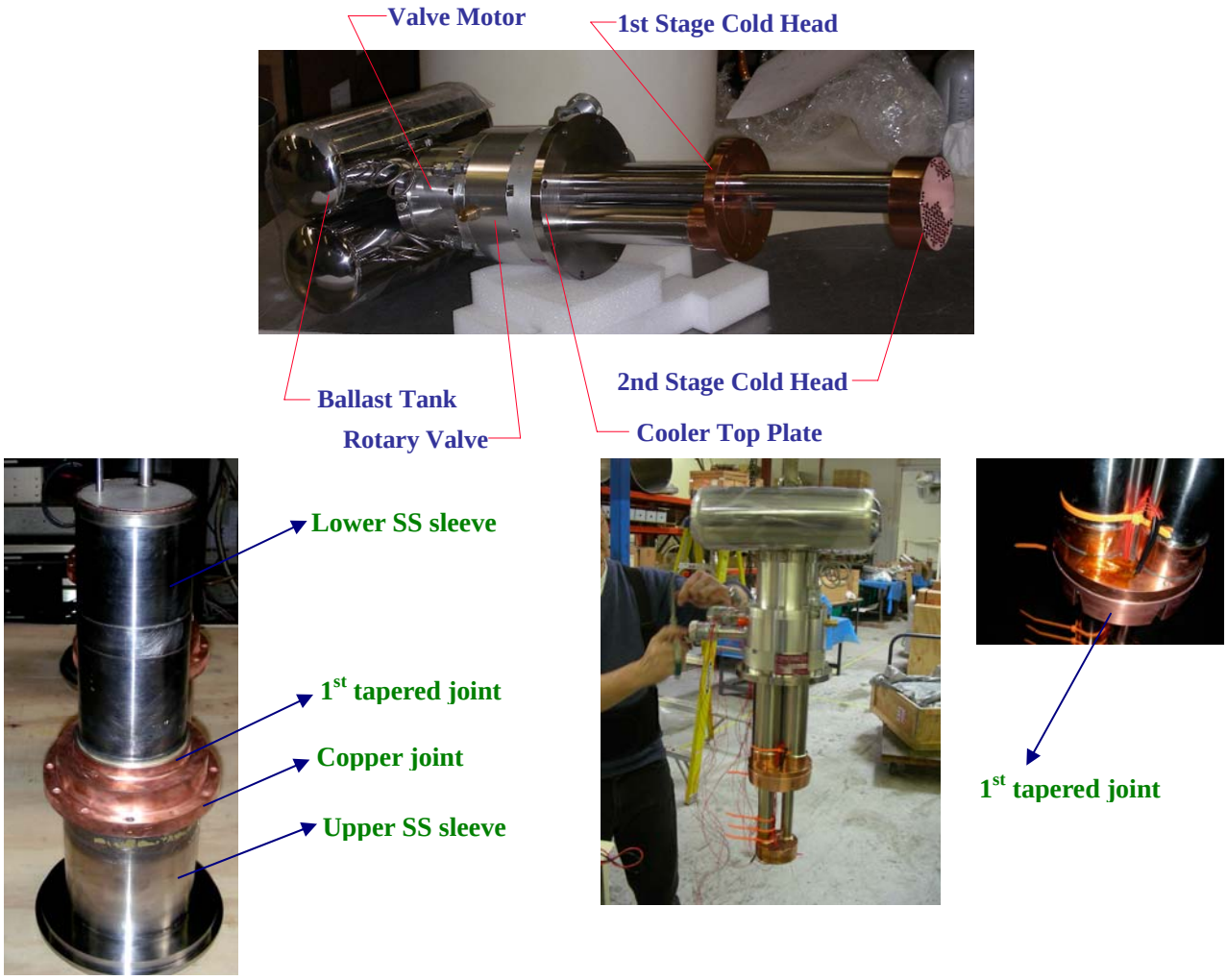

Fig.4-3-7 Drop-in PTR415

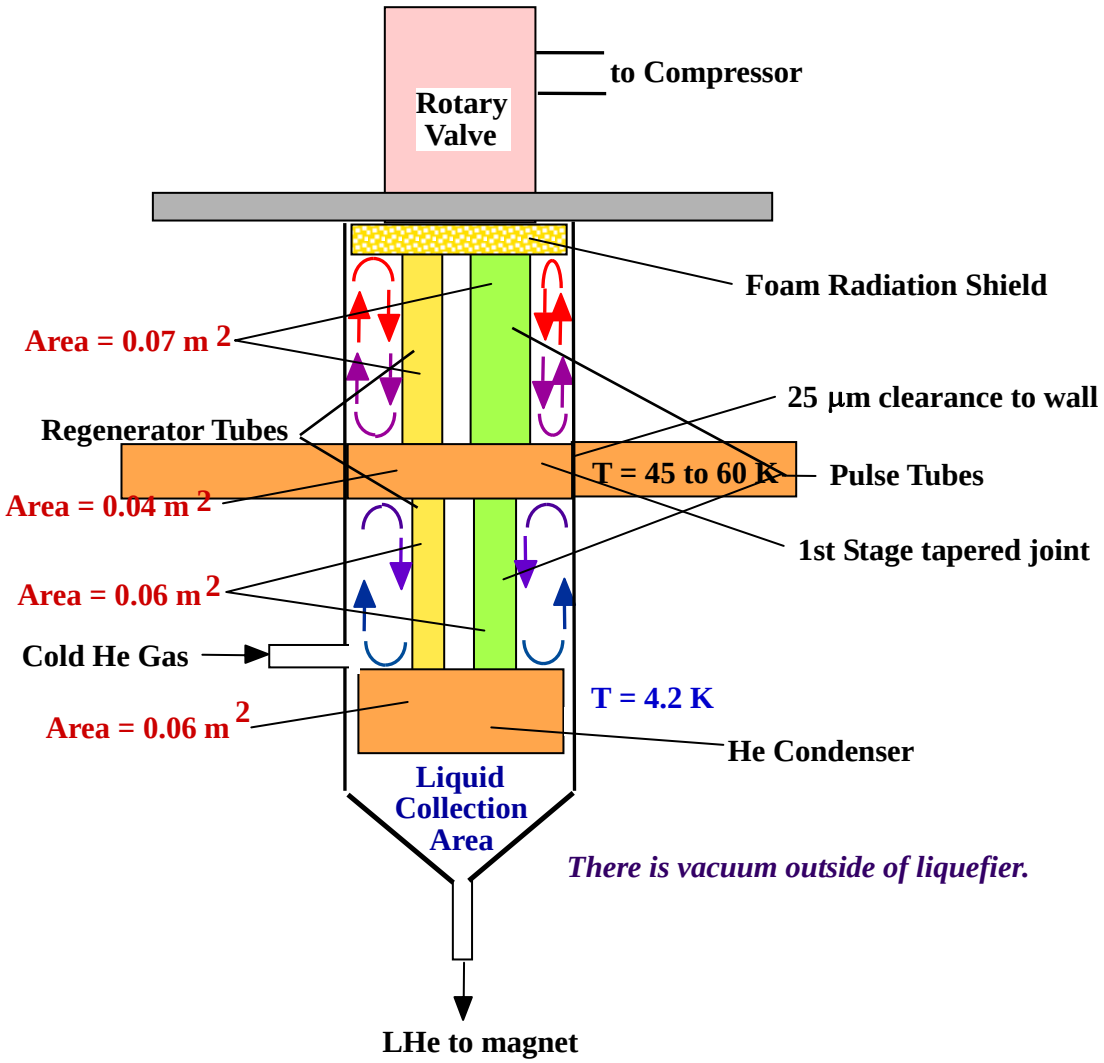

Fig. 4-3-8 An illustration of drop-in cooler

4.3.7 Effects of stray magnetic field on cryocooler drive motor

The only part that is sensitive to the magnetic field for the pulse tube cooler is the rotary slide valve drive motor. The magnetic field around the valve motor is 0.19~0.21 T and that around the PTR cooler second stage cold head is 0.6 to 0.7 T as shown in Fig.3-1-5. The highest field at the cooler occurs when the magnet is in the flip mode at p = 240 MeV/c and beta = 420 mm.

The performance of the valve motor will be affected under the field higher than 0.05T. Hence, there are two ways to reduce the stray field at the rotary valve motor: 1) The valve is moved to a low field location up to 1 meter from the rest of the cold head, which will reduce the cooler performance on both stages by 10 percent. 2) The valve motor is shielded with an iron shield. The latter is to be adopted, because the cooler performance on either stage is important for the magnet cooling. The induction in the motor with a 33 mm thick shield will be lower than 0.05 T. A rotary valve with thick iron case instead of aluminum case fabricated by the cooler vender will be applied on the coupling magnet.

4.4 Thermal shields

The intermediate temperature shields are to be used in the coupling magnet in order to reduce the heat leakage directly from the room temperature to 4.2K cold mass. The shields consist of inner shield, outer shield, and two end shields as shown in Fig.4-4-1. The outer shield is divided into two parts: upper neck part and main part, which are connected together by flexible Al strips for releasing additional thermal stress during cooling down. The upper neck part is welded to the copper plate attached to the cold heads of cryocoolers by copper-aluminum transition parts. It is supported to the top plate of the cryostat. The neck shield can be disassembled on both its front and back sides for maintenance of HTS leads. The main shields around the magnet cold mass are to be supported individually by 8 tension rods. The shields are made of 1100 aluminum and to be conduction cooled by the first stage cold heads of the magnet coolers. The highest temperature on the shields is required less than 80K.

The shields are designed so that no closed current loops are formed around the solenoid during a magnet quench, charging and discharging. They are slit into two parts and covered by non-conductive (electrically) material such as G-10 so that radiation from room temperature does not pass through them. They will be insulated with multilayer insulation (MLI) of 50~60 layers.

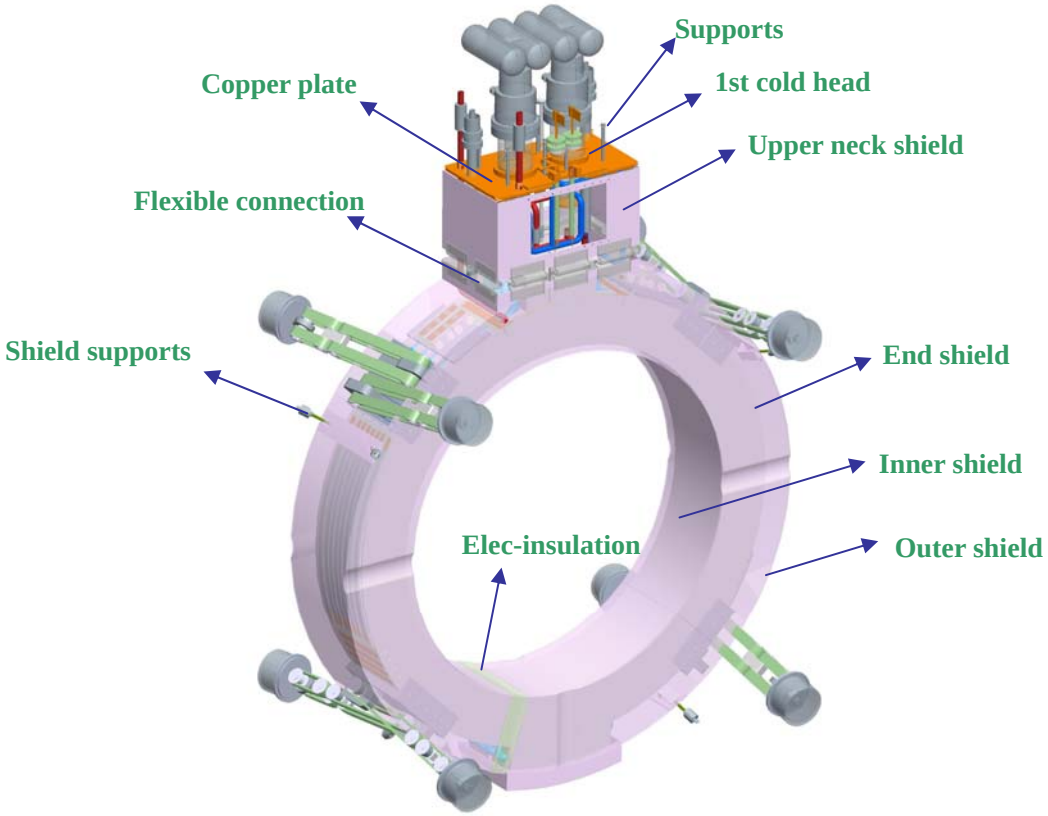

Fig. 4-4-1 3D view of thermal shields in coupling magnet cryostat

4.4.1 Thermal analyses

The thermal shields are to be cooled by conduction through the copper plates attached to the 1st

cold heads of cryocoolers. The hot spot temperature on the shields should be less than 80K. The heat leakage from room temperature to the shields includes radiation heat, conduction heat form intermediate temperature intercepts of cold mass supports, conduction heat form shield supports, conduction heat from intercepts of cooling tubing, vent piping, instrument tubing, neck tubes and instrument wires to the copper plate. The refrigerating capacity of the 1st stage of the cryocooler is 40W at 40K, 45Wat 50K, 55Wat 60K. Table 4-4-1 lists the heat leaks to the shields.

Table 4-4-1. Heat leakage to shields

	Heat load(W)
Copper leads	19.30
Cold mass supports	9.9
Radiation heat to 60K thermal shields	8.7
60K Intercepts for instrumentation wires	1.0
60K intercepts for neck tubes	4.823
Heat shield supports	4.0
Upper neck shield supports	0.62
Total	47.343

The thermal shields are considered as the symmetric and modeled as a half 3-D model as shown in Fig.4-4-2. The main dimensions of the thermal shields are shown in Table 4-4-2. The shields and flexible strips are made of 1100 aluminum, and the connection plate to the cooler and thermal intercepts to the cold mass supports are made of pure copper with RRR 60.

Table 4-4-2. Dimensions of shields

Inner shield ID (mm)	1431
Outer shield OD (mm)	2056
Shield width (mm)	389
Height/width/length of neck shield (mm)	522/389/920
Width/length/thickness of flexible strip (mm)	1500/150 /8

4.4.1.1 Assumptions

- ✧ To assume the flexible strips are straight;
- ✧ To assume no heat resistance between the copper connection plate and 1st cold head;

4.4.1.2 Operating conditions

- ✧ Radiation heat load (half of 8.5 W) is applied to all external surfaces of the model;
- ✧ Heat loads of from cold mass supports are applied to the copper blocks (1.236 W per block);
- ✧ Heat loads from shield supports are applied to the position of shield supports (2 W totally);
- ✧ Heat loads from various intercepts are applied to the connection plate.

✧ The temperature at the copper plate is set at 60K.

✧ 50W of refrigeration capacity is put onto the copper plate.

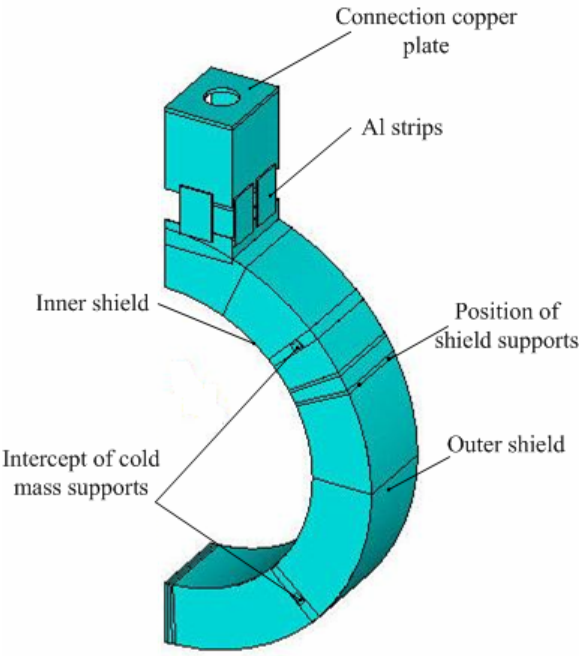

Fig. 4-4-2 FE Model for thermal shield simulation

4.4.1.3 Simulation results and analyses

Fig. 4-4-3 shows the temperature distribution on the shields with thickness of 3mm and 4 mm, respectively, when the temperature on the cold connection plate is set at 60 K. Fig. 4-4-4 shows the hot spot temperature and the temperature difference on the shields.

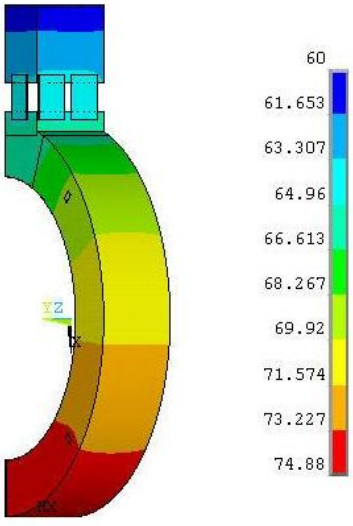

Fig. 4-4-3a Temperature on 4mm shields

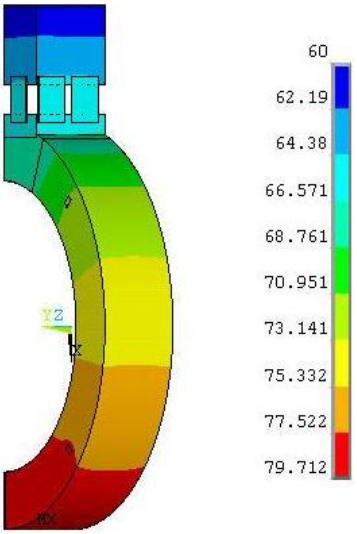

Fig. 4-4-3b Temperature on 3mm shields

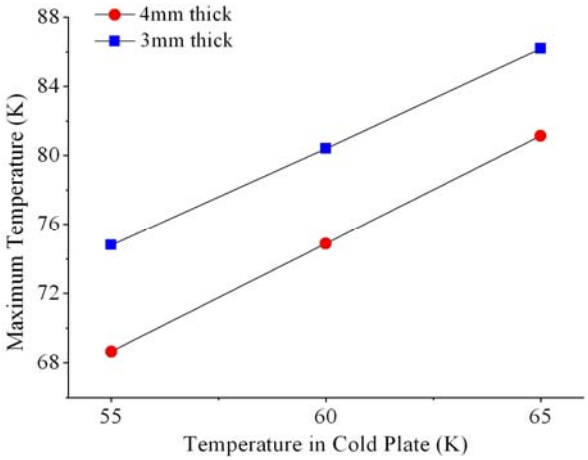

Fig. 4-4-4a Hot spot temperature on shields

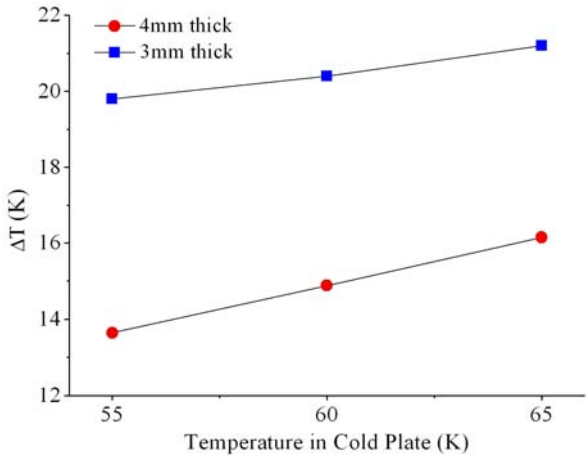

Fig. 4-4-4b The maximum ΔT on shields

From Fig. 4-4-3 and 4-4-4, one can see that the hot temperature on the shields occurs at their bottom due to the symmetric, about 75K with 4mm thickness and 80K with 3mm thickness. With the increasing of the shield thickness, the maximum temperature difference drops down, about 15K with 4mm thickness and 20K with 4mm thickness at 60K of connection plate. The shields are to be designed as the thickness of 4 mm.

4.4.2 Thermal shield flexible connection

As shown in Fig.4-4-1, the Al shields are to be conduction-cooled through the upper neck part connected to the first stage cold heads of cooler. During cool down, there exists stress induced by thermal contraction between the shields and the connection copper plate, as well as weight of the shields (about 120kg). In order not to affect the performance of cryocoolers, the flexible connection is applied for the shields, and the shields are divided into two parts which supported respectively. The flexible connection is composed of Al strips with both ends welded to the upper neck shield and the main shield separately, which is designed to keep the temperature difference along the strips at 2 to 2.5K. Fig.4-4-5a shows the structure of the flexible connection.

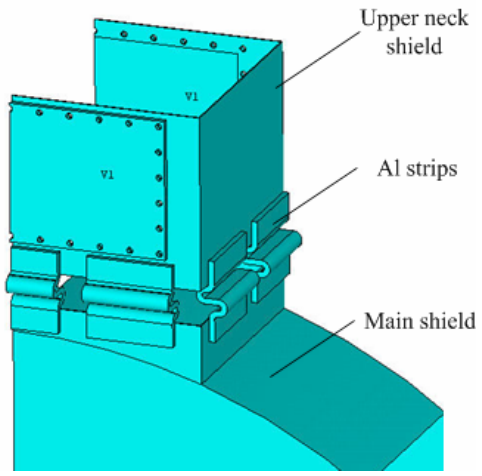

Fig 4-4-5 3D view of flexible connection for shields

Table 4-4-3. Dimensions of flexible connection

Thickness (mm)	8
Welding length (mm)	40
Total width (mm)	1500
Length of flexible strip (mm)	150
ΔT	<2.0K

The dimensions of the flexible connection are calculated and shown in Table 4-4-3. Fig. 4-4-6 shows the relationship between the conduction cross-sectional area and temperature difference along the connection at different length of flexible part. Fig.4-4-7 presents the relationship between the total width and the total temperature difference from the neck shield to the lower end of the connection at different thickness of the connection.

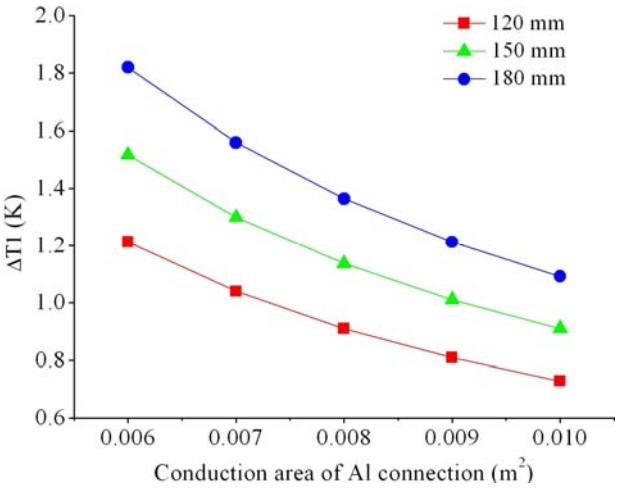

Fig. 4-4-6 Relationship between the conduction cross-sectional area and temperature difference along the connection at different length of flexible part

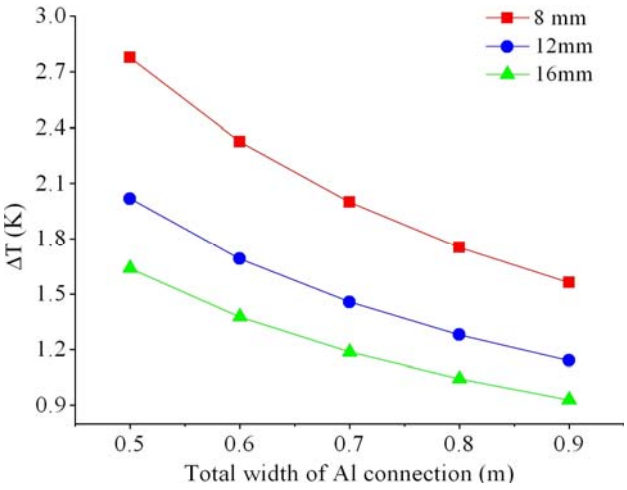

Fig. 4-4-7 Relationship between the total width and the total temperature difference from the neck shield to the lower end of the connection at different thickness of the connection

4.4.3 Supports for thermal shields

The main shield is to be supported by 4 pairs of supports, four located at each end shield, which is shown in Fig 4-4-1. First, the shield supports are required to withstand shipping loads of 2.5g at any direction at room temperature as well as its weight. Second, after cooled down, they must withstand a certain amount of forces due to shrinkage of the shield towards mechanical center besides its weight. Third, in order to reduce the heat leakage through the supports, they should be made of the material with small thermal conductivity. Therefore, the supports are mainly made from the G-10 rod and the stainless steel base. The G-10 rod will be glued into the SS base by epoxy. The structure schematic is shown in Fig 4-4-8. The supports will be sealed by a welded cap at the warm end after the final alignment at room temperature before transportation. The tensile stress applied to the supports is transferred as the shear stress of epoxy, so the maximum tensile force is set as the

shear force of epoxy. The designed main dimensions of the supports are listed in Table 4-4-4. The maximum shear stress on epoxy at one end is up to 7kN, which is acceptable. The heat load through each support is calculated as 0.38W.

Table 4-4-4. Dimensions of shield supports

G-10 rod diameter D (mm)	8
Overlapping depth L2 (mm)	15
Length L1 (mm)	20

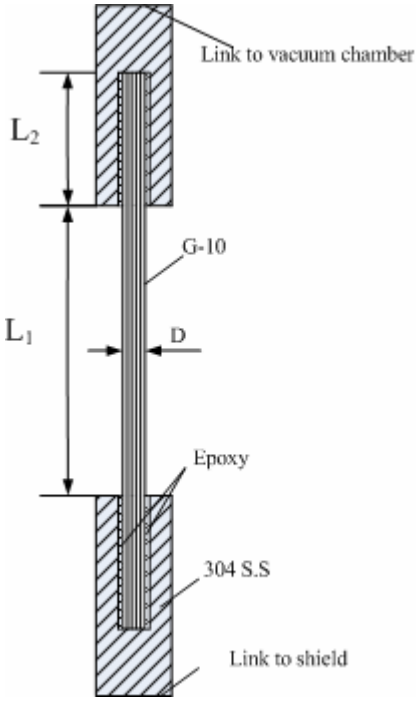

Fig. 4-4-8 The schematic of shield supports

4.5 Vacuum chamber and interface design

The 300K vacuum chamber consists of inner vacuum shell, end flanges and outer vacuum shell. The inner vacuum vessel is 1387 mm in inner diameter, 489 mm wide and 4 mm thick. The outer vacuum shell is divided into two parts, one is rectangular neck to mount the cryocoolers, and the other is cylindrical part. The cylindrical shell is 2278 mm in outer diameter and 4 mm wide. Two opposite side walls in the neck are removable for easy disassembly and maintenance. There are three indented sections on each end flange for the 130 mm OD coupler tubes of RF cavities. The indented section is 4 mm thick with a radius of 68 mm. The non-magnetic vacuum vessel made of 304SS is designed to satisfy both the ASME pressure vessel code and Chinese pressure vessel code (see details in section 4.7). The relief valve setting will be 0.14 bar (2 psig). The rupture disc relief pressure will be 0.3 bar (4.4 psig). The whole vacuum vessel assembly will be vacuum leak tight to helium at room temperature at 1 atmosphere at the rate of $1x10^{-8}$ Pa·m^3/s ($1x10^{-7}$ mbar·liter/s).

The magnet current leads and all the instrumentation wires are to be brought out of the cryostat on the rectangular neck, as well as the neck tubes for the rupture disc and the relief valve for the magnet cooling system and two bayonets for cool down piping. A 40-mm diameter vacuum pump out port for the cryostat vacuum is provided. The pump out port will have a flange to allow a pump out valve and relief valve to be attached for the vacuum cryostat space. The room-temperature ends of the cold mass supports are mounted on the vacuum vessel through a stainless steel sleeve. The major force imposing on the vacuum vessel is the pre-tension force transferred from cold mass support straps. The reinforcement around the stainless steel sleeve connection is designed as shown in Fig. 4-5-1. The FEA on the stress and deflection on the vacuum vessel is worked out by using ANSYS.

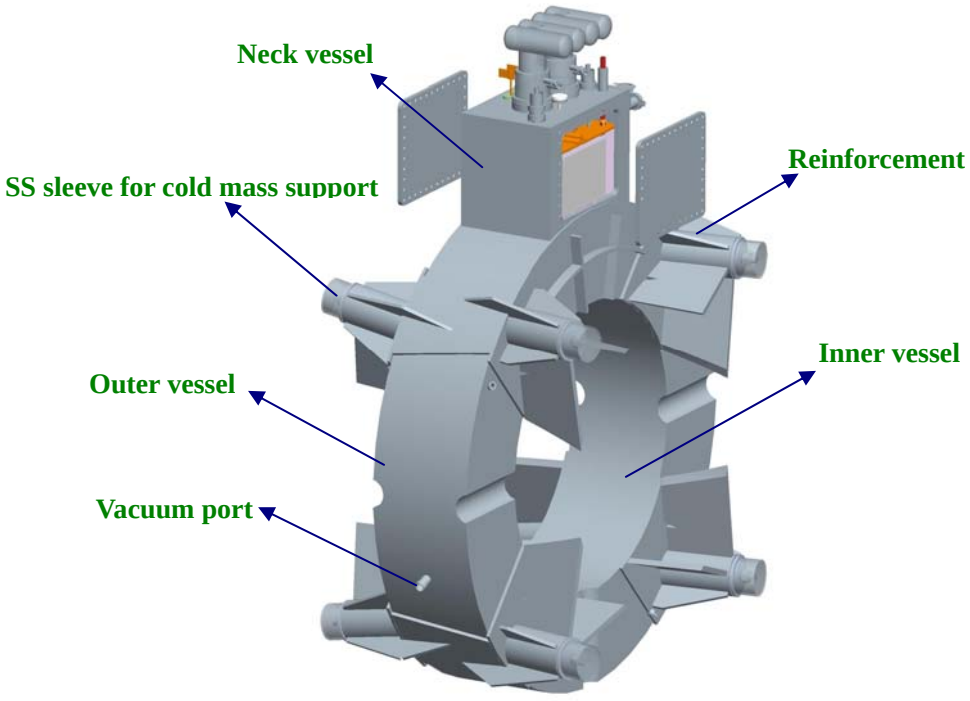

Fig. 4-5-1 A 3D view of MICE coupling magnet vacuum vessel

4.6 Instrumentation and feedthrough design

Instrumentation

For each coupling magnet, there will be installed: 15 to 17 Platinum temperature sensors, 13 to15 Cernox temperature sensors, one liquid helium level gauge, one DC heater of 3W, one pressure transducer, and 26 voltage taps.

4.6.1.1 Temperature sensors

The temperature sensors' location on each coupling magnet is shown in Fig.4-6-1.

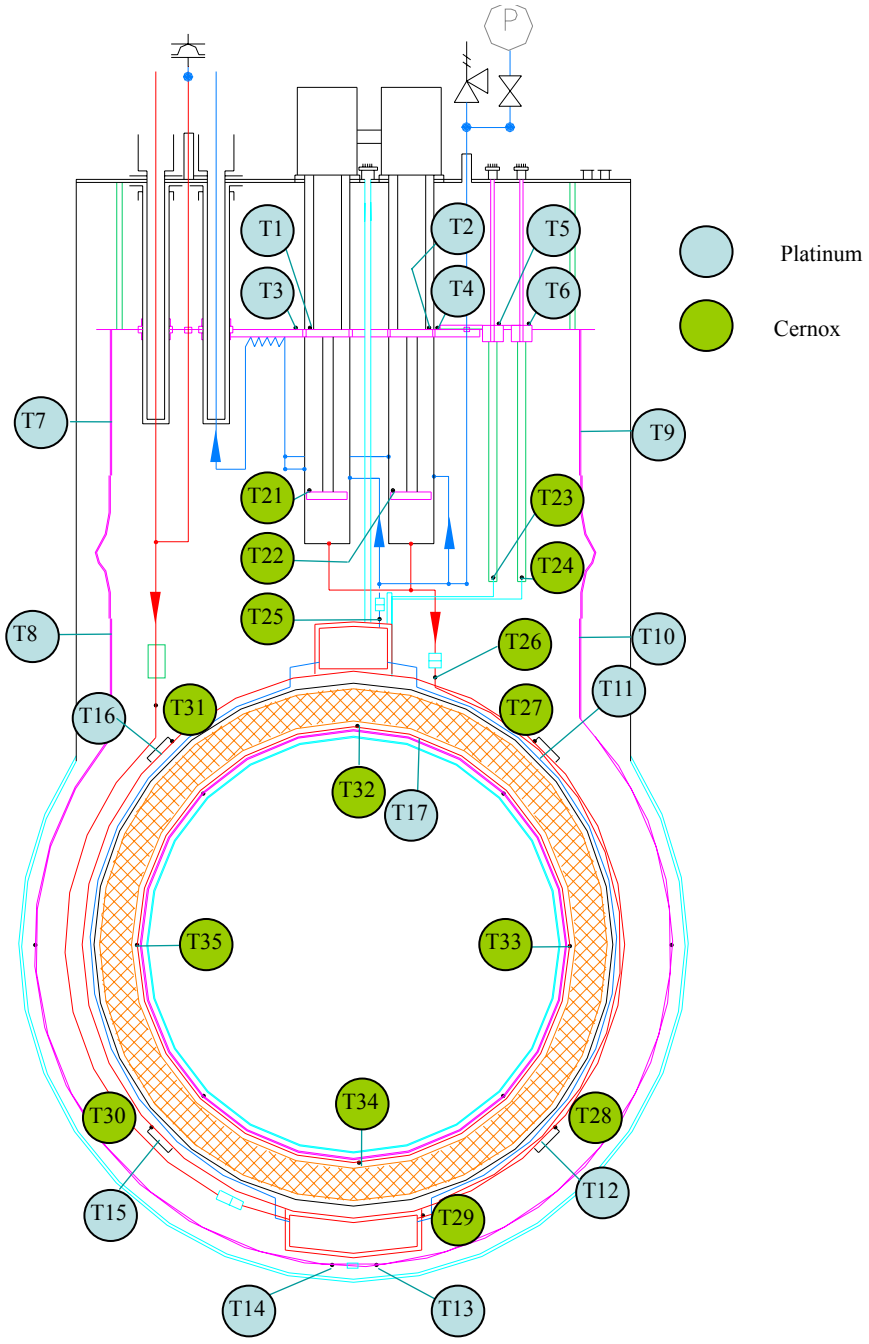

Fig. 4-6-1 Temperature sensors in coupling magnet

The temperature sensor is used to monitor the temperature in the coupling magnet during normal operation and off normal operation such as cold down, quench and warm up. Two kinds of temperature sensors are to be applied. One is kind of standard platinum resistance thermometer to be used for temperature monitoring ranged from 40K to 300K, which has interchangeable accuracy of 0.25K and typical magnetic field-dependent temperature error ΔT/T at 40K and 8 Tesla less than 3%. The other is kind of Cernox RTD for the temperature range of 3.5K to 300K, which has low magnetic field-induced errors, high sensitivity at low temperature and good sensitivity over a broad range. The Cernox sensors on piping are suggested to be mounted on aluminum tubes but stainless steel tube if possible. The sensors at cold ends of HTS leads should be electrically insulated from the leads. During cool down process, in order to control the cool down speed of the coil cold mass less than 30~40K, two sensors are to be placed on the helium supply and return piping, and the backups are recommended.

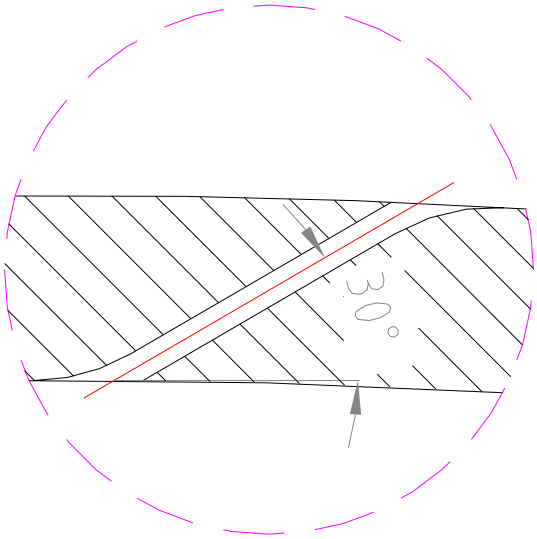

Fig. 4-6-2 Lead hole of heater in the coil bobbin

4.6.1.2 Helium level meter

A liquid helium level sensor is put inside the top helium collection vessel of the coil assembly to monitor the liquid level during operation. To avoid the helium leakage resulting from using the feed-through at cryogenic temperature, an SS instrument tube is connected to the top flange of magnet vacuum vessel from the helium collection vessel, through which the level sensor may be inserted into or demounted from the helium vessel.

4.6.1.3 Electrical heater

A 20×10×0.1mm Kapton film-coated heater of 60 ohms will be installed on the bobbin along the central line in axial direction, which may supply 3W heating into the coil cold mass. The heater will be placed between the coil bobbin and the G-10 insulation sheet, and its lead will be brought

out from a declining-drilled hole as shown in Fig. 4-6-2.

4.6.1.4 Pressure transducer

A pressure transducer is to be installed on the helium return tubing from the magnet to the cooler re-condensers in order to monitor the pressure in the cooling system.

A vacuum gauge that can operate in a magnetic field of 1.5 T will be mounted to the cryostat vacuum port.

4.6.1.5 Magnet voltage taps

The purpose of voltage taps is to provide coil resistance measurement during the magnet cool down (with a small current running through the coils) and to provide voltage monitoring when the magnet coil is charged, discharged and during a quench. Totally 13 pairs of voltage taps are to be adopted for the coupling magnet, which include 1 pair to be attached at the terminals of the coil, 8 pairs for the quench protection sub-sections, and 4 pairs for power leads.

Feed-through

The wires from sensors will be fed to room temperature electrical feed-through on the vacuum chamber. Two kinds of feed-through will be applied. One with 1kV withstand voltage is for instrumentation wires, including temperature sensor, liquid level sensor and heater. In total 4 feed-through of 32 pins and 1 feed-through of 4 pins are needed as listed in the Table 4-6-1. One with 5kV withstand voltage is for voltage taps and 3 feed-through of 10 pins are needed as listed in the Table 4-6-2.

All the feed-through should meet the vacuum leak tightness requirement. The instrumentation wires that come through the cryostat vacuum will have thermal interceptions to the first stage cold heads of the coolers. The voltage taps should be coated with insulation which can stand 5kV voltage to ground inside the vacuum vessel.

Table 4-6-1. Feed-through pin assignments for instrumentation wires

Tag No.	Sensor Type	Location	Pin no. of Feedthrough
T1	Platinum RTD	1st stage of 1st cryocooler	F01-1, 2, 3 ,4
T2	Platinum RTD	1st stage of 2nd cryocooler	F01-5, 6, 7, 8
T3	Platinum RTD	50K thermal sink plate	F01-9, 10, 11, 12
T4	Platinum RTD	50K thermal sink plate	F01-13, 14, 15, 16
T5	Platinum RTD	Joint of copper lead and HTS lead	F01-17, 18, 19, 20
T6	Platinum RTD	Joint of copper lead and HTS lead	F01-21, 22, 23, 24
T7	Platinum RTD	Outer 50K thermal shield at neck	F01-25, 26, 27, 28
T8	Platinum RTD	Outer 50K thermal shield at neck	F01-29, 30, 31, 32
T9	Platinum RTD	Outer 50K thermal shield at neck	F02-1, 2, 3 ,4

T10	Platinum RTD	Outer 50K thermal shield at neck	F02-5, 6, 7, 8
T11	Platinum RTD	Outer 50K thermal shield	F02-9, 10, 11, 12
T12	Platinum RTD	Outer 50K thermal shield	F02-13, 14, 15, 16
T13	Platinum RTD	Outer 50K thermal shield	F02-17, 18, 19, 20
T14	Platinum RTD	Outer 50K thermal shield	F02-21, 22, 23, 24
T15	Platinum RTD	Outer 50K thermal shield	F02-25, 26, 27, 28
T16	Platinum RTD	Outer 50K thermal shield	F02-29, 30, 31, 32
T17	Platinum RTD	Inner 50K thermal shield	F04-29, 30, 31 ,32
EH1	Electrical heater	Inner diameter of bobbin	F05-1, 2
T21	Cernox-1050	2nd stage of 1st cryocooler	F03-1, 2, 3 ,4
T22	Cernox-1050	2nd stage of 2nd cryocooler	F03-5, 6, 7, 8
T23	Cernox-1050	Cold end of HTS lead	F03-9, 10, 11, 12
T24	Cernox-1050	Cold end of HTS lead	F03-13, 14, 15, 16
T25	Cernox-1050	Gaseous helium return tube of cold mass	F03-17, 18, 19, 20
T26	Cernox-1050	Liquid helium injection tube of cold mass	F03-21, 22, 23, 24
T27	Cernox-1050	Outer diameter surface of cold mass	F03-25, 26, 27, 28
T28	Cernox-1050	Outer diameter surface of cold mass	F03-29, 30, 31, 32
T29	Cernox-1050	Bottom helium tank of cold mass	F04-1, 2, 3 ,4
T30	Cernox-1050	Outer diameter surface of cold mass	F04-5, 6, 7, 8
T31	Cernox-1050	Outer diameter surface of cold mass	F04-9, 10, 11, 12
T32	Cernox-1050	Inner diameter surface of cold mass	F04-13, 14, 15, 16
T33	Cernox-1050	Inner diameter surface of cold mass	F04-17, 18, 19, 20
T34	Cernox-1050	Inner diameter surface of cold mass	F04-21, 22, 23, 24
T35	Cernox-1050	Inner diameter surface of cold mass	F04-25, 26, 27, 28
LV1	——	Top helium tank of cold mass	F06-1, 2, 3, 4

Note: Because the temperature sensors, which are intended to mount on the 1st and the 2nd stage cold heads of cryocoolers, should be attached along with their instrumentation wires, a feed-through with at least 8 pins for each cryocooler is needed. The temperature sensor wires have to be brought out from inside the cooler sleeves with the helium-filled to the room temperature. This requires the customized fabrication of the cooler top plate. Therefore, T1, T2, T21, T22 are option for use.

Table 4-6-2. Feed-through pin assignments for voltage taps

Tag No.	Full scale	Location	Pin no. of Feedthrough
V1	0-200mV	Copper lead (+)	HF01-1
V2	0-200mV	HTS lead (+)	HF01-2, 3
V3	0-200mV	Copper lead (-)	HF01-4
V4	0-200mV	HTS lead (-)	HF01-7, 8
V5	0-20V	Both coil lead	HF01-9, 10

V6	0-20V	Coil subsection of No. 1	HF02-1, 2
V7	0-20V	Coil subsection of No. 2	HF02-3, 4
V8	0-20V	Coil subsection of No. 3	HF02-5, 6
V9	0-20V	Coil subsection of No. 4	HF02-7, 8
V10	0-20V	Coil subsection of No. 5	HF02-9, 10
V11	0-20V	Coil subsection of No. 6	HF03-1, 2
V12	0-20V	Coil subsection of No. 7	HF03-3, 4
V13	0-20V	Coil subsection of No. 8	HF03-5, 6

4.7 Pressure vessel & pressure piping design and ASME code verification

In the coupling coil cryostat, the vacuum vessel and helium vessels are designed as pressure vessels. All the helium pipes in the cryostat are pressure pipes. The helium vessels are designed at a pressure of 4 bara (44 psig). The helium pipes are designed at a pressure of 20 bar (290psig). The vacuum vessel is designed at external design working pressure of 0.1MPa (15psi.). The design for them is required to conform to the ASME Pressure Vessel Code.

Herein ASME code for shell stress and end plates are employed to verify the ASME stress and thickness requirement and then compare with design thickness. The verification results show that the design satisfy ASME code, and conservative.

4.7.1 ASME Code verification calculation for vacuum vessel

The vacuum vessel is composed of inner vessel, outer vessel and two end flanges made of 304 stainless steel. The main design dimensions are given in Table 4-7-1. The results of verification calculations for vacuum vessel are shown in Table 4-7-2 and Table 4-7-3.

Table 4-7-1 Main design dimensions of vacuum vessel

Design dimension (mm)	ID	OD	Thickness	Length
Inner Vessel	1387	1395	4	489
Outer Vessel	2258	2278	10	489
End Flange	1395	2258	10	489

Table 4-7-2 Verification calculation of vacuum vessel under external pressure

Under External Pressure	Outer Vessel (Leak check)	Inner Vessel (Vacuum Break)
Material	S.S-304	S.S-304
Shell Thickness (mm)	10	4
Max. allowable P (MPa)	0.675	0.26
Actual Working P (MPa)	0.1	0.1
Hook stress=AWP*OD/4/thk (MPa)	5.695	8.72
Longitudinal Stress =AWP*OD/2/thk (MPa)	11.29	17.44

Table 4-7-3 Verification Calculation of vacuum vessel under internal pressure

Under Internal Pressure	Outer Vessel (Vacuum Break)	Inner Vessel (Leak check)
Design Pressure (MPa)	0.1	0.1
Stress Limit (MPa)	120.6	120.6
Joint Efficiency	0.7	0.7
Thickness Required=DPres*IR/(SLtd*JE-0.6) (mm)	1.35	0.827
Actual design thickness (mm)	10	4
Hook Stress=Dpres*2*IR/4/ADThk (MPa)	5.645	8.68

Longitudinal Stress=Dpres*2*IR/2/ADThk (MPa)	11.29	17.36

Note: Factor A is independent of material.

Stress Limit=Yield Strength/S.F=241.2/2=120.6 MPa

Actual Working P <Max allowable P、Hook stress<Stress Limit and Lstress< Stress Limit, OK.

4.7.2 Verification calculation of end flanges

The calculations for end flanges are according to 《ROARK'S FORMULAS FOR STRAIN AND STRESS》, and the result is shown in Table 4-7-4.

Table 4-7-4. Verification calculation of end flanges

ID (mm)	OD (mm)	Thickness (mm)	Maximum Stress (MPa)	Allowable Stress (MPa)
1395	2258	10	82.4	124.1

4.7.3 Verification calculation of pressure pipes

The calculations for helium piping in the cryostat is according to the chinese code-"Design code for industrial metallic piping (工业金属管道设计规范) GB50316-2000" which are consistent with the ASME code. The following formular is used for allowable thickness calculation.

$$t_s = \frac{PD_o}{2([\sigma]^t E_j + PY)} \quad (1)$$

$$t_{sd} = t_s + C \quad (2)$$

Table 4-7-5 Verification results of pressure pipes

Material	6061-T6Al	Copper		SS304		
Allowable stress [σ] (MPa)	72	45		137		
Welding joint coefficient E_j	0.8	0.8		0.9		
Coefficient Y	0.4	0.4		0.4		
Design internal pressure (bara)	21	21		21		
Outer Diameter D_o (mm)	30	8	10	18	22	25
Calculated thickness t_s (mm)	0.539	0.228	0.285	0.152	0.186	0.211
Additional thickness C (mm)	0.35	0.03	0.03	0.6	0.6	0.6
Allowable min thickness t_{sd}(mm)	0.889	0.258	0.315	0.752	0.786	0.811
Used pipe	Φ30×3	Φ8×1	Φ10×1	Φ18×1	Φ22×1	Φ25×1

The thickness of the helium piping used in the coupling magnet cryostat is at least 1mm, which is larger than the allowable minimum thickness.

4.7.4 Verification calculation of helium vessels

4.7.4.1 LHe distribution vessel

The Lhe distribution vessel made of 6061 T6 aluminum are designed using ANSYS. Table

4-7-6 shows the main its main parameters.

Table 4-7-6 Table Main parameters of LHe distribution vessel

Parameters	Value
Inner diameter of inner vessel (mm)	1866
Height of side plate (mm)	150
Length of long side plate (mm)	460
Length of short side plate (mm)	290
Thickness of upper and lower plate (mm)	15
Thickness of long side plate (mm)	15
Thickness of short side plate (mm)	15
Design internal pressure (bara)	4
Peak stress (MPa)	51.1
Allowable stress (MPa)	66

Considering symmetry of the LHe container, 1/4 model is developed. The load for the FEA model is internal pressure of 4bara. Fig.4-7-1 shows the FEA analysis results using ANSYS. The max von Mises stress is located at the center point of the contact line of the long side plate and lower plate, and its value is 51.1MPa. According to the chinese code-"Aluminium welded vessels (铝制焊接容器) JB/T4734-2002" which is consistent with the ASME code. The allowable stress of 6061 T6 aluminum is 66MPa. The design can meet the code requirement.

4.7.4.2 LHe collection vessel

The LHe collection vessel made of 6061 T6 aluminum are designed using ANSYS. Table 4-7-7 shows its main parameters.

Table 4-7-7 Main parameters of LHe collection vessel

Parameters	Value
Inner diameter of inner vessel (mm)	1866
Height of side plate (mm)	140
Length of long side plate (mm)	320
Length of short side plate (mm)	290
Thickness of upper and lower plate (mm)	15
Thickness of long side plate (mm)	15
Thickness of short side plate (mm)	15
Design internal pressure (bara)	4
Peak stress (MPa)	35.6
Allowable stress (MPa)	66

Considering symmetry of the LHe collection box, 1/4 model is developed. The load for the FEA model is internal pressure of 4 bara. Fig.4-7-2 shows the FEA analysis results using ANSYS. The max von Mises stress is located at the center point of the contact line of the long side plate and up plate, and its value is 35.6MPa. According to the chinese code-"Aluminium welded vessels (铝

制焊接容器) JB/T4734-2002" which is consistent with the ASME code. The allowable stress of 6061 T6 aluminum is 66MPa. The design can meet the code requirement.

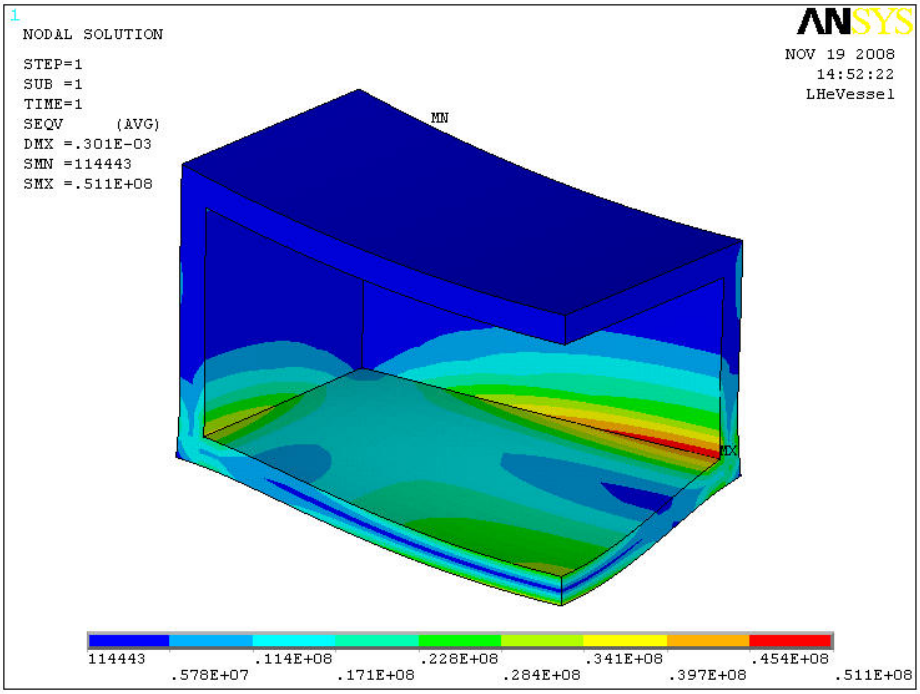

Fig.4-7-1 Von Mises Stress for LHe distribution container

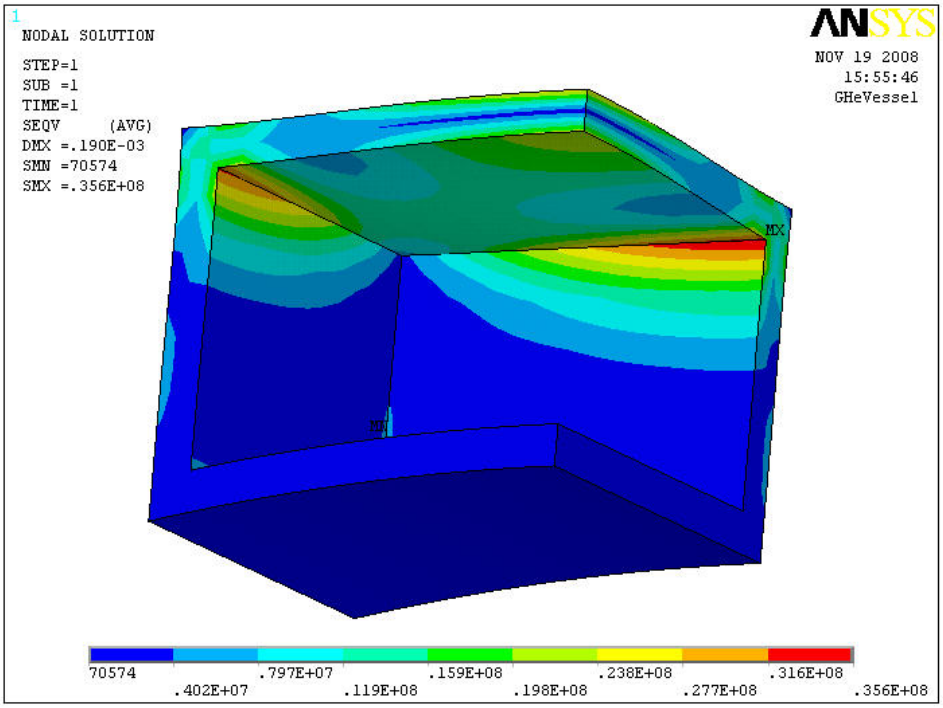

Fig.4-7-2 Von Mises Stress for LHe collection vessel